Glacier surging in the West Kunlun Shan

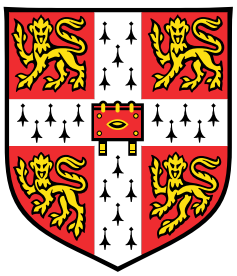

Thomas Russell Chudley

Scott Polar Research Institute

University of Cambridge

This dissertation is submitted for the degree of

Master of Philosophy

Downing College

June 2016

For my grandfather, who will be sorely missed.

Declaration

I hereby declare that except where specific reference is made to the work of others, the contents of this dissertation are original and have not been submitted in whole or in part for consideration for any other degree or qualification in this, or any other university. This dissertation is my own work and contains nothing which is the outcome of work done in collaboration with others, except as specified in the text and Acknowledgements. This dissertation contains fewer than 20,000 words excluding tables, captions, appendices, and list of references.

Thomas Russell Chudley

June 2016

Acknowledgements

I would firstly like to thank Ian Willis for supervising this study, whose support, insight, and near-bottomless list of contacts made this thesis possible. Thanks must also go to Toby Benham and Nick Töberg, for their advice and guidance regarding velocity tracking; TJ Young, who helped me to tackle the Chinese literature; and Duncan Quincey, who responded to a steady stream of emails with encouraging words and invaluable recommendations.

For providing additional data to support this study, I am further grateful to Amaury Dehecq, who was kind enough to share his excellent and comprehensive velocity fields, and Shiyin Liu, who provided the meteorological station data from the Chinese Meteorological Administration.

SPRI is fantastic research community, and the various staff and students of SPRI have been a source of excellent support and encouragement. In particular, I would like express my gratitude to Evan Miles and Andrew Williamson, for their generously provided knowledge and advice on all things glaciology; to Bob Headland, for his liberal application of red pen to a first draft of this thesis; and of course, to the rest of the MPhil Polar Studies cohort, who were an unending source of support and entertainment throughout the year – good job team.

I was incredibly privileged to have been financially supported through this degree by both Newton College and John Whitworth Master's Studentships. I am indebted to the Isaac Newton Trust and Downing College for providing this funding.

Abstract

The cryosphere of High Mountain Asia represents the third-largest glacial system on Earth, with a glacierised area of $\sim$40 800 km^2 (Bolch et al., 2012) and a mass balance of -26 $\pm$ 12 Gt a^{-1}: $\sim$10% of the global contribution of the cryosphere to sea level rise (Vaughan et al., 2013). The glaciers of the Karakoram and West Kunlun Shan represent the second major global centre of surge activity (Sevestre and Benn, 2015) and also mark a region of anomalous glacier behaviour known as the 'Karakoram Anomaly' (Hewitt, 2005), whereby widespread glacier stability and even growth contrasts with the global norm (Bhambri et al., 2013; Gardelle et al., 2012; Kääb et al., 2015). Despite the motivations presented by this unusual behaviour, understanding of glacial dynamics in the region is underdeveloped due to a scarcity of data and studies in the area, with even the dominant surge mechanism remaining unclear (Quincey et al., 2015).

This study aims to expand the current dataset of surging in the region by characterising a series of surges identified in a small range at the western end of the West Kunlun Shan. This site exists between the Karakoram and the site of the one previous surging study in the region (Yasuda and Furuya, 2015), allowing for the analysis of surging behaviour across a wide longitudinal range. The objectives of this study are: (i) to identify the long-term spatial and temporal distribution of surges in the study region; (ii) to assess surge dynamics over the course of the most recent surges; and (iii) to characterise observed surge behaviour in the context of established surge mechanisms and regional climatic and glaciological behaviour. A combination of a decadal-scale range of remotely sensed imagery, manual tracking of terminus position change, and cross-correlation feature-tracking methods are used to identify and characterise surge dynamics in the range.

A total of ten glaciers were observed to surge between 1972–2016 – 11.3% of the total population. Statistical analysis showed that these glaciers were more likely to be wider than non-surging glaciers, which is in line with previous findings, and terminate at lower altitudes, which is a new finding that here is linked to the increased likelihood of warm beds at lower altitudes. Distribution is biased to the northern range in the study area, which could be related to differing topographies in the north and south ranges, but could also be linked to geological differences.

Surge dynamics do not conform to classical understandings of surge mechanisms. Some characteristics are indicative of thermal (Svalbard-type) surges, with relatively slow velocities and build-up and termination periods lasting months–years. However, some unusual behaviours are also reminiscent of hydrological surges, including shorter return periods ($\sim$4 decades) and surge periods ($\sim$2–6 years) than typical thermal surges. These factors have been previously identified in adjacent studies (Quincey et al., 2015; Yasuda and Furuya, 2015), suggesting that the unusual behaviours observed across various surge studies in HMA are not anomalous, but instead indicative of a unique surge mechanism that is related to, but distinct from, traditional surge mechanisms.

Finally, observations were made of eight glacier surges that are temporally coincident to an unusual degree, which conflicts with understandings of glacier surging as a behaviour forced entirely by internally regulated mechanisms. Although conclusions presented here are highly speculative, links were made to a hydro-thermodynamic mechanism recently put forward by Dunse et al. (2015) to explain hydrologically forced thermal surging on an outlet glacier of the Austfonna ice cap. This conclusion is supported by records of anomalously high temperatures during the surge initiation period, and can also be interpreted in the context of long-term climate changes in the region, recently linked to increased surge incidence in the Karakoram.

This study has expanded the record of surges in the WKS, and made an unusual discovery that further validates recent literature proposing a relationship between surging and climate. These findings are important both in terms of understanding more about regional glaciology and climate, but also in better understanding surge behaviour as a whole.

Table of Contents

List of Figures

List of Tables

List of Nomenclature

Roman Symbols

A	Area
g	Gravitational acceleration (m^2 s^{-2})
H	Glacier thickness (m)
L	Length
N	Effective pressure (Pa)
P_i	Ice overburden pressure (Pa)
P_w	Water pressure (Pa)
W	Width

Greek Symbols

α	Ice surface slope (°)
ρ_i	Density of ice (kg m^{-3})
σ	Uncertainty in velocity calculations (m a^{-1})
τ_d	Driving stress (Pa)

Acronyms / Abbreviations

(G)DEM	(Global) Digital elevation model

a.s.l.	above sea level
ASTER	Advanced Spaceborne Thermal Emission and Reflection Radiometer (satellite sensor)
DoY	Day of Year
ELA	Equilibrium-line altitude
HMA	High Mountain Asia
ImGRAFT	Image GeoRectification And Feature Tracking (toolbox)
IPCC	International Panel of Climate Change
LOWESS	Locally Weighted Scatterplot Smoothing
NDSI	Normalised Difference Snow Index
RGI	Randolph Glacier Inventory
VNIR	Visible and Near-Infrared
w.e.	water equivalent
WKS	West Kunlun Shan

Chapter 1

Introduction

1.1 Rationale

The cryosphere of High Mountain Asia (HMA) represents the third-largest glacial system on Earth, with a glacierised area of $\sim$40 800 km^2 (Bolch et al., 2012) and a mass balance of -26 $\pm$ 12 Gt a^{-1}: $\sim$10% of the global contribution of the cryosphere to sea level rise (Vaughan et al., 2013). The ranges to the northwest of the system form the second major global centre of surge activity (Sevestre and Benn, 2015) and represent a region of distinct glacier behaviour known as the 'Karakoram Anomaly' (Hewitt, 2005), where widespread glacier stability, and even growth, contrasts with the global norm (Bhambri et al., 2013; Gardelle et al., 2012; Kääb et al., 2015). Despite motivations to understand this unusual phenomenon, knowledge of glacier behaviour and dynamics in the region remains underdeveloped due to the physical and geopolitical difficulty of conducting fieldwork in this region. Advances in remote sensing techniques in recent decades have gone some way to alleviating data scarcity, but the region is still remarkably under-researched compared with other glacier systems, such as in Alaska and the Alps.

This study is specifically motivated by two research themes related to the region. The first is the recent extension of HMA satellite altimetry and area change studies (Cogley, 2016; Kääb et al., 2015). These have identified that the Karakoram Anomaly extends well into the West Kunlun Shan (WKS) and may, in fact, be centred over the range. This

provides motivation to increase the understanding of glacier dynamics in the WKS, which has seen relatively few glaciological studies. The second motivation relates to the unusual surge dynamics that have recently been described in the Karakoram (Quincey et al., 2015). Glaciers appear to display behaviours that conflict with traditionally understood surge mechanisms, and the exact nature of surging in the region is yet to be ascertained. Recently, the first major study of surging in the WKS – centred on the region surrounding the Liushi Shan – has confirmed similarly unusual surge behaviours (Yasuda and Furuya, 2015), and thus motivates further studies into surges across a wider span of the WKS.

1.2 Study Objective and Aims

In light of the motivations outlined above, this study aims to use a decadal-scale range of satellite imagery to expand the understanding of glacier surging in the WKS. Three research objectives are identified:

1. Identify surge activity

To assess the incidence of surging in an as-yet unexamined area of the WKS. Using multitemporal Landsat satellite imagery, regular observations can be made over several decades. This will allow the identification of the characteristics of active surges and evidence of past surge activity. Following identification of surge-type glaciers, statistical analysis can be used to compare the characteristics of surging glaciers with non-surging glaciers (e.g. glacier size, hypsometry) to identify glacier characteristics that may predict surge activity in the region.

2. Assess surge dynamics

To assess changes in glacier behaviour throughout the active phase, and use this information to speculate on a potential surge mechanism. This research objective will be composed of two major parts. The first is to track changes in terminus positions, allowing the recent history of glacier retreat and advance to be analysed. The second is to assess changes in

glacier velocity using cross-correlation feature tracking methods, specifically using the open-source ImGRAFT software (Messerli and Grinsted, 2015). This combination of methods will allow key surge characteristics (e.g. velocity, active phase length, seasonal variation) to be detected and determined.

3. Explain surge mechanisms

In the context of the information gained above, an attempt will be made to interpret surge behaviour in terms of potential mechanisms, and to place observations into a glaciological and climatic context. This is of particular interest given the ambiguous conclusions of adjacent surge studies, which identify distinct differences when compared to traditionally understood surge mechanisms.

1.3 Thesis Structure

This thesis is divided into seven chapters. This chapter introduced the basic motivations for the study and outlined the major aims. The second chapter reviews literature relevant to (i) glacier surging and (ii) the glaciology and surge behaviour of HMA. The third chapter introduces the study area, reviewing climate and glaciology with specific reference to the WKS. Chapter 4 details the data sources and methods used in this study. Results are presented in chapter 5 and discussed in chapter 6. Finally, chapter 7 reviews the major conclusions made in this study before recommending avenues for future research.

Chapter 2

Literature Review

2.1 Glacier Surging

Surges are internally driven cyclic oscillations of glacier behaviour estimated to occur on approximately 1% of glaciers worldwide (Jiskoot et al., 1998). A surge cycle consists of a switch from a slow-flowing 'quiescent' to a fast-flowing 'active' regime, recurring over uniform periods (Meier and Post, 1969). Phases tend to be of relatively consistent periods for individual glaciers (although exhibiting high inter-glacier variability), with active phases lasting from months–decades and quiescent periods lasting from decades–centuries . During the active phase, ice-flow rates may increase by as much as three orders of magnitude, accompanied by chaotic crevassing and often terminus advance (fig. 2.1). Surge activity has been observed for over a century (e.g. Tarr, 1907), but even today, a unified theory of surging remains an active topic of research (Sevestre and Benn, 2015). Motivations to study and understand surge events range from the perspectives that may be gained on subglacial processes (Benn and Evans, 2010) to the hazards they represent to local communities (Hewitt, 2014).

2.1.1 Surge Mechanisms

In the quiescent phase of a surging glacier, ice velocities are below that of balance velocity, resulting in ice accumulating in a 'reservoir area' in the upper region of the glacier (Meier

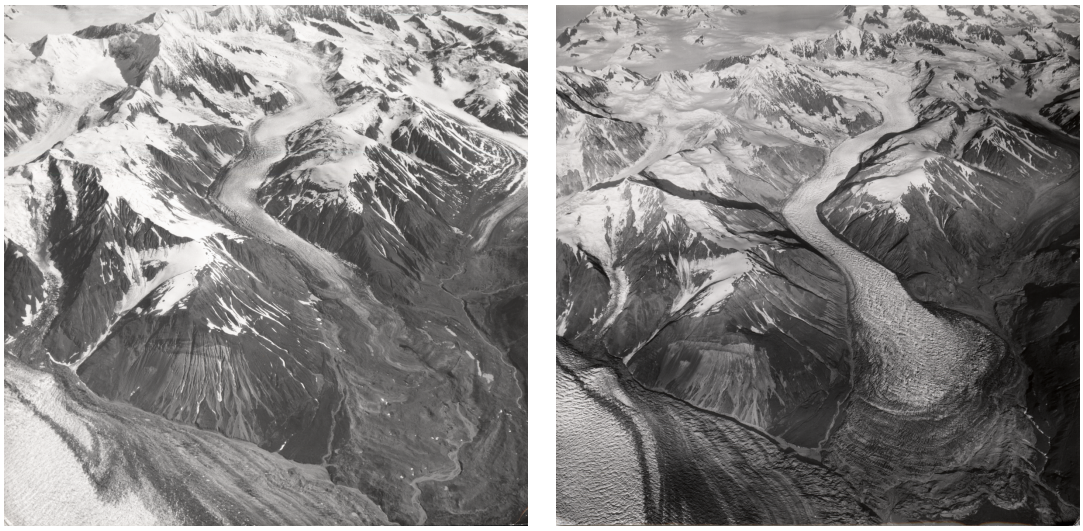

(a) 29th August 1964 (b) 22nd August 1965

Fig. 2.1 Aerial photos of Variegated glacier, (a) pre-surge, and (b) post-surge. Photographs by Post (1964, 1965), retrieved from the National Snow and Ice Data Center Glacier Photograph Collection (NSIDC, 2015).

and Post, 1969). As a result, ice surface gradient increases in the lower part of the reservoir area during this period. Meanwhile, ice mass decreases in the 'receiving area' in the lower glacier. As ice accumulation in the reservoir increases profile thickness, driving stress (τ_d) at the base increases in line with equation 2.1.

$$\tau_d = \rho_i g H \alpha \tag{2.1}$$

Where ρ_i is ice density, g is gravitational acceleration, H is ice thickness, and α is ice surface gradient. At a critical τ_d threshold, the active phase of the surge initiates and reservoir ice is rapidly transferred downstream to the receiving area, resulting in a rapid surface lowering in the reservoir area of 10–100 m, and an inverse response in the receiving area. This rapid acceleration occurs due to enhanced basal sliding rates, which can be triggered through multiple mechanisms. Early work considered the potential of external forcing, including tectonic activity and climate (Meier and Post, 1969). Considering the semi-regular recurrence interval and asynchronous surges of adjacent glaciers, recent research has settled on a definition of surging driven solely by internal oscillations in subglacial

dynamics, distinct from externally driven speed-ups (Sharp, 1988). As research into surging glaciers has progressed, two distinct triggering mechanisms, here termed 'hydrological' and 'thermal', have emerged (Murray et al., 2003).

Hydrological Surges

Hydrological (also known as 'Alaskan' or 'temperate') surges occur at temperate glaciers and are attributed to changes in basal hydrology. Quiescent phases can last decades, and active phases months or years, commonly initiating during the winter months and terminating during the summer. The basic model assumes a hard bed, which is not always favoured by the limited observations that exist of surging glaciers. Alternative, analogous models of temperate surging exist that account for soft beds (Cuffey and Paterson, 2010), but the mechanism discussed here remains the most commonly cited in the relevant HMA surge literature (e.g. Quincey et al., 2011), a region where the subglacial environment remains poorly known.

The model was developed based on seminal studies of the 1982–1983 surge of Variegated glacier (Kamb, 1987; Kamb et al., 1985). In 1981, prior to the surge proper, velocities ranged from 0.1–1.0 m day^{-1}, higher in the upper glacier. After 4–6 summer 'minisurges' of up to 1–3 m d^{-1} occurring between 1978–1982, the surge proper began in January 1982. Velocity peaked in the upper glacier on 26th June 1982 at 10.4 m d^{-1} (the lower glacier was not affected). The termination was rapid, decelerating to <50% of this speed in a few hours, and to $\sim$1 m d^{-1} in by mid-August. This marked the first phase of the surge, taking place in the upper glacier. In October 1982, the second phase started, reaching a maximum up $\sim$15 m d^{-1} in the upper glacier between May–June 1982 and decreasing to 0.2 m d^{-1} (less than pre-surge velocities) in late July. During phase two, the surge front also propagated rapidly downglacier, increasing velocities from 0.2 m d^{-1} to between 40–60 m d^{-1} in June (again reducing to $\sim$0.4 m day^{-1} by late July).

The principal mechanism to explain these behaviours is a seasonal transition in subglacial drainage system. In traditional warm-based glaciers, large inputs of meltwater to the subglacial system in the late ablation season can maintain an efficient, channelised subglacial

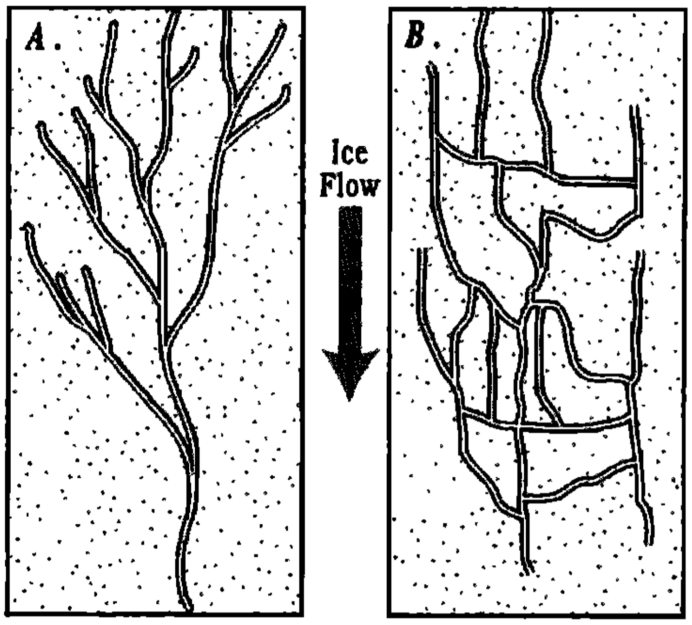

Fig. 2.2 Idealised plan view of (a) efficient 'channelised' and (b) inefficient 'distributed' subglacial hydrologies, reproduced from Fountain and Walder (1998).

drainage network through high rates of thermal erosion. However, following a reduction in meltwater in the winter, these large channels can no longer be maintained, as closure via ice creep can occur. This switches the system to an inefficient, distributed network existing as a series of cavities ($\sim$1 m high and $\sim$10 m wide) formed in the lee of bedrock bumps, linked by small conduits ($\sim$0.1 m in diameter) (Kamb, 1987, fig. 2.2). As surface meltwater production begins again in spring, increased basal water pressures occur as the meltwater cannot be efficiently evacuated by the inefficient system. This results in low effective pressures (N), defined as in equation 2.2:

$$N = P_i - P_w \tag{2.2}$$

N dropping beneath zero can initiate ice-bed separation, or 'hydraulic jacking', allowing enhanced ice flow by reducing friction at the bed (Cuffey and Paterson, 2010). Finally, as the summer progresses, increased meltwater supply begins to force a new system of efficient channels, reducing basal P_w, and hence increasing N and reducing glacier velocities.

This seasonal perturbation is common in hydrologically surging glaciers. This is supported by observational data at Variegated Glacier: on 9thth June 1983, dye-tracing experiments showed slow subglacial water velocities of $\sim$0.02 m s^{-1}, indicative of an inefficient system (Kamb et al., 1985). However, a transition to an inefficient system is also common in non-surge temperate glaciers and ice sheets (Bartholomew et al., 2010; Nienow et al., 1998), indicating that this is a necessary but not sufficient component of surge activity.

Eisen et al. (2005) hypothesise that, during quiescent phases, low H (and hence τ_d), meltwater from sources such as strain heating and geothermal heat are sufficient to keep the channelised system open through the winter. As H in the reservoir area increases through the quiescent phase, the system is increasingly predisposed to the collapse of the channelised system. Eventually, transition occurs late in the melt season, trapping subsequent rain or meltwater within the subglacial system and resulting in extremely high winter P_w that induces surge velocities Kamb (1987). Additionally, Fowler (1987) proposed that high-pressure, linked-cavity drainage systems are stable at higher ice velocities. Hence, beyond a critical threshold of τ_b the system preferentially switches to a stable distributed system with fast flow velocities.

Temperate glacier surges terminate rapidly upon switching to an efficient drainage system in early-mid summer. For instance, by the 14th July 1983 (post-termination), Kamb et al. (1985) showed subglacial flow velocities at Variegated Glacier to have increased to $\sim$0.7 m s^{-1}, typical of flow in open channels. This switch occurs in response to increased meltwater supply enlarging preferential channels through frictional melting of channels walls. For instance, the 1995 surge of Variegated Glacier terminated after two days of record high temperatures, producing large quantities of meltwater (Eisen et al., 2005). This channel enlargement initiates a positive feedback whereby low P_w in the channels preferentially drains the surrounding high-pressure pathways. As water drains across only a small portion of the bed in a channelised system, high ice-bed contact increases basal friction, and thus terminates high surge velocities.

Thermal Surges

Thermal (also known as 'Svalbard' or 'polythermal') surges occur in polythermal glaciers where cold ice exists at the bed, and are attributed to changes in thermal regime. Models of thermal surges were based upon studies of glaciers such as Bakaninbreen, Svalbard (Murray et al., 1998, 2000), which surged between 1985 and 1995. Thermal surges occur over longer periods than hydrological surges. Following an acceleration phase lasting months, active surges last for years–decades ($\sim$10 years for Bakaninbreen), with peak ice velocities slower than hydrological surges (1–3 m d^{-1} for Bakaninbreen). Following deceleration, quiescent phases may last for decades–centuries. Surges are sometimes associated with slowly propagating surge boundaries (at Bakaninbreen, the surge front advanced 2.5–4.7 m day^{-1} for the first 4 years of the surge), but this is not always the case – uniform acceleration is observed at marine-terminating glaciers such as Monacobreen (Murray et al., 2000).

A theoretical model of thermal surging was presented by Fowler et al. (2001). During the quiescent phase, cold-based or polythermal conditions dominate. Ice accumulation in the reservoir area increases H and hence τ_d (eq. 2.1), initiating higher creep rates. These higher creep rates generate heat through strain heating, and as H increases, heat loss from the base via conduction will decrease. Both factors increase basal temperatures. Once the pressure melting point is reached, basal meltwater production will increase pore P_w in the underlying till, weakening the sediment and initiating deformation. Deformation will dilate the till, increasing water storage and further weakening it. Till deformation produces further frictional heating, inducing further melt and higher P_w in a positive feedback that increases basal motion.

Once P_w equals or exceeds P_i ($N \leq 0$), Fowler et al. (2001) suggest water is stored in 'blisters', prevented from draining by the cold ice and permafrost downglacier – these observations are supported by ground penetrating radar measurements at Bakaninbreen (Murray et al., 2000). At the margins of this blister, τ_d and hence ice deformation is increased, and thus a positive feedback expands the surge area. Fowler et al. (2001) term this the 'thermal activation wave', moving both up- and down-glacier – and when the propagation of

this wave is slow relative to ice speed (i.e. when there is restriction to flow at the margins of the blister), this is also expressed as a surge front progressing downglacier. The surge terminates when subglacial water is able to discharge through the thawed till or faults, reducing P_w accordingly until pre-surge pressures are reached. A reduction in ice thickness will also increase heat loss, refreezing the bed in temperate regions (Cuffey and Paterson, 2010). In the model of Fowler et al. (2001), termination occurs when a subglacial till layer thaws completely and water is able to escape.

2.1.2 Surface Features

Surge activity can result in a number of diagnostic surface features. Looped medial moraines may form during tributary surges, responding to velocity differences between tributaries and the main trunk, which are then carried downstream to form a repeating geomorphic signature (Meier and Post, 1969). During active phases, chaotic crevassing is also a common expression of surface velocities. Lawson (1996) used historic aerial photography to identify widespread crevasse development on Variegated Glacier during the 1947-48, 1964-65, and 1982-83 surges. The quiescent phase is marked by generally sparse crevassing, but towards the end of the phase, crevassing occurs in the upper glacier as a response to increasingly steep gradients. Towards the end of the active phase, three zones were identified: (i) a narrow upper zone of arcuate transverse crevasses, above the surge activity and recording tensional stresses; (ii) a large middle zone of superimposed, often chaotic, longitudinal and transverse crevasses, where longitudinal crevassing formed by compressive flow ahead of the velocity peak precedes transverse crevassing behind it; and (iii) a narrow lower zone of longitudinal crevasses where only compressive flow is experienced.

2.1.3 Controls on Surging

Surges can occur across a wide range of glacier sizes, hypsometries, thermal regimes, and climatic environments. Surging glaciers are unevenly distributed globally, and Sevestre and Benn (2015) identify two major clusters (fig. 2.3): the first the ‘Arctic Ring’ (including

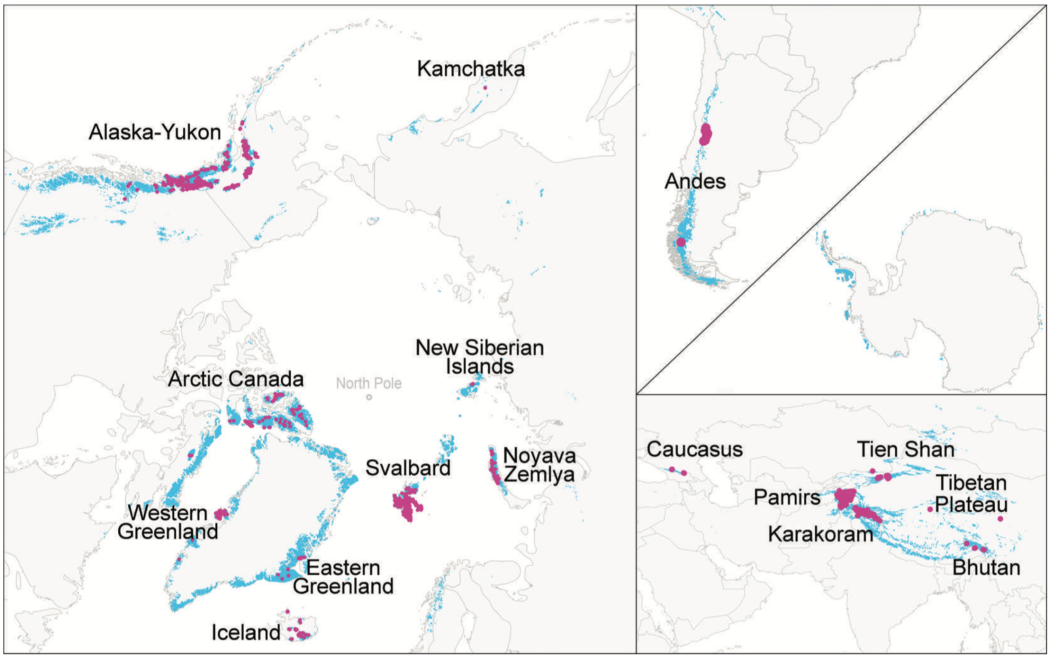

Fig. 2.3 Global distribution of surge-type glaciers, reproduced from Sevestre and Benn (2015). Global glacier outlines are presented in blue from the Randolph Glacier Inventory (RGI) version 3.2, and pink dots represent surge-type glaciers.

Alaska-Yukon, Arctic Canada, parts of Western and Eastern Greenland, Iceland, Svalbard, and Novaya Zemlya), and the second in HMA (including the Karakoram, Pamirs, and western Tien Shan).

Statistical analyses have been performed to link the distribution of surging glaciers to various environmental and geometric influences. Studies have identified a number of statistically significant indicators of surge incidence. For instance, surge incidence has been correlated with glacier length in a wide range of regions including the Yukon (Clarke, 1991), Svalbard (Hamilton and Dowdeswell, 1996), the Karakoram (Barrand and Murray, 2006) and Novaya Zemlya (Grant et al., 2009). Long glaciers are hypothesised to relate to longer subglacial erosion times, with the subsequent finer-grained and thicker till possibly relating to flow instability through increased permeability (Jiskoot et al., 2000). However, correlations are not always uniform – for instance, no relationship with length occurs in East Greenland (Jiskoot et al., 2003). A positive correlation with steep surface slopes has been found in Svalbard (Jiskoot et al., 1998, 2000), but a negative correlation exists in Novaya Zemlya

(Grant et al., 2009) and Iceland (Björnsson et al., 2003) – although the latter has been argued to be a by-product of the relationship between slope and glacier length (Clarke, 1991; Sevestre and Benn, 2015). Some studies have found significant correlations with underlying lithology. For instance, fine-grained sediments host more surge-type glaciers in Svalbard (Jiskoot et al., 2000). However, once again, this relationship is not global: no geological relationships have been found in East Greenland (Jiskoot et al., 2003) or Iceland (Björnsson et al., 2003).

A recent statistical analysis of a global geodatabase of 2317 known surge-type glaciers by Sevestre and Benn (2015) attempted to assess comprehensively relationships between surging, glacier geometries, and (for the first time) climate across regions. They found that the surge clusters existed within a well-defined climatic envelope of mean annual temperature and mean annual precipitation, with two subzones: a 'cold-dry' region for Arctic Canada and the Tibetan Plateau, where glaciers have much larger areas and greater lengths than normal; and a 'warm-humid' region for the remainder of the Arctic Ring and HMA, in which surge-type glaciers, whilst still larger, tend to be closer in size to the norm. As such, they propose that surge incidence is explained at the first order by climatic controls, and glacier geometries only modify the effects of climate.

2.2 High Mountain Asia

2.2.1 Cryosphere of High Mountain Asia

The cryosphere of HMA represents the third-largest glacial system on Earth, with a glacierised area of $\sim$40 800 km^2 (Bolch et al., 2012). It exhibits an estimated mass balance of -26 $\pm$ 12 Gt a^{-1} – $\sim$10% of the global contribution of mountain glaciers and ice caps to sea level rise (Vaughan et al., 2013). The system is also regionally important for water security. More than 1.4 billion people depend on water from the major rivers of HMA, and in river basins such as the Indus where desert conditions predominate, seasonal water availability is dependent on snow and glacier meltwater (Immerzeel et al., 2010). Glaciers in HMA also present local hazards, as lakes formed by glacial processes may be at risk of breaching and initiating

outburst floods (Bajracharya and Mool, 2010; Hewitt and Liu, 2010). Despite this importance to human activity on a number of scales, geopolitical and physical constraints on access have resulted in HMA being understudied in comparison to the global cryosphere as a whole.

Regional Glacier Characteristics

The extreme high relief of HMA gives glaciers distinctive characteristics that complicate basic models of mass balance. The first is significant debris supply from steep headwalls, which contributes to extensive debris covering in the ablation area. This acts to increase ablation where thin ($<\sim$2 cm), due to a reduced albedo, and reduce ablation where thick, due to their insulating effect (Benn and Lehmkuhl, 2000). The latter effect greatly modifies glacier responses in the region, with heavily debris-covered glaciers more likely to have stable, albeit stagnant, termini (Scherler et al., 2011b). Supraglacial ponds play a unique role in accelerating melt rates on debris-covered tongues, accelerating surface downwasting through calving and by exposing clean ice at ice cliffs (Benn et al., 2012), as well as acting as heat sinks to transfer energy to the englacial and subglacial environments, in total increasing melt rates by up to an order of magnitude (Immerzeel et al., 2014).

The second distinctive characteristic of the HMA cryosphere is that glaciers can be significantly or predominantly avalanche-fed. Common terminology in the regional literature refers to 'Turkestan' type glaciers almost entirely fed by avalanching with no accumulation zone as normally understood (<20% of area above the snowline), and 'Mustagh' types also predominantly avalanche fed but with flow commencing in a recognisable accumulation zone (20–50% of area above the snowline), both distinct from traditional 'Alpine' types fed predominantly by precipitation (Hewitt, 2011). High, steep headwalls thus extend the effective accumulation zone beyond the bounds of the glacier itself, and may result in a patchwork of accumulation zones (i.e. avalanche cones) in the lower regions of a glacier that would be part of the ablation zone if responding to climatic indices alone (Benn and Lehmkuhl, 2000). Both debris-cover and avalanching characteristics result in complex and non-linear mass balance profiles that complicate a simple theoretical understanding of glaciers based on

climatic equilibrium line altitudes (Benn and Lehmkuhl, 2000). As such, projection of glacier behaviour into the 21st century in this critical region is quite uncertain (Cogley, 2011).

Response to Climate Change

Glaciers in HMA have been found to be retreating in conformity with global trends. Cogley (2016) reviewed 155 publications on glacier area changes, finding that from 1960–2010, the average glacier retreated 0.57% a^{-1}, with slower rates extending from the southern Pamir to the Kun Lun ranges. This observed change in area is supported by studies measuring mass and volume losses, including a mass balance of -35.0 $\pm$ 5.8 Gt a^{-1} as estimated from GRACE gravimetry (Yi and Sun, 2014) and a mean -0.37 $\pm$ 0.10 m a^{-1} glacier elevation change from ICESat altimetry (Kääb et al., 2015).

One important but poorly-understood regional behaviour is termed the 'Karakoram Anomaly' (Hewitt, 2005), whereby widespread glacier stability and even growth is observed in the Karakoram-Himalaya, as assessed through both elevation and area change studies (Bhambri et al., 2013; Gardelle et al., 2012; Kääb et al., 2012). This could be partly a feature of the size dependence of glacier retreat rate – glaciers at 34–37°N are on average larger than elsewhere (Cogley, 2016). Additionally, alternative explanations have proposed that as much as 70% of the increase in total glacier area can be attributed to surge events (Bhambri et al., 2013). However, as even smaller non surge-type glacers are shown to be stable or advancing (Bhambri et al., 2013), it is likely also an actual function of mass balances. Explanations identify that the response of mid-latitude westerlies to climate change is increasing accumulation in the highest catchments of the Karakoram (Kapnick et al., 2014; Wiltshire, 2014).

Whilst termed the 'Karakoram Anomaly' (Hewitt, 2005), recent large-scale glacier change studies that have extended their study regions to the north and east (Cogley, 2016; Kääb et al., 2015) identify, in their expanded analyses, that the anomaly is larger than previously determined, extending well to the northeast of the Karakoram proper. Indeed, in their ICESat altimetry study, Kääb et al. (2015) identify the West Kunlun Shan as the centre of the mass

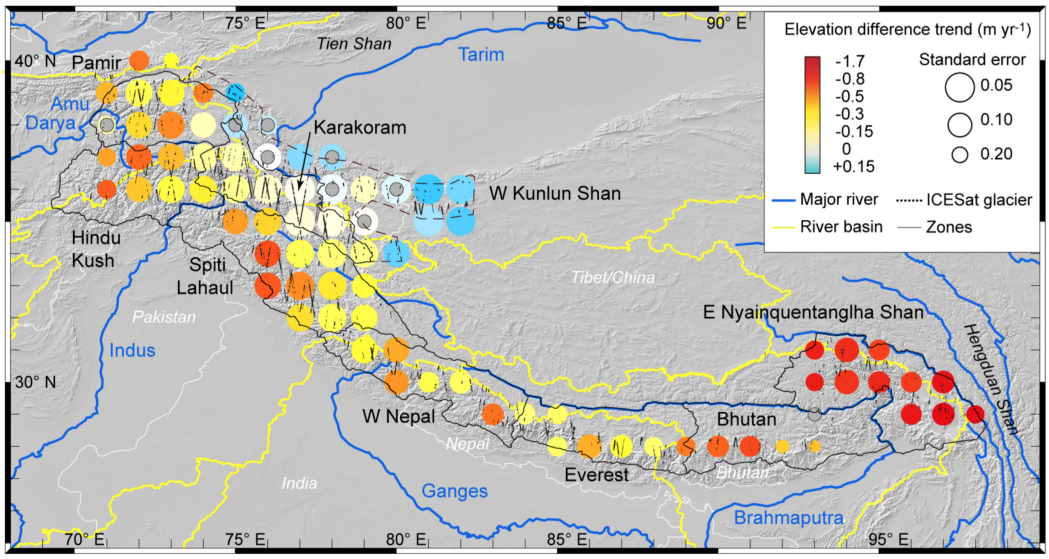

Fig. 2.4 Regional trends in glacier elevation changes based on on autumn ICESat acquisitions, reproduced from Kääb et al. (2015). Data shown on a 1° grid with overlapping rectangular geographic averaging cells of 2° by 2°. Grey centres mark cells where trends are not statistically significant. Zones where ICEsat footprints cross glaciers shown with dotted line.

change anomaly ($+0.05 \pm 0.07$ a^{-1}), with the Karakoram and Pamir as peripheral zones (fig. 2.4). This motivates further detailed investigation into glacier dynamics in this region.

2.2.2 Surge Activity

Despite the northwestern Himlaya-Karakoram marking the second major cluster of surging globally, HMA remains a notably under-researched region with regards to surge activity. The limited number of surge studies in the Pamirs (Kotlyakov et al., 1997, 2008), the Tien Shan (Narama et al., 2010; Pieczonka et al., 2013), and the WKS (Yasuda and Furuya, 2015) have largely focussed on identifying surges, often as part of a larger multitemporal glacier change analysis. Instead, the most comprehensive databases, and most detailed research into surge dynamics, have focussed on the Karakoram (Copland et al., 2011; Hewitt, 2007; Quincey et al., 2011, 2015; Rankl et al., 2014), where 55 surges have been identified since the mid-1860s, involving 46 glaciers (Hewitt, 2014), and one estimate suggests that 12.6% of glaciers are surge-type (Barrand and Murray, 2006). As such most literature referenced in

this section will refer to this range, and the limited WKS literature will be examined in section 3.3.3.

Surge Mechanisms

Attributing surges to an established mechanism in HMA is complex. In principle, with diverse altitudinal ranges, thermal regimes, and accumulation patterns, both hydrological and thermal surges could be expected, and a lack of studies of subglacial environments makes attribution difficult (Hewitt, 2014). Early observations reported that surges display sudden onsets, high velocities and advances, then sudden terminations suggestive of a hydrological surge type (Hewitt, 1969). More recently, using observations and modelling, Mayer et al. (2011) concluded the 2003–2007 surge of North Gasherbrum Glacier to be hydrological. Observations and estimates suggest return periods between 20–40 years (Guo et al., 2013; Quincey and Luckman, 2014), again conforming to a hydrological mechanism.

Other evidence suggests thermal mechanisms also play a role. Polythermal regimes are thought to dominate, with extreme vertical climate gradients. Quincey et al. (2011) highlight observations indicative of a thermal control: (i) a lack of seasonal cycle in observed surges; (ii) an acceleration of several years before peak velocity is reached; and (iii) peak velocities in the lower 10 km of glaciers. This agrees well with suggestions that glaciers are polythermal, cold-based at the tongue, margins, and higher elevations, and warm-based in the middle (Copland et al., 2009; Quincey et al., 2009). The effect of the large debris supply on subglacial processes is largely unknown due to a paucity of fieldwork, although limited studies have highlighted that soft sediment underlies at least some glaciers in the region (Owen and Derbyshire, 1989).

Very recent studies conclude that mechanisms are probably more complex, existing between those two end-member behaviours. For instance, Quincey and Luckman (2014) suggest Khurdopin Glacier exhibits characteristics of both thermal and hydrological surges, with acceleration over several years and late summer maxima in velocities (thermal), but a relatively sudden increase in summer velocities and an absence of a surge front (hydrological). Quincey et al. (2015) examine eight recent surges in the Karakoram. They describe events

lasting 3–5 years, indicative of hydrological surging. However, velocities do not exceed 2 km a^{-1}, there appears to be no consistent seasonal control on the timing of the initiation and termination of the surges, and the length of the buildup and termination phases can last for months or even years – all suggestive of thermal surging. Additionally, they note that where surge fronts occur, they override significant obstacles such as debris, dead ice, and thermokarst, such that surge fronts may be a consequence of glacier configurations rather than a feature indicative of a thermal or drainage boundary.

Ultimately, Quincey et al. (2015) conclude that no clear single mechanism can be defined for the region, particularly with such a distinct lack of knowledge about basal conditions and large heterogeneity in thermal and sedimentological conditions. With the high altitudes and reliefs involved, they speculate that the classic dichotomy may not be even appropriate.

Controls on Surging

Karakoram surge-type glaciers occur along the main crest of the range, on the highest, coldest, steepest, and snowiest glaciers fed by avalanche nourishment (Hewitt, 2014). Unlike relationships between surging and length/steepness identified in other regions (section 2.1.3), analyses suggest controls in the Karakoram to be slightly different.

Multivariate analysis of surges by Barrand and Murray (2006) show that whilst significant positive correlations between surging and glacier length, area, perimiter, width, and debris cover exist, after accounting for colinearity the strongest relationship was with perimeter size. They explain this in the context of an increased incidence of avalanching, which provide snow and debris. Some have suggested that increased debris may act to alter thermal regimes in the ice and sediments at the base (Gardner and Hewitt, 1990), but Barrand and Murray (2006) suggest that avalanching controls surge incidence by increasing the supply of snow and ice to the glacier, rather than by directly affecting basal processes.

Relevance to Wider Understanding

The unique surge behaviour exhibited in HMA is of importance as research moves towards a unified model of surging (e.g. Sevestre and Benn, 2015), which must explain the unique characteristics observed in surges in this region. Better understanding the nature of glacier surges in HMA is also of particular relevance to local communities, for whom surges may represent particular hazards for communities living in valleys: occupying land, disrupting transport routes to water sources, and causing outburst flood risks by damming streams (Hewitt, 1998, 2007, 2014).

Chapter 3

Study Area

3.1 West Kunlun Shan

Extending more than 2000 km from the Yarkand river valley to the west to the Amne Machin group in the east, the Kunlun Shan is one of Asia's longest mountain ranges, with some peaks exceeding 7000 m above sea level (a.s.l) (Ward, 1989). Traditionally separated at $\sim$83°E into the western and eastern ranges, the WKS acts to separate the Tibetan Plateau, Aksai Chin, and Karakoram to the south from the Tarim basin to the north. The most studied glaciated area in the region (marked as the study site of Yasuda and Furuya (2015) in fig. 3.1) is a dense collection of glaciers between Aksayqin and Keriya Pass, centred around the Liushi Shan (35°19' N, 80°55′ E), which at 7167 m a.s.l. is the highest peak in the Kunlun Range. This region (hereafter the Liushi region) attracts attention by containing the largest glaciers – such as the Duefeng Glacier – and the 120 km^2 Guliya Ice Cap, the largest ice cap in China (Zhang et al., 1989).

The specific study area examined is a $\sim$40 x 60 km zone of the WKS in the Hotan Prefecture of Xinjiang Autonomous Region, China – $\sim$150 km to the west of the Liushi region, and $\sim$250 km east-northeast of the Karakoram. The village of Dahongliutan is situated immediately southwest of the area (36°0′ N, 79°12′ E) and the one named peak in the study area is Qierlizuoke Feng (6802 m, 36°1′ N 79°28′ E) (figure 3.2). Glaciers in the study area feed the watersheds of the Karakash (to the west) and the Yurungkash (to the east). To the

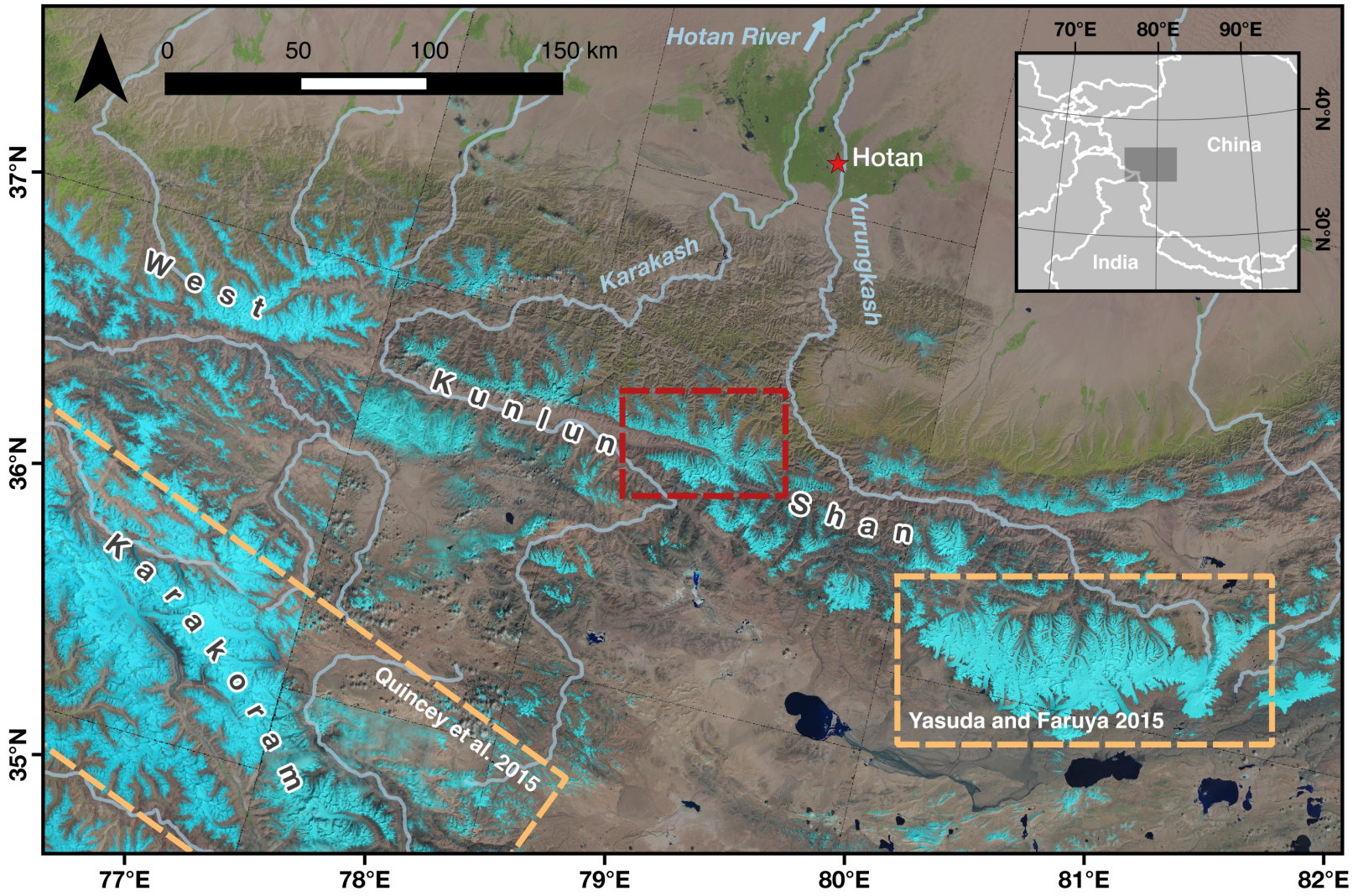

Fig. 3.1 Region map showing location of study area (red box). Also identified are the two adjacent surge studies (light boxes) and the town of Hotan (red star). Projected in WGS 84 / UTM zone 44N. Map background is LandSatLook "Natural Colour" imagery 2013–2015, from `earthexplorer.usgs.gov`.

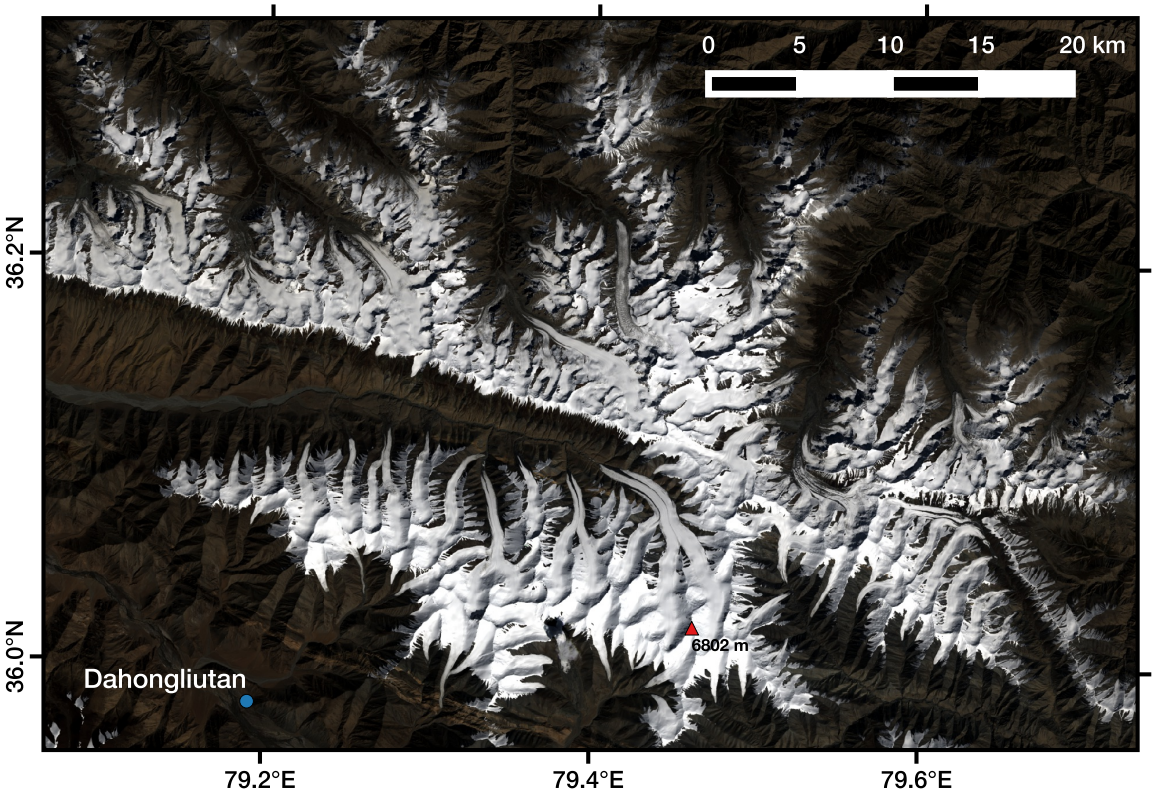

Fig. 3.2 False colour Landsat 8 OLI image of study area (taken 2013-09-18). The village of Dahongliutan and the highest peak (Qierlizuoke Feng) are marked.

north of the study area, both rivers flow into the the Hotan River, one of the major tributaries of the Tarim River.

3.2 Climate

3.2.1 Climate of the West Kunlun Shan

The region surrounding the West Kunlun has a continental climate, cold and very dry (Bao et al., 2015; Zhao et al., 2004). Westerlies supply moisture from the Indian Ocean, but supply is limited by orographic rain shadow effects due to the Karakoram and WKS (Zhang et al., 1989; Zhang and Jiao, 1987). Most precipitation occurs in the summer, from May–August (Zhang et al., 1989). High altitude glaciated catchments experience more precipitation and lower temperatures than the plains. This difference can be marked: Shangguan et al. (2009)

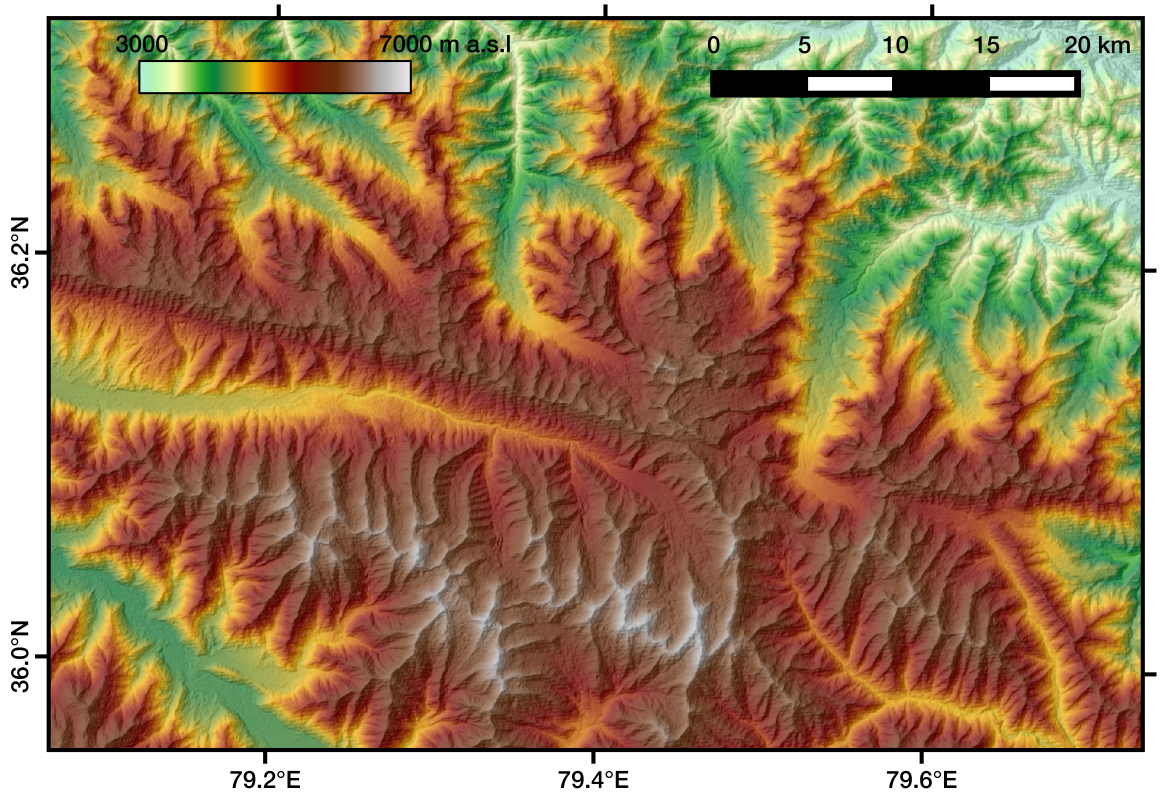

Fig. 3.3 Hillshaded ASTER GDEM v2.0 of study area.

report that whilst precipitation on the plains of the north slopes of the Liushu region might be under 40 mm a^{-1}, by 1800-3000 m a.s.l. precipitation has been reported to be 100–200 mm a^{-1}, and by 5700 m a.s.l. is 571 mm a^{-1}.

Sparse short-term observations exist to help quantify the climate at high altitudes. Various estimates place the equilibrium line altitude (ELA) for the Liushi region between 5300–6200 m a.s.l. (Scherler et al., 2011a; Shi et al., 2006; Zhang and Jiao, 1987), although recent studies (Bao et al., 2015; Ke et al., 2015; Neckel et al., 2014) use the ELA value of 5930 m obained by Ageta et al. (1989) for the Chongce ice cap. ELAs in the current study area are probably lower, as some glaciated catchments do not reach 5900 m a.s.l., even at their peaks (fig. 3.3). Zhang and Jiao (1987) report that at the snow line of the northern slopes of the Liushu region ($\sim$5900 m a.s.l.) mean annual temperature was -14.7 ℃ and precipitation $\sim$460 mm. Similarly, Shi et al. (2006), using short-term observations and proxy data, have

reported the annual precipitation at the ELA to range from 200–500 mm, and the mean annual and summer temperatures to be -10 ℃ and -1 ℃ respectively.

3.2.2 Climate Change in the Hotan Basin

A particular feature of climate change in northwest China, and particularly the Tarim Basin, is a notable shift to warmer and wetter climate occurring ∼1986–1987 (Borth et al., 2015; Chen et al., 2006; Shangguan et al., 2009; Shi et al., 2007). Causes of the regional-scale climate change in northwest China have been proposed to be: (i) a switch in 1987 to an atmospheric pattern favourable to enhanced southern wind and water vapour transport to the north, resulting in an increase in the transport of atmospheric water vapour from the Indian ocean, or (ii) an enhanced water cycle resulting from increased Indian Ocean temperatures (Shi et al., 2007).

Across 128 weather stations in Northwest China, the period 1987–2000 was 0.7 ℃ warmer than the period 1961–1986 (Shi et al., 2007). This temperature increase was highest in the winter (Zhang et al., 2009; Zhao et al., 2004), although positive trends exist in all seasons (Peng et al., 2014). Additionally, southern Xinjiang, and in particular the Hotan catchment, experienced muted effects. The warming trend is smaller here compared to the rest of Xinjiang (Tang et al., 2014). To the south, in the northern Tibetan Plateau, overall temperature has decreased by 0.6 ℃ in the past 30 years (Shi et al., 2006; Wang et al., 2003). This suggests that the West Kunlun range lies at the far edge of the climate shift.

Precipitation displays similar trends to temperature. Whilst southern Xinjiang saw an increase in annual precipitation of 17.4 mm (33%) in 1987–2000 compared to 1961–1987 (Shi et al., 2007), precipitation trends for the Hotan basin were also notably less, with two meteorological stations showing small but opposite trends (Shangguan et al., 2009), and various studies reporting insignificant precipitation changes (e.g. Xu et al., 2013; Zhang et al., 2009). This again suggests that the West Kunlun/Hotan catchment climate change is of a lower magnitude than Xinjiang as a whole.

3.2.3 Climate Changes at High Altitudes

Given the muted climate trends in southern Xinjiang, extrapolating low-altitude meteorological station observations to high-altitude glaciated catchments is difficult. Evidence suggests that runoff data might make an accurate proxy for the net effects of temperature and precipitation changes at these high altitudes. Chen et al. (2006) report that glaciers and snow melt form 48.2% of the total runoff of the Tarim river, but in particular emphasise that for the Hotan River – unlike other tributaries – streamflow displays a stronger correlation coefficient with summer temperature than precipitation, suggesting that meltwater may be a particularly important source of runoff in the catchment (see also Xu et al., 2013). As Kalakash and Yurungkash hydrological stations are located above regions where anthropogenic activity (e.g. irrigation) exerts an influence on streamflow, such changes in runoff might be a reliable indicator of changes in glacier and snow melt behaviour.

Shi et al. (2007) report a 5–40% increase in runoff in 18 of the 26 rivers in Xinjiang in 1987–2000 compared with 1956–1986. However, during the same period, river runoff originating from the WKS reduced by 1.6–9.2%, and similar declines are observed in other studies (Chen et al., 2006; Huang et al., 2009; Zhang et al., 2009). As such, it is unlikely that a shift to negative mass balances is occurring. This suggests that the climate changes observed at low altitudes probably correspond to changes at high altitudes. This is supported by MODIS observations of snow line altitudes for the Liushi region, which show that whilst altitudes varied between 5929–6061 m a.s.l. between 2003–2013, negligible trends were observed overall (Bao et al., 2015).

3.3 Glaciers

3.3.1 Glacier Characteristics

Early reports of glaciers in the WKS from western literature can be traced back to the expeditions of Sir Aurel Stein (e.g. Stein, 1912). The second half of the 20th century saw increasing scientific study on the range, but the remote location and difficult access

requirements means that in-situ measurements are lacking. Most glaciers in the WKS drain into the Hotan River system (Zhang et al., 1989), including the glaciers examined in this thesis.

The cold, dry climate has traditionally been thought to give rise to cold-based, polythermal glaciers (Shi and Liu, 2000), although in-situ measurements are rare and conditions at the bed largely unknown. Where boreholes exist – for example, in the accumulation zone of Shule Nanhan glacier in the East Kunlun Shan, more than 1000 km east of the current study area (Liu et al., 2009) – glaciers display temperatures below the pressure melting point down to the base. To remedy this in-situ data gap, Yasuda and Furuya (2013) used radar data to assess short-term (sub-annual) variation in velocity profiles in the Liushi region of the WKS. They suggest that 'normal-flow' (i.e. non-surge) glaciers display features inconsistent with a uniformly frozen bed, such as clear seasonality in velocity. At Duofeng Glacier, the largest glacier in the WKS, mean velocity profiles are 70 $\pm$ 7 m a^{-1} between October–February, and 92 $\pm$ 10 m a^{-1} between May–September. As a result, they suggest that a strictly cold-based model of these glaciers is simplistic, and observations are consistent with regions of warm bed.

The topography and geology of the range exerts considerable control on glacier morphology and distribution. The south slope of the range, backing the Tibetan Plateau, is flat and wide, with a height difference between peaks and foothills of <2000 m, whilst the steep northern slopes, extending down to the Tarim Basin, can reach 5000 m difference, with deep valleys (Zhang et al., 1989). Mean local relief is lower than other glaciated ranges in HMA, and the upper ablation area is generally shallow, allowing large interconnected accumulation areas to exist in the central massif (albeit with comparatively slower flow velocities, on the order of tens of metres per year) (Scherler et al., 2011a). Glaciers with a mean aspect between northwest and northeast (i.e. on northerly slopes) occupy $\sim$70% of the total area (Zhang et al., 1989), as well as extending to lower altitudes. However, southern slope glaciers can exhibit unique morphology, particularly at the Guliya Ice Cap, where distinct piedmont tongues occur where glaciers flow beyond the constraints of valley walls. The proportion of debris-covered glaciers is relatively low compared to the rest of the Hindu Kush Himalaya

(Scherler et al., 2011b; Yasuda and Furuya, 2013; Zhang et al., 1989), with a mean debris cover of <3% (Scherler et al., 2011a), indicative of only minor hillslope fluxes at the headwall.

3.3.2 Glacier Changes

For the most part, glaciers in Tarim Basin catchments are retreating, having lost 6.6% of their area and 3.8% of the volume since the 1960s (Liu et al., 2006). This conforms to, albeit at a lower rate than, the HMA cryosphere as a whole (section 2.2.1). This trend is likely because observed increases in precipitation have not outweighed increased temperatures with regards to changing mass balances since 1987 (Liu et al., 2006). Remote sensing studies assessing changes in the WKS/Hotan catchment are sparse. Studies also tend to sample exclusively from the Liushu region, making reports of change in the WKS potentially biased to these larger glaciers (e.g. Ding et al., 2006; Scherler et al., 2011b; Yasuda and Furuya, 2013), which are known to respond more slowly to climatic warming.

For glaciers in the Hotan river basin, Shangguan et al. (2009) used the Chinese Glacier Inventory to assess 2487 glaciers. Glaciers retreated 0.7% between 1970 and 2000, the smallest retreat of any Tarim river subbasin (mean -3.3%). This negligible long-term retreat has been supported by a number of studies (Ding et al., 2006; Liu et al., 2006; Shangguan et al., 2007). However, a recent study by Bao et al. (2015) at a higher temporal resolution identifies that retreat has probably halted in recent decades: whilst glaciers in the Liushu area retreated between 1970–1990 (-3.2 $\pm$ 3.1%), change was negligible between 1990–2010 (-0.2 $\pm$ 2.5%), suggesting that there has been sharp deceleration after 1990. This change would agree with the distinct climatic change in the late 1980s described in section 3.2.2.

This shift away from negative mass balances since the 1990s is supported by altimetry studies. As part of wider global and regional analyses, Gardner et al. (2013) reported a mean 2003–2009 elevation change of +0.17 $\pm$ 0.15 m a^{-1} for glaciers in the WKS, Neckel et al. (2014) +0.04 $\pm$ 0.29 m a^{-1}, and Kääb et al. (2015) +0.05 $\pm$ 0.07 m a^{-1}. Focussing on the WKS, Ke et al. (2015) identify heterogeneous surface changes in the Liushi region, reporting mean elevation changes of +0.20 $\pm$ 0.04 m a^{-1} from 2003–2008. High between- and within-glacier heterogeneity was observed, attributed to the complicated structure of

glaciers here: with large elevation ranges and variations in aspect, hypsometry, glacier length and ice flow. Finally, Bao et al. (2015) report recent elevation/mass balance gains (+0.22 $\pm$ 0.07 m a^{-1}, or +0.23 $\pm$ 0.24 m water equivelent (w.e.) a^{-1}, between 2003–2009). These gains were largely in the accumulation areas and change was negligible in the ablation areas (+0.42 $\pm$ 0.09 m a^{-1} versus +0.01 $\pm$ 0.10 m a^{-1}). Hence, the slight positive trends observed in glacier mass balances align with the positive anomalies observed in the Karakoram, as demonstrated by recent reports that the Karakoram Anomaly is in fact centred over the WKS (Cogley, 2016; Kääb et al., 2015). However, Yasuda and Furuya (2015) indicate that ICESat tracks often cross surging glaciers in the region, making it difficult to ascribe the cause of such changes to climate.

3.3.3 Glacier Surges

Studies of WKS surge glacier dynamics are limited to those of Yasuda and Furuya (2013, 2015) for the Liushu region. Of the 31 major valley glaciers in the area, nine have been identified as surge type (with a further eight potential candidates showing some geomorphic indicators), and at least four have surged in the first decade of the 21st century. No glacier surged more than once during the observation period, suggesting a recurrence interval exceeding 42 years. Surging glaciers in these studies were longer and larger than non-surging glaciers, and individual quiescent phase characteristics were dependent on whether glaciers were on the north or south slope of the range – the shallower south slope glaciers retreated more slowly.

Yasuda and Furuya (2015) used feature tracking to measure surface velocities at high temporal resolutions (up to 11 days). Observed characteristics are indicative of both thermal and hydrological surging, similar to reports by Quincey et al. (2015). They found that increases in ice velocity were gradual and peak velocities reached 200–1000 m a^{-1}, indicative of thermal surging. However, velocity showed clear seasonal modulations by as much as 200% in the early winter compared with the early summer, indicative of a significant hydrological influence on glacier dynamics. Consequently, whilst temporal durations are reminiscent of thermal surging, Yasuda and Furuya (2015) suggest that glacier surges here,

whilst occurring under a polythermal regime, are largely a result of hydrological activity. They speculate that the colder and drier climate results in a lower summer meltwater supply than traditional temperate hydrological surges, thus an efficient drainage network fails to fully develop in the summer. Hence, more of the summer meltwater supply is maintained into the winter, and thus subglacial meltwater storage sufficient to increase winter basal P_w can occur. Pressure melting and frictional heating may also generate additional water subglacially. Despite this, winter P_w remains lower than in temperate surges, resulting in the smaller peak velocities observed in the WKS. This subsequently means that the reservoir area is emptied at a slower rate, allowing the surge to continue for longer periods than a temperate glacier surge, whilst still exhibiting hydrologic seasonal velocity variation.

The tentative hypothesis of a polythermal, yet still hydrological, surge proposed by Yasuda and Furuya (2015) can explain a number of the unusual characteristics of these surges, such as the seasonal velocity variation of a hydrological surge and the long phase durations and low velocities of a thermal surge. This interpretation of contradictory surge characteristics displays similarities to that of Quincey et al. (2015), who, whilst not speculating on any specific processes, suggest that Karakoram surges do not fit neatly into either classical model. This is significant as the Karakoram is only slightly further away from the current study area than the Liushi region examined by Yasuda and Furuya (2015) ($\sim$250 km versus $\sim$150 km).

Chapter 4

Methods

4.1 Data Sources

The primary data used in this study were satellite images from the Landsat MSS (Multispectral Scanner System), Landsat TM (Thermal Mapper), Landsat ETM+ (Enhanced Thematic Mapper), and and Landsat OLI (Operational Land Imager), forming a suite of Landsat imagery from 1972–2016. All available Landsat scenes (path 146, row 035) with <40% cloud were downloaded from `earthexplorer.usgs.com` – a complete list of which is detailed in appendix A. Landsat imagery was provided at level 1T (terrain corrected), and as such was already orthorectified by the USGS. Visual analysis suggested that this orthorectification was correct to within a pixel for the study area, and hence no further correction or coregistration was necessary.

4.2 Surge Identification

Surging glaciers were identified based on a systematic analysis of summer Landsat imagery from 1972–2016, following the descriptors and classification of Copland et al. (2003). This classification has been used successfully by Yasuda and Furuya (2015) to classify surging glaciers to the east. The procedure uses features readily visible in optical Landsat imagery –

particularly the 15 m panchromatic band available for the Landsat 7 ETM+ and Landsat 8 OLI sensors – to classify glaciers into four distinct phases, as below:

1. **Observed surging.** The active phase is clearly observed, with distinct surface features and rapid terminus advance.
2. **Likely surge-type.** Many distinct surge features are present, but the active phase is not directly observed.
3. **Possibly surge-type.** There are fewer, or less distinct, surge features present (e.g. surface crevassing), and no active phase.
4. **Non-surging.** No surge features are present.

Actively surging glaciers are readily identified by severe surface crevassing, shear margins at the fast flow boundary, a surge bulge, rapid advance of the glacier surface not present in adjacent glaciers, and a strandline of ice on the surrounding bedrock where ice surface elevation has fallen rapidly. A number of features can also indicate a surging glacier even in the quiescent phase, including looped medial moraine, rapid terminus retreat, and potholes on the glacier surface.

4.3 Characteristics of Surging Glaciers

4.3.1 Glacier Characteristics

To identify glacier characteristics that might be favourable for surge activity, a glacier inventory was constructed and various glacier characteristics calculated. Initially, outlines from the Randolph Glacier Inventory (RGI) version 4.0 (Pfeffer et al., 2014) for the study area were assessed for their suitability, but it was concluded that these were inappropriate, tending to overestimate glacier cover. Indeed, RGI outlines are known to overestimate glaciers in HMA when compared to manually delineated imagery, with the Glacier Area Mapping for Discharge from the Asian Mountains (GAMDAM) inventory having a total glaciated area 24% lower than the equivalent RGI coverage (Nuimura et al., 2015). Instead, glacier outlines

were manually delineated based on Landsat ETM+ band 8 (15 m resolution panchromatic) imagery from the 2000 ablation season. The year 2000 is recommended for generation of baseline datasets by Paul et al. (2010), and has the advantage of containing no actively surging or recently surged glaciers, thus giving a representative view of all glaciers in the quiescent phase. Clouds obscure at least some ice-covered surface across all Landsat ETM+ scenes in the 2000 late ablation period, so a combination of Days of Year (DoY) 218 and 282 are used (neither scene has significant snow cover, despite 282 being in October). Only glaciers with an area >1 km^2 were delineated, as smaller glaciers are not prone to surges. This threshold has been previously used in surge studies such as Dowdeswell et al. (1995).

After the construction of a basic set of outlines, glacier characteristics could be calculated. These characteristics were chosen to align with the study by Barrand and Murray (2006) of surging glaciers of the Karakoram. The variables assessed consisted of glacier area, length, perimeter, mean slope, aspect, average width, mean, minimum, and maximum elevation, elevation range, debris cover, and glacier complexity. Area and perimeter could be calculated directly from glacier outlines. Length was determined from manually delineated glacier centrelines. Glacier aspect and elevation parameters were calculated in combination with topographic data provided by the ASTER Global Digital Elevation Model (GDEM) version 2, a product of METI and NASA and provided by the USGS at `earthexplorer.usgs.com`.

The percentage of debris cover was calculated by using the Normalised Difference Snow Index (NDSI) to identify bare ice using bands 2 and 5 of Landsat ETM+ imagery as in equation 4.1:

$$NDSI = \frac{B_2 - B_5}{B_2 + B_5} \tag{4.1}$$

Where B_n refers to the bands used. NDSI was calculated for DoY 218 and 282 for the year 2000, using manually chosen thresholds of 0.35 and 0.40 respectively to identify ice-covered pixels. Following this, the percentage of pixels within glacier outlines classified as debris was calculated. As with glacier outlines, two images were used to account for

clouds cover across scenes – where data for both images were available, an average of the two scenes was used.

Finally, estimates of glacier average width and complexity were calculated based on approximations used by Barrand and Murray (2006): glacier complexity was calculated by dividing the perimeter by the area; and average width was calculated by dividing the area by the length. For all continuous variables where the relationship to surge incidence was non-linear, log transformations were applied.

4.3.2 Statistical Assessment

Standard linear regression models based on ordinary least squares (OLS) regression are inappropriate for assessing potential explanatory relationships between glacier characteristics and surge incidence (Jiskoot et al., 1998). First, these models assume that variables are (i) independent, and (ii) normally distributed, whilst glacier characteristics will display covariable and non-normal distributions. Second, surge incidence is a Boolean response variable (i.e. surge or non-surge), whilst standard linear models assume a continuous variable response. Instead, multivariate logit regression models, which can be fitted as generalised linear models (GLMs), have been commonly used to assess surge predictors (e.g. Atkinson et al., 1998; Barrand and Murray, 2006; Jiskoot et al., 1998, 2000). These allow categorical dependent variables (where surge-type = 1 and non-surge = 0), as well as both continuous and categorical explanatory variables, which is useful in this instance for glacier aspect data, processed as categorical data. An in-depth discussion of the use of multivariate logit modelling with regards to geomorphological purposes, including glacier surging, is given by Atkinson et al. (1998).

In this study, logit modelling was performed using R. The success of any individual model can be assessed by examining the extent which model deviance is reduced compared to a null model. R provides a measure of statistical significance (where $p < 0.05$ was deemed significant), but as a rule of thumb the 0.05 significance level lies at the point where the estimated model coefficient is at least twice the calculated standard error. In the first round, univariate logit regression was used for individual variables to assess statistically signifi-

cant relationships. The significant predictor variables were then ranked by the magnitude of reduction in model deviance against the null model. Then, a multivariate model was constructed using a stepwise strategy, fitting the predictor variables one by one so that covariable predictors can be excluded. If, after adding a predictor to the model, a statistically significant reduction in model deviance was not observed, then the variable was rejected in future rounds.

4.4 Glacier Dynamics

4.4.1 Terminus Changes

The relatively coarse temporal resolution of the Landsat satellite record used in this study – particularly after accounting for cloud cover – may leave periods of over a month without useful observations, especially when considering the high image quality necessary for velocity tracking using optical satellite imagery. Additionally, even qualitatively comparing satellite imagery of two or more different time periods can be difficult, especially when assessing minor changes indicative of early surge initiation. As a result, identifying changes in terminus position can be useful when assessing surge dynamics. An advancing terminus position is relatively easy to assess, and, as a secondary effect of surge activity, can be used to infer information about surge velocity and behaviour. Additionally, as locating the terminus position requires only the snout of the glacier to be visible, it allows useful information to be extracted from satellite imagery that might otherwise be of too poor quality for wider assessment – for instance, due to cloud cover, or following the loss of the Landsat 7 ETM+ scan line corrector (SLC) in 2003.

Assessment of terminus changes for the most recent glacier surges followed Yasuda and Furuya (2015) in their study of WKS surging glaciers, in using the protocol of Moon and Joughin (2008). First, a rectangular polygon was drawn around the full spatial extent of terminus variation for the study period, extending to an arbitrary reference line, or gate, upstream (fig. 4.1). A digitised ice front position was manually delineated for each time period using Landsat imagery. Second, the mean length (L) of the polygon was calculated

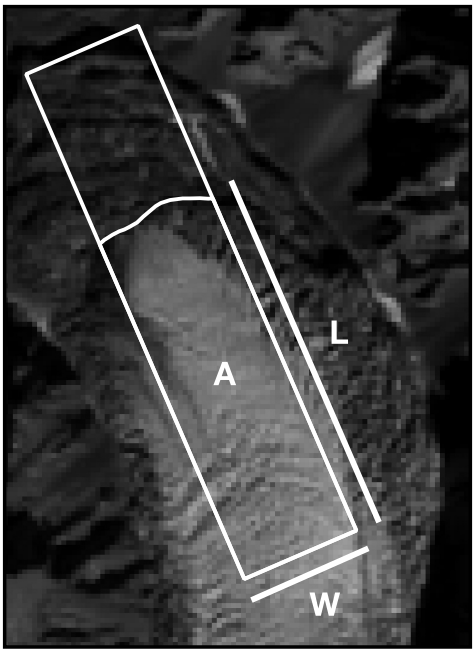

Fig. 4.1 Schematic showing variables collected in process of identifying length change, including the area (A), width (W), and length (L).

by dividing the area of the polygon (A) with the known width (W). As the gate position and polygon width remains constant between measurements, the average polygon length across the terminus front can be calculated, accounting for uneven changes across the ice front better than the measurement of single flowlines. Total glacier length at any time period can then be calculated by adding the mean polygon length to the remaining length of the glacier centreline from the gate to headwall.

4.4.2 Glacier Velocity – Cross-Correlation Feature Tracking

Remotely sensed data have provided the opportunity for efficient assessment of surge dynamics in many remote areas. Velocity data can be derived using cross-correlation feature tracking from synthetic aperture radar or optical satellite imagery, and has been used successfully for glaciological purposes for over two decades (Scambos et al., 1992). Cross-correlation produces velocity fields from pairs of digital satellite images, tracking the

movement of small-scale surface features – in the context of surging glaciers and in particular HMA, crevasses and surface debris patterns are a particularly useful feature for this purpose. Early applications primarily used synthetic aperture radar (SAR), but recent studies have seen the successful use of optical satellite imagery such as panchromatic Landsat 7 and 8 imagery, including in the Karakoram (Quincey et al., 2015).

The feature-tracking package used was the 'Image GeoRectification and Feature Tracking' (ImGRAFT) toolbox (Messerli and Grinsted, 2015), a complete and open-source module for MATLAB. Although originally developed for use with terrestrial oblique imagery (e.g. time-lapse photography), the package has been used successfully with Landsat 8 imagery (Messerli et al., 2014). Satellite images were primarily sourced from Landsat ETM+ and Landsat 8 OLI imagery, although the failure of the ETM+ scan line corrector leaves a gap in this dataset between May 2003 and the first usable OLI imagery in May 2013. Level 1T ASTER imagery was used to attempt to fill this gap, but a complete suite of data from the visible and near-infrared (VNIR) telescope was not available for the study period, and those that remained were unable to provide high-quality results.

Images were pre-processed by applying a high-pass filter to highlight high-frequency signals (i.e. crevasses) and reduce the effects of differing illumination directions. The template size was set to 21x21 pixels, as recommended for Landsat imagery in the ImGRAFT documentation (`imgraft.glaciology.net`), and search areas were manually determined, between 41x41 and 71x71 pixels depending on the image. Search area can be conceptualised as a sum of the template size and the maximum expected displacement – hence, periods of faster flow necessitated larger search areas for optimal pattern recognition.

4.4.3 Glacier Velocity – Error Assessment

Error will be introduced into the displacement data due to registration in the georeferenced L1T satellite imagery. Quincey et al. (2015) suggest that a reasonable assumption for this error is the $\sim$5 m accuracy estimated by Lee et al. (2004) for multitemporal Landsat 7 ETM+ imagery from the same path and row. Presuming greater georeferencing error, such as the

30 m estimate of Messerli et al. (2014), the resultant uncertainty is $\sim$2 m d^{-1} for intervals >15 days.

However, further error results from correlation failures introduced by changes in crevasse and surface debris patterns through time, or through the mismatch of surface features. These were often distinctly visible in the resultant velocity fields as sectors of anomalously high velocities, often in random flow directions. These errors were dealt with as in Quincey et al. (2015). First, areas with a high signal-to-noise (SNR) ratio were removed. Following experimentation, a threshold ratio of 4.5 was found to be most effective for the dataset. Second, extreme velocities were removed by applying a realistic upper threshold, based on the highest-quality velocity fields for each period. This upper limit varies between 100 and 1500 m a^{-1}, largely dependent on whether glaciers were in their quiescent or active phases. Finally, data were filtered to remove those deviating from dominant flow directions beyond a set threshold (between 45–90°). After these procedures were applied, pixels were assumed to be robust. Scenes providing only a minority of useful data were removed from the analysis.

After filtering, an estimate of the final uncertainty (σ) was made using a modified form of the uncertainty equation of McNabb et al. (2012), as described by Quincey et al. (2015):

$$\sigma = 365\frac{(C_{pix} + C_{match})\Delta x}{\Delta t} \tag{4.2}$$

Where C_{pix} is the uncertainty in coregistration and C_{match} is the uncertainty of the matching algorithm (both assigned typical values of 0.5 pixels), Δx is the image resolution (15 m), and Δt is the time interval between the image pair in days.

Chapter 5

Results

5.1 Surge Identification and Description

Of a total of 88 glaciers >1 km^2 in the study area, 10 glaciers were identified as type 1 (i.e. a clear active phase was observed in Landsat imagery between 1972–2016). Locations and principal characteristics for these glaciers are presented in figure 5.1 and table 5.1. Additionally, readers are directed to the supplementary material located at `http://www.repository.cam.ac.uk/handle/1810/256047`, consisting of animations of stacked Landsat satellite imagery from 1972–2016 (scale and coordinate information are detailed in appendix B) for surge-type glaciers 01 – 08. Animated gifs have found recent use in visualising glacier surges in other parts of HMA (Paul, 2015). The presentation of multitemporal satellite imagery in an animated format is useful not only for intuitive assessment of surge dynamics as a moving image, but allows the complete suite of satellite imagery to be available to the reader through the examination of individual frames.

5.1.1 Surging Glaciers

Of the 10 surge-type glaciers, only 2 (glaciers 09 and 10) surged prior to 2000. These are identified by a rapid advance in terminus position between Landsat imagery in 1976 and 1989, although due to sparse image availability between these two years the surges themselves are missed. Following this, the glaciers underwent decay in the lower tongue

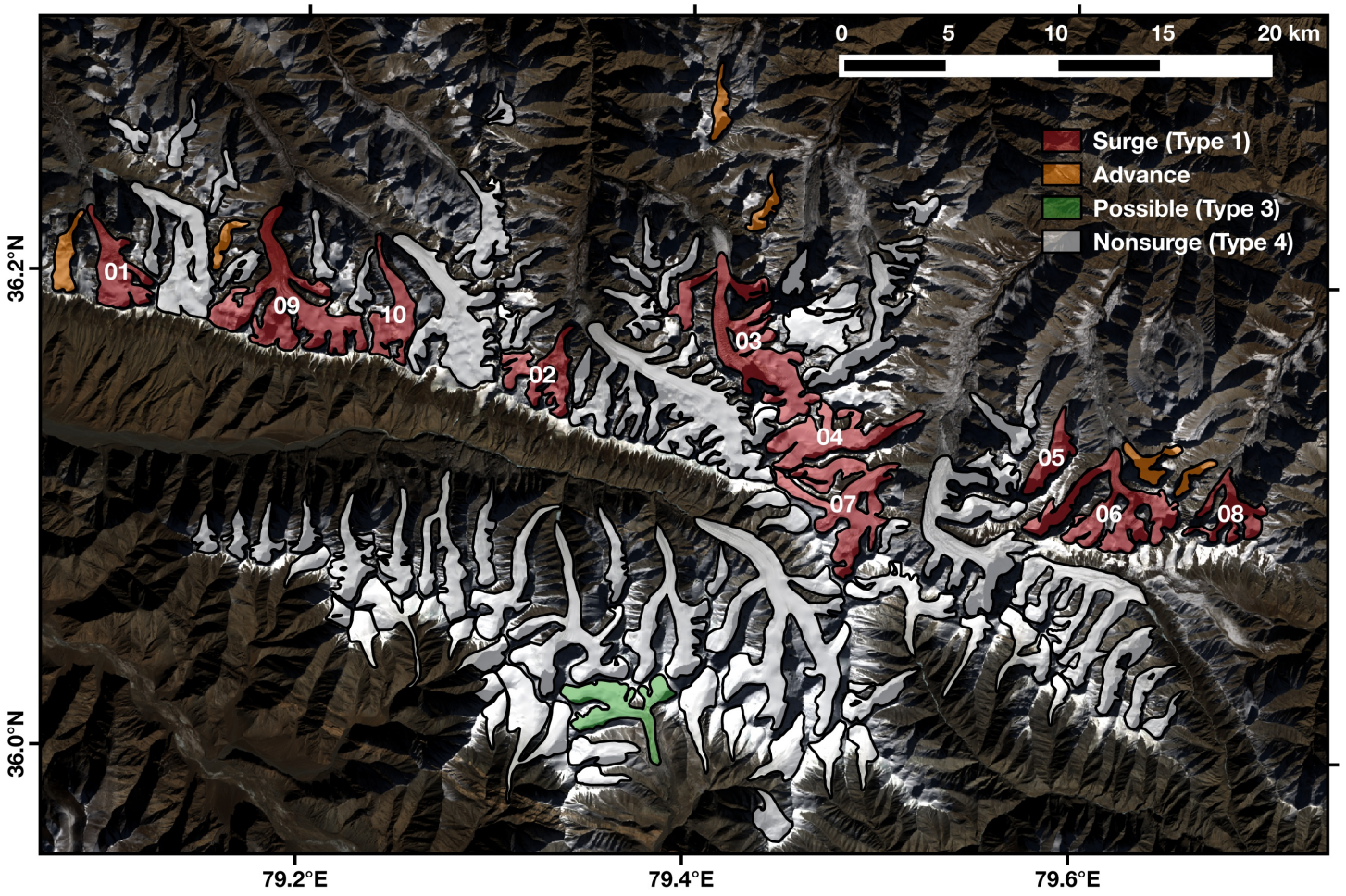

Fig. 5.1 Map showing glacier outlines >1 km^2 for the year 2000, with colours indicating (i) glaciers with surge events observed (red), (ii) glaciers displaying some advance but of uncertain surge status (orange), and (iii) possible surge glaciers displaying some evidence of prior surges but without a surge event observed. Surge-type glaciers are given IDs for reference. Map background is Landsat 7 ETM+ imagery, year 2000 DoY 282.

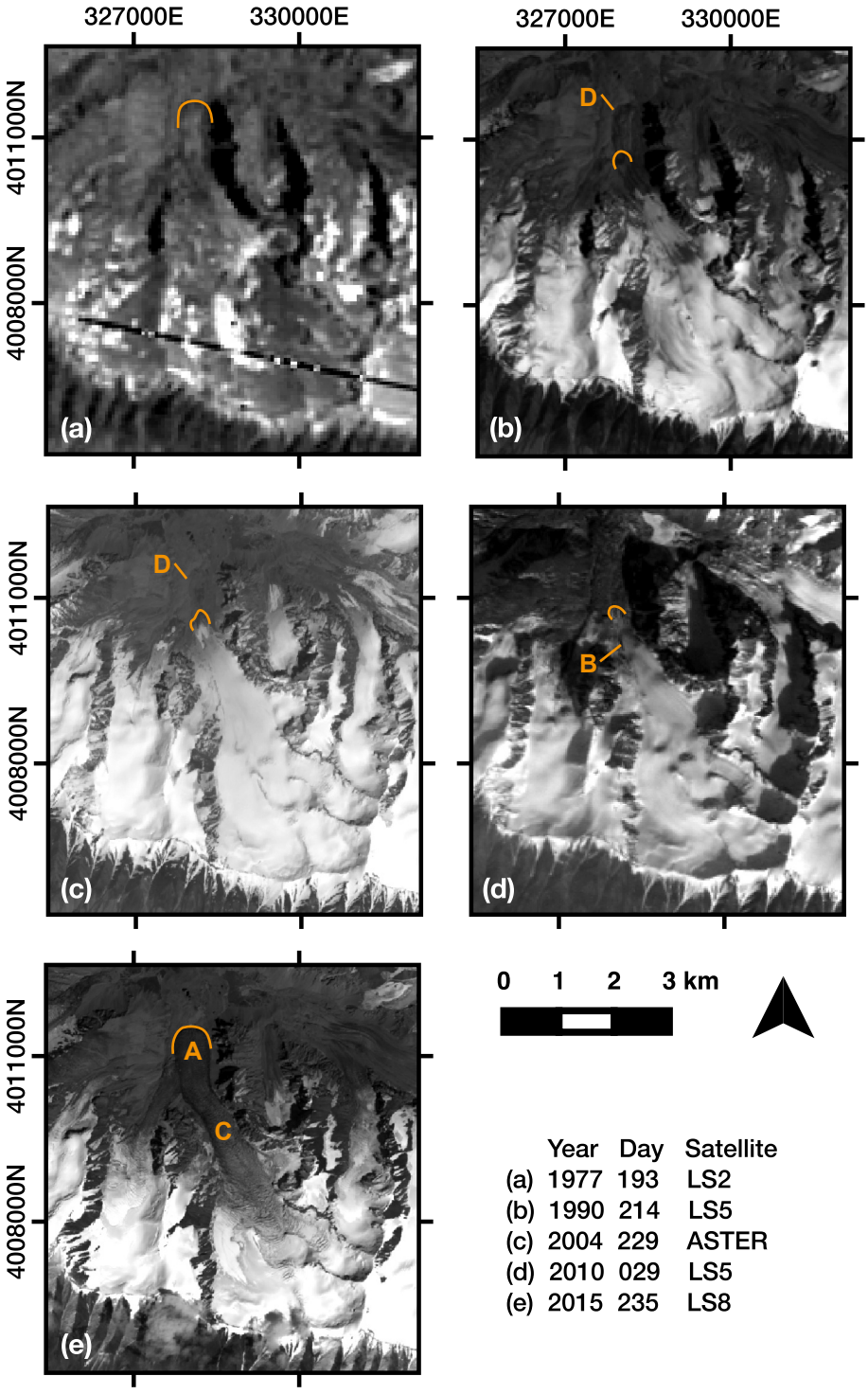

Fig. 5.2 Satellite imagery showing the evolution, and key indicators, of the surge of glacier 01. Glacier termini are highlighted. Also marked are cases of glacier advance (A), surge bulges (B), crevassing (C), and decaying ice (D). Projection and coordinates in UTM 44N. Please see animated gifs in supplementary material (appendix B) for further imagery at high temporal resolution.

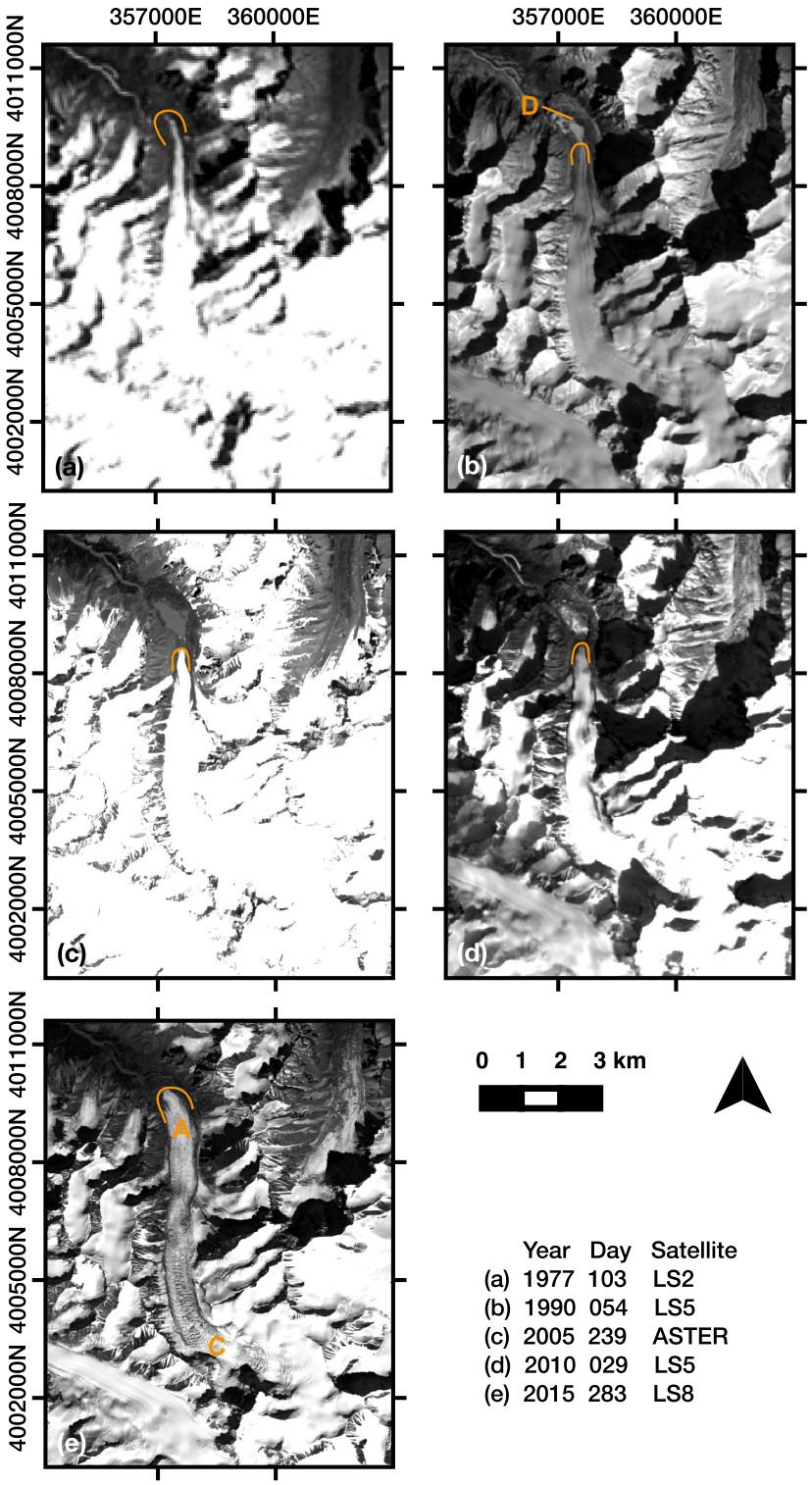

Fig. 5.3 Satellite imagery showing the evolution, and key indicators, of the surge of glacier 03. Glacier termini are highlighted. Also marked are cases of glacier advance (A), surge bulges (B), crevassing (C), and decaying ice (D). Projection and coordinates in UTM 44N. Please see animated gifs in supplementary material (appendix B) for further imagery at high temporal resolution.

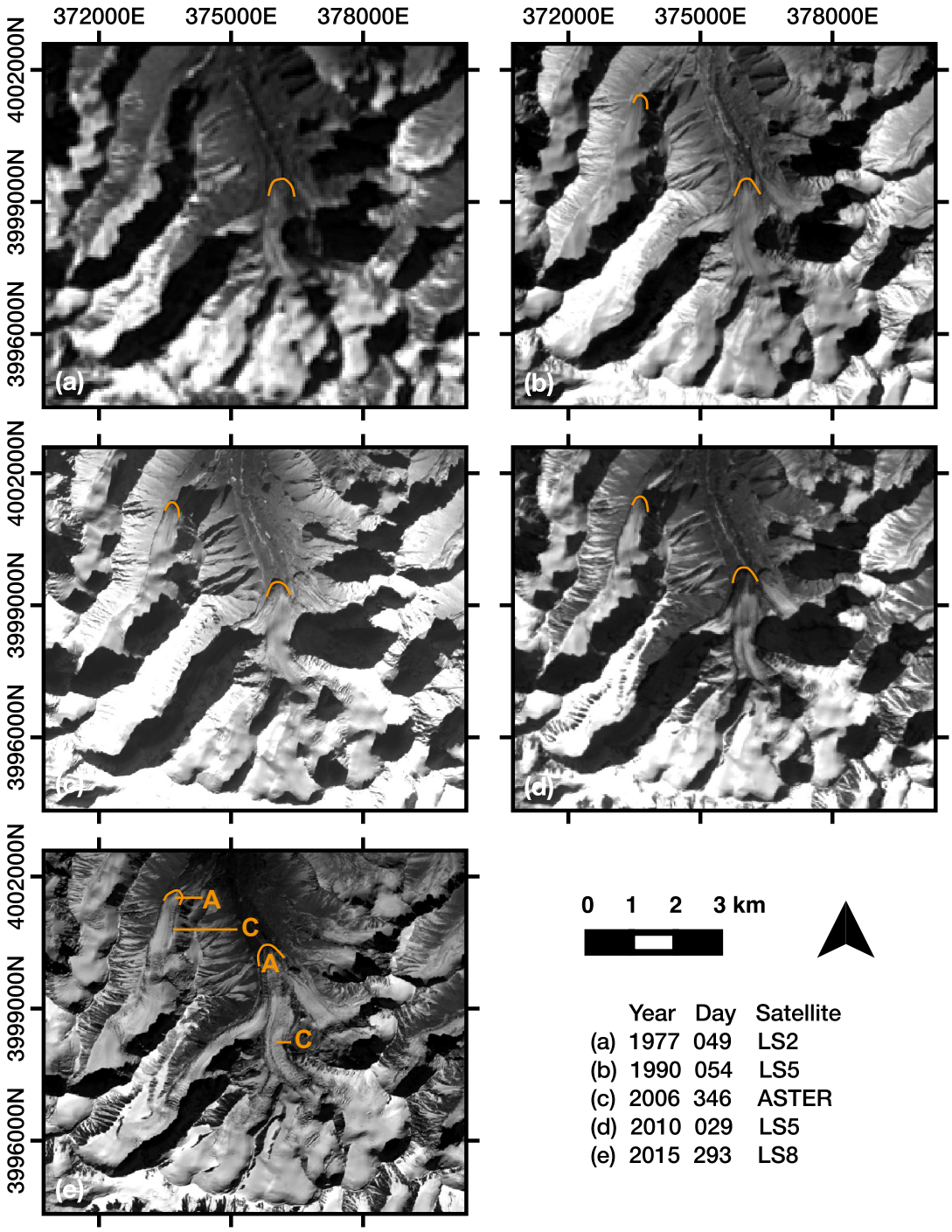

Fig. 5.4 Satellite imagery showing the evolution, and key indicators, of the surges of glaciers 05 and 06. Glacier termini are highlighted. Also marked are cases of glacier advance (A), surge bulges (B), crevassing (C), and decaying ice (D). Projection and coordinates in UTM 44N. Please see animated gifs in supplementary material (appendix B) for further imagery at high temporal resolution.

Table 5.1 Locations, and measured glacier characteristics, for the 8 confirmed surge-type glaciers.

ID	Lat. (°)	Long. (°)	Area (km^2)	Length (km)	Debris Cover (%)	Mean Slope (°)	Mean Elev. (m a.s.l.)	Elev. Range (m)
01	36.20	79.10	6.51	5.50	0.78	17.0	5290	1304
02	36.16	79.32	6.05	4.73	0.54	20.1	5475	1356
03	36.19	79.42	17.02	10.33	2.72	17.3	5442	1746
04	36.13	79.48	9.14	7.89	2.88	15.9	5651	1672
05	36.13	79.59	3.46	4.62	1.15	19.2	5112	946
06	36.11	79.63	13.00	5.91	2.28	18.4	5286	1438
07	36.11	79.48	12.45	7.03	0.93	16.4	5625	1287
08	36.12	79.68	4.80	4.73	9.52	23.3	5044	1282
09	36.22	79.18	17.02	9.24	17.52	18.4	5442	1746
10	36.19	79.25	5.703	6.49	1.33	18.0	5307	1029

visible in subsequent imagery. The remaining surges (glaciers 01–08) occurred from $\sim$2006 onwards, and comprehensive satellite coverage allows for a detailed qualitative assessment to be made.

Relatively uniform behaviour was observed between surges. Apart from glaciers 08 and 09, which were notably debris-covered (table 5.1), glaciers displayed a quiescent phase dominated by clean ice with minimal crevassing, except in the upper zones of larger glaciers (fig. 5.3b). A pre-surge phase lasted months-years, where the glacier snout underwent noticeable thickening and some advance of the order of hundreds of metres (cf. figs. 5.2c-d; 5.3c-d; 5.4c-d). Finally, the surge phase was associated with a rapid advance of the terminus of between 0.5–1.5 km, as well as glacier-wide crevassing (figs. 5.2e, 5.3e, 5.4e). In glaciers 02 and 03, this phase lasted 2 years before significant deceleration occurred. In other glaciers, the active phase has been occurring for 3–5 years – displaying only preliminary signs of deceleration as of January 2016.

When surging, the glaciers display extensive regions of transverse crevassing in the central and lower regions, with a notable reduction in albedo in the active phase. However, in contrast to the three-zone model of crevassing described by Lawson (1996) (section 2.1.2), glaciers in their active phase display widespread transverse crevassing from the upper regions of the glacier down to the snout. Crevasses only tend to be perpendicular at

the terminus, especially where the glacier displays arcuate snout morphology (e.g. glaciers 01, 03, 06). In smaller glaciers (04, 07), crevassing does not extend far past the lower regions of the glacier, but in larger glaciers (01, 02, 06, 08), crevassing can extend up into multiple (although in the case of glacier 01, not all) tributaries.

Qualitative examination does not reveal any obvious 'source zone' for surges. Perhaps a side-effect of the coarse temporal resolution of satellite imagery, crevassing apparently initiates across the glacier in a relatively uniform fashion. Only glacier 01 displays an obvious surge bulge (fig. 5.2d) that travels downstream – visible from $\sim$2006, it develops only $\sim$400 m behind the terminus position at the time, and slowly advances for several years before overriding the terminus position and rapidly advancing in 2012.

Glaciers 01 and 03 display indirect evidence of previous surges in the form of notably advanced terminus position in the 1972–1977 Landsat 2 imagery (figs. 5.2a, 5.3a). Over the next 20 years, the fronts decay (in the case of glacier 03, developing a substantial proglacial lake – see figs. 5.3b–d) until a new, relatively stable terminus position forms $\sim$2000, where they stay until the next active phases begins in the late 2000s. No obvious terminus advance can be observed between 1972–1977, hence the previous active phase was not directly observed. However, given the subsequent relatively rapid decay of the lower glacier, it is likely that the surges occurred in the years immediately preceding 1972. Given that glacier 01 and 03 surge in the late 2000s, this gives a lower bound on quiescent phase period to be $\sim$40 years. However, other glaciers do not show this behaviour in the early imagery, despite having clear proglacial zones of hummocky moraine and dead ice, indicative of relatively recent glacial activity. As a result, these glaciers must have had earlier active phases, and thus longer surge periods.

5.1.2 Other Glaciers

It is notable that no type 2 glaciers are identified, indicating a lack of distinctive looped moraines that are visible in Landsat imagery of other surging glaciers, even in the nearby Karakoram (Paul, 2015). Glacier 08 does display the distinctive contorted moraines prior to rapid advance, but the direct observation of the active phase elevates its status to a type

1 glacier. The lack of looped moraines could be a side effect of a lack of debris cover in general, but even glacier 09, which is the most debris-covered ($\sim$17.5%), does not display any obvious moraine features indicative of unstable flow. Instead, a lack of looped moraine features could be a consequence of the relatively small glacier sizes in the study area, resulting in a lack of tributary glacier surges onto trunk glaciers of a significant velocity. Whilst glacier 02 does surge onto a main trunk glacier (or at least, the dead ice of a prior trunk glacier), it is apparent that the stagnant velocities in this area will not result in a clean pattern of looped moraines in the immediate future.

Only one glacier displays any alternative evidence of surge activity, classifying it as a type 3 glacier (see fig. 5.1). This glacier exhibits a very clearly rapidly decaying tongue between 1977–2000, similar to that observed in glaciers 01, 03, 09, and 10, but has not as yet exhibited a new active phase.

Of the remaining glaciers, 74 are classified as non-surging (type 4). However, a further six smaller (<3 km^2) glaciers, here referred to as 'advancing', are not classified with certainty. They display some ambiguous evidence of surge behaviour – such as crevassing and the terminus advance – but these features are small, often with limited crevasse cover and advances <200 m. Given the relatively heterogeneous behaviour of even non-surge glaciers in the WKS, it could not be ascertained whether these are small surges or simply glaciers displaying terminus advance in response to positive mass balances.

5.2 Glacier Characteristics and Controls on Surging

5.2.1 Descriptive Results

As a preliminary exploration, simple descriptive statistics and data visualisation techniques were used to explore the data. Of the continuous variables collected, area, length, width, perimeter, slope, and debris did not display a normal distribution, showing distinctive skew and failing a Shapiro-Wilks test of normality ($p<0.05$). For these variables, the median was used as a measure of central tendency. Additionally, data were visualised using a log-normal distribution, after which they approximated a normal distribution for most datasets. Simple

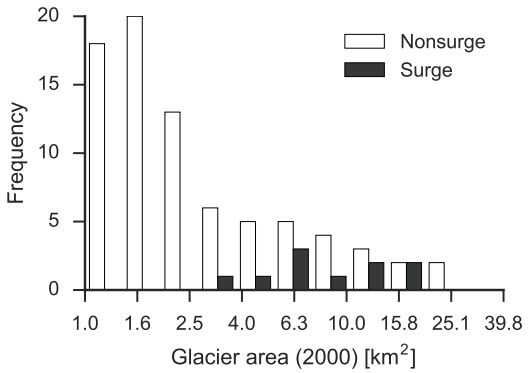

(a) Area (note that x-axis is log-scale)

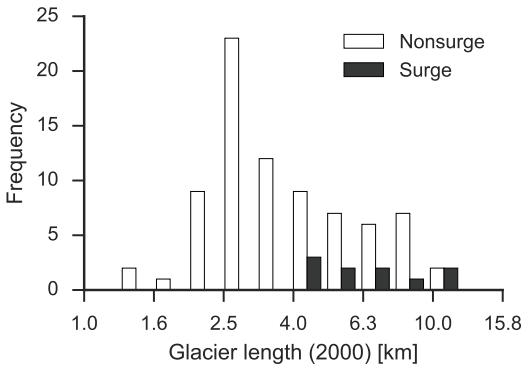

(b) Length (note that x-axis is log-scale)

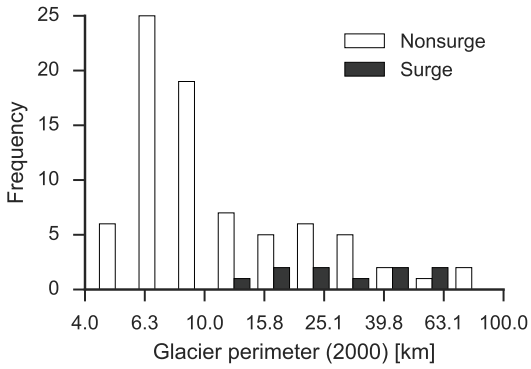

(c) Perimeter (note that x-axis is log-scale)

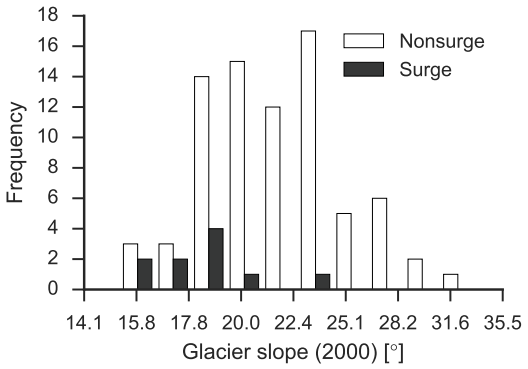

(d) Mean Slope (note that x-axis is log-scale)

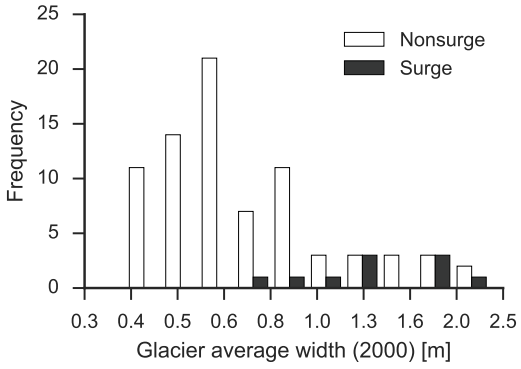

(e) Width (note that x-axis is log-scale)

Fig. 5.5 (a-e) Histograms comparing distributions of surging and nonsurging glacier across various measured characteristics. Note that non-normally distributed continuous variables are presented using a log-normal scale.

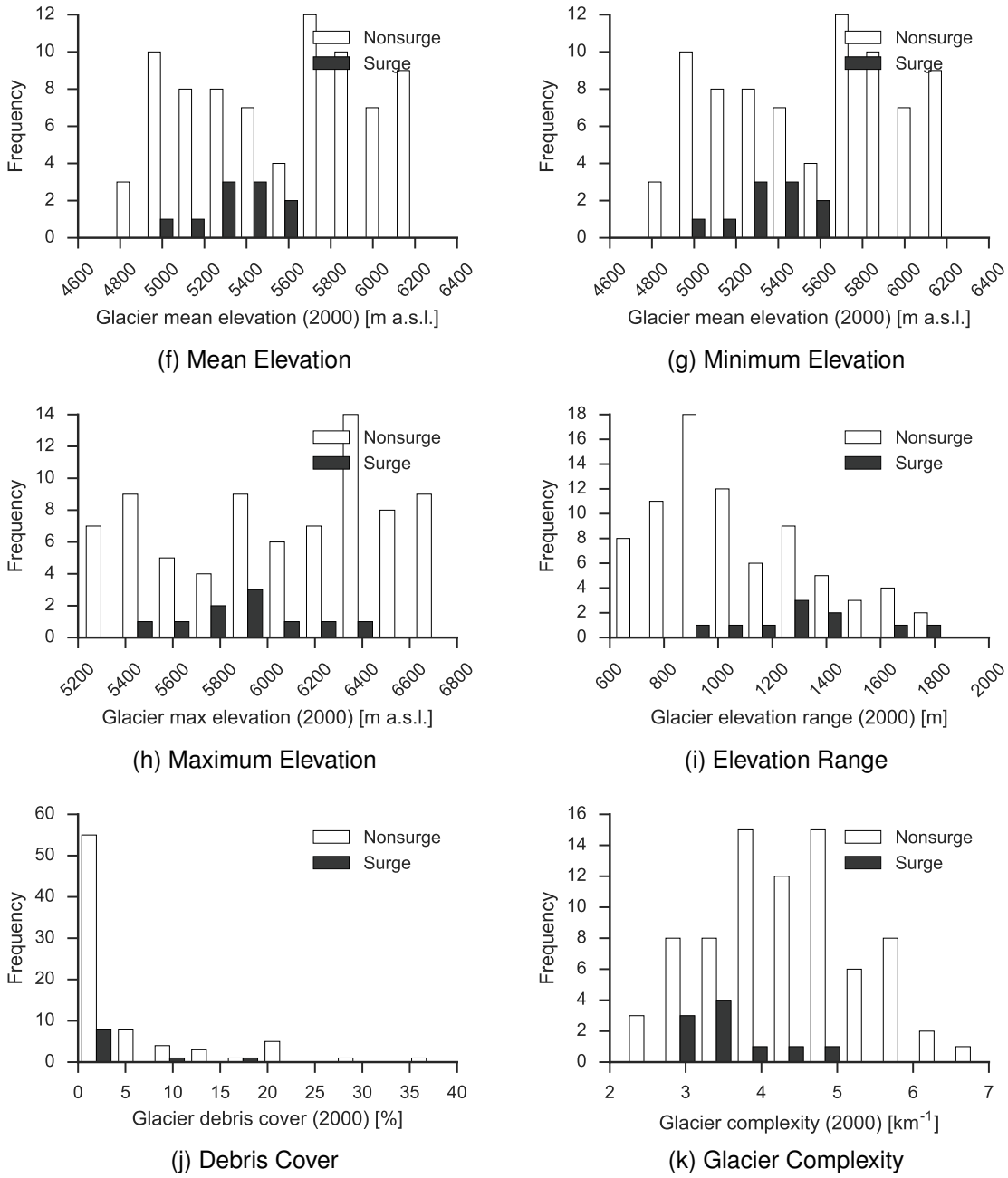

Fig. 5.5 (f-k) Histograms comparing distributions of surging and nonsurging glacier across various measured characteristics. Note that non-normally distributed continuous variables are presented using a log-normal scale.

Table 5.2 Descriptive statistics for surging and non-surging glacier characteristics. Characteristics marked with an askerisk display non-normal distributions, and as such averages presented are medians rather than means. The p-value represents the results of a two-tailed Mann-Whitney *U*-test testing for differences between surging and nonsurging populations: significant results (p<0.05) are displayed in bold.

Characteristics	Min	Max	Total Average	Nonsurge Average	Surge Average	p-value
Area* (km^2)	1.00	27.88	2.22	1.99	7.82	**5E-5**
Length* (km)	1.26	12.05	3.62	3.39	6.12	**5E-4**
Perimeter* (km)	4.32	91.17	9.29	8.79	27.43	**4E-5**
Mean Slope* (°)	15.28	33.43	20.85	21.56	18.21	**1E-3**
Av. Width* (km)	0.39	2.35	0.65	0.64	1.23	**4E-5**
Mean Elev. (m a.s.l.)	4769.5	6248.4	5534.6	5556.3	5365.2	0.16
Min. Elev. (m)	4352	5780	4938.3	4983.2	4588.1	**1E-3**
Max. Elev. (m)	5219	6769	6041.6	6057.8	5915.7	0.21
Elev. Range (m)	613	1834	1103.2	1074.6	1327.6	**9E-3**
Debris Cover* (%)	0.00	38.68	1.41	1.40	1.81	0.45
Complexity (km^{-1})	2.21	6.99	2.24	4.33	3.59	**0.02**

descriptive statistics are in table 5.2, as well as the results of a two-tailed Mann-Whitney *U*-test to assess differences in the medians of surging and non-surging populations (here, 'surging' refers only to type 1 glaciers). Additionally, histograms for a subsection of the variables are in figure 5.5.

Variables in some way related to size (i.e. area, length, width, perimeter) displayed distinct and colinear patterns. Observations were biased towards smaller glaciers, but surging glaciers tended to be larger than the norm. For instance, the median area was 2.2 km^2 for the total glacier population, 2.0 km^2 for non-surging glaciers and 7.8 km^2 for surging glaciers, suggesting a difference in the population of surging glaciers. A Mann-Whitney *U*-test confirms a significant difference between these two populations (p<0.05). This pattern continues through the rest of the glacier size variables (table 5.2; fig. 5.5a–c, e).

Another characteristic displaying significant difference between surging and nonsurging glaciers was mean slope (fig. 5.5d), where surging glaciers tended to be shallower than nonsurging glaciers (18.21° and 21.56° respectively). Interestingly, minimum elevation

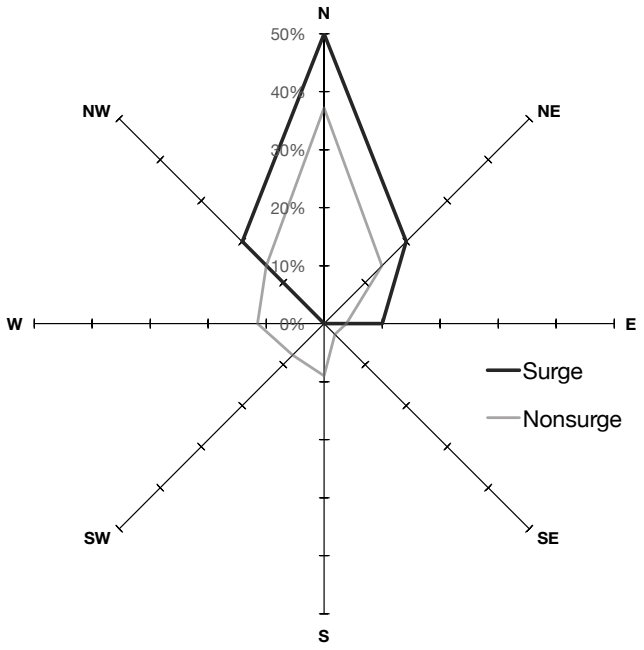

Fig. 5.6 Windrose showing glacier aspect for surging and non-surging glaciers, expressed as percentages of their respective populations.

and elevation range displayed significant differences between the two populations (surging glaciers were extended lower, and over a greater range, than non-surging glaciers – see fig. 5.5e-f), whilst maximum and mean elevation showed no difference. Surging glaciers tended to be less complex (i.e. have a lower perimeter:area ratio) than non-surging glaciers (3.59 and 4.33 respectively). Finally, percentage debris cover did not display a significant difference between the two populations.

Figure 5.6 displays the the aspect of glaciers, expressed as percentages of their respective populations. It is apparent that most glaciers in the range have a northerly aspect, but surge-type glaciers may be more likely to be oriented NW–NE, with only one glacier oriented in another direction (E). Non-surging glaciers share this distribution, but are also more likely to be oriented on a W–SE plane. However, differences are not distinct between these two populations.

Table 5.3 Univeriate logit regression models with each variable fitted seperately. Significance coding: '***' = p<0.001; '**' = p<0.01; '*' = p<0.05; '^' = p<0.1. Variables significant to p<0.05 are presented in bold.

Variable	Subgroup	Estimate	Standard Error	p-value	Deviance	△ Deviance
–	"Null Model"				62.31	
Area	intercept	-4.274	0.912	3E-06***		
	log area	3.352	1.008	0.0008***	48.05	14.26
Length	intercept	-5.881	1.498	9E-05***		
	log length	5.519	1.882	0.003**	51.60	10.71
Perimeter	intercept	-7.270	1.738	3E-05***		
	log perimeter	4.183	1.230	0.0007***	47.17	15.14
Mean Slope	intercept	23.280	8.797	0.008**		
	log slope	-19.563	6.908	0.004**	51.51	10.80
Average Width	intercept	-1.863	0.397	3E-06***		
	log av. width	6.752	1.949	0.0005**	46.84	15.47
Aspect	intercept	-3.296	1.018	0.001**		
	NW-N-NE	1.561	1.081	0.149	59.35	2.96
Debris Cover	intercept	-1.989	0.395	5E-07***		
	debris cover	-0.015	0.051	0.770	62.22	0.09
Mean Elevation	intercept	4.744	4.841	0.327		
	mean elevation	-0.001	0.001	0.165	60.25	2.06
Max. Elevation	intercept	2.339	4.563	0.608		
	max elev	-0.0007	0.0007	0.339	61.39	0.92
Min. Elevation	intercept	17.465	7.403	0.018*		
	min elev	-0.004	0.002	0.010*	50.86	11.45
Elevation Range	intercept	-5.417	1.536	0.0004***		
	elevation range	0.003	0.001	0.016*	56.05	6.26
Complexity	intercept	1.580	1.620	0.328		
	complexity	-0.925	0.431	0.032*	56.71	5.60

5.2.2 Univariate Logit Regression

The results of the univariate logit regression analysis are presented in table 5.3. For non-normal data, log-transformed data were used to better approximate results, as in comparable studies (e.g. Barrand and Murray, 2006; Jiskoot et al., 1998). Exact p-values are presented (as a rule of thumb, regressions are significant ($p<0.05$) where the parameter estimate is double that of the standard error).

Of the twelve explanatory variables tested, eight provided significant results: log area, log length, log perimeter, log mean slope, log average width, minimum elevation, elevation range, and complexity. These variables are the same as those assessed by the Mann-Whitney *U*-test to display significant differences between surging and nonsurging glaciers (table 5.2). Area, length, perimeter, width, and elevation display positive relationships with surge incidence, whereas possibility of surging decreases with increased gradients, higher minimum elevations, and increased complexity. Of the significant relationships, the strongest is that of log average width, which results in a reduction in model deviance from the null model of 15.47, with a positive parameter estimate (6.75) indicating that the log-odds of a glacier being of surge type increases with glacier average width. Following this, from the strongest relationship (i.e. largest reduction in deviance from the null model) to the weakest, is glacier perimeter, area, minimum elevation, mean slope, length, elevation range, and complexity.

In line with Mann-Whitney *U*-test results, univariate logit models based on debris cover, mean elevation, maximum elevation, and aspect (aggregated into two classes, NW-N-NE and E-SE-S-SW-W, based on descriptive results) showed no statistically significant reduction in model deviance.

5.2.3 Multivariate Logit Regression

The second stage of logit analysis was to perform a multivariate analysis. This is because the effects of colinearity may result in certain relationships being misinterpreted, and the contribution of certain glacier characteristics to be overstated, in univariate models. For

Table 5.4 Multivariate logit regression models. The null model and univariate average width model are also retained for comparison. Significance coding: '***' = p<0.001; '**' = p<0.01; '*' = p<0.05; '^' = p<0.1.

Variable	Subgroup	Estimate	Standard Error	p-value	Deviance	Δ Deviance	Degrees of Freedom
–	"Null Model"				62.31		87
Av. Width	intercept	-1.863	0.397	3E-06***	46.84	15.47	86
	log av. width	6.752	1.949	0.0005**			
Av. Width	intercept	-4.147	3.925	0.291	46.47	15.84	85
+ Perimeter	log av. width	4.057	4.849	0.403			
	log perimeter	1.779	3.013	0.555			
Av. Width	intercept	-2.07	2.039	0.308	46.83	15.48	85
+ Area	log av. width	6.188	5.565	0.266			
	log area	0.303	2.808	0.914			
Av. Width	intercept	16.236	8.363	0.052^	39.17	23.14	85
+ Min. Elev.	log av. width	5.926	2.005	0.003**			
	min elevation	-0.004	0.002	0.035*			
Av. Width	intercept	8.038	10.380	0.439	45.87	16.44	85
+ Slope	log av. width	5.177	2.394	0.031*			
	log slope	-7.656	8.069	0.343			
Av. Width	intercept	-2.077	2.039	0.308	46.83	15.48	85
+ Length	log av. width	6.490	3.095	0.036*			
	log length	0.303	2.808	0.914			
Av. Width	intercept	-4.212	1.777	0.018*	44.79	17.52	85
+ Elev. Range	log av. width	6.167	2.046	0.002**			
	elev. range	0.002	0.001	0.159			
Av. Width	intercept	-3.333	2.337	0.154	46.43	15.88	85
+ Complexity	log av. width	7.896	2.698	0.003**			
	complexity	0.386	0.596	0.517			

instance, it is intuitive that glaciers with a larger area are likely to be longer and wider, as well as extending to a lower elevation. The multivariate model built on the univariate model displaying the greatest reduction in deviance (average width), adding each of the subsequent significant explanatory variables in their significance order (log perimeter, log area, minimum elevation, log slope, log length, elevation range, and complexity).

The results of these multivariate analyses are presented in table 5.4. These results show that no additional size-related variable adds significantly ($p<0.05$) to the reduction in model deviance, showing that characteristics relating to glacier size are indeed highly interdependent. This is also true of elevation range and glacier complexity. However, a multivariate model consisting of both the log average width of glaciers and minimum glacier elevation does result in an optimal, and statistically significant, explanatory model that improves upon the univariate average width model alone.

5.3 Glacier Dynamics

5.3.1 Quantified Terminus Change Positions

Changing terminus positions in the eight recent glacier surges, relative to a 2000 baseline, are presented in figure 5.7, both as (a) raw data points and (b) a curve smoothed by locally weighted scatterplot smoothing (LOWESS). From these data, three significant observations are apparent.

The first is that glaciers in the study area appear to display distinctive pre- and post-surge acceleration and deceleration phases to the terminus advance, resulting in a smooth, sigmoidal pattern on the time-series figures. The pre-surge phases, where termini accelerate from a stable front to their maximum advance rate, last between 2–4 years, and the post-surge deceleration phases, although not captured in their entirety, appear to be similar. This is very different to the rapid acceleration and termination that can be observed when tracking the terminus positions of hydrologically surging glaciers (e.g. Zhongfeng Glacier, Yasuda and Furuya, 2015). Assuming that terminus advances can be used as a proxy for glacier dynamics and velocity, these months-long pre- and post-surge acceleration/deceleration

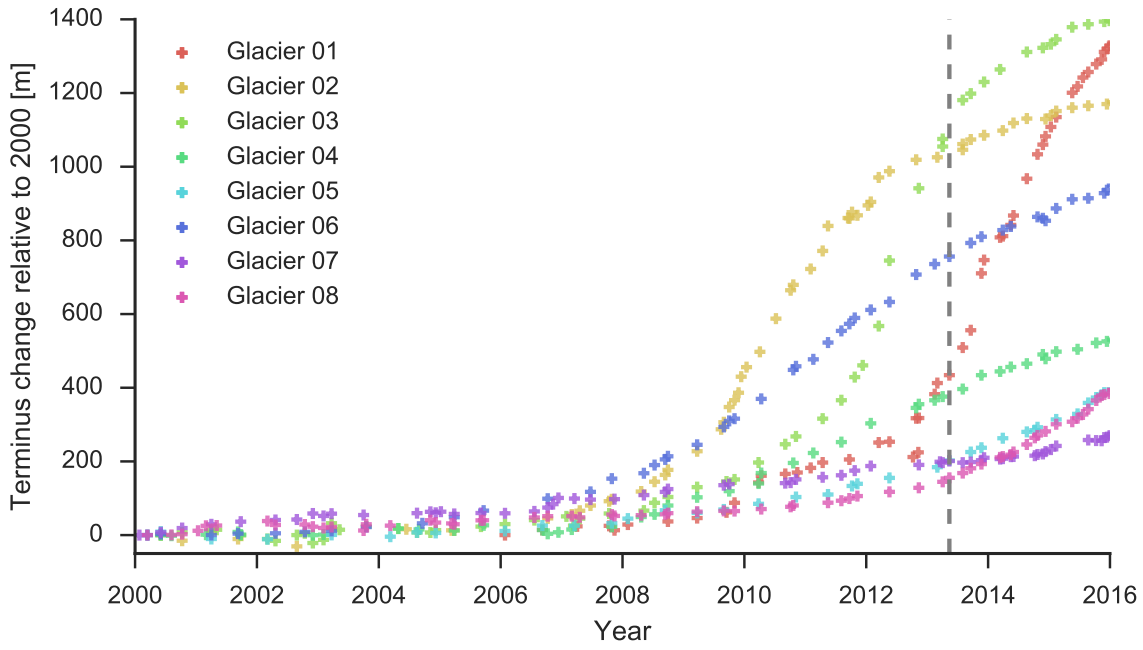

(a) Scattergraph of measurements.

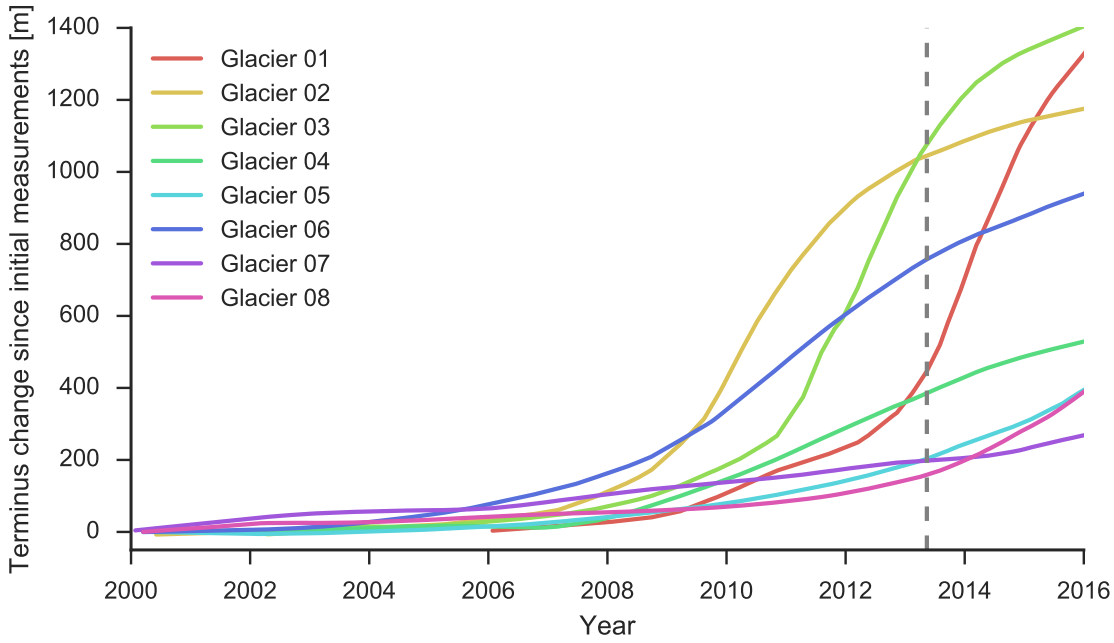

(b) LOWESS-smoothed line.

Fig. 5.7 Graphs showing terminus changes relative to 2000 baseline for surging glaciers (glacier 01 data shows advance of surge bulge rather than terminus). Vertical line marks the commencement of Landsat 8 OLI imagery suitable for feature tracking (2013-05-13).

phases are more analogous to the pre- and post-surge velocity phases described for thermal surges (Murray et al., 2000).

The second is that – assuming the acceleration and deceleration in terminus advance rate are indeed analogous to the pre- and post-surge phases of a traditional temperate surge – the length of the subsequent 'active phase' can be identified. Glaciers where a clear post-surge phase can be delineated (i.e. a deceleration in surge advance has begun) include glaciers 01, 02, 03, 04, and 06. Active surge phases for these glaciers range between $\sim$2 years (glacier 02) to $\sim$5 years (glacier 04), and are associated with a terminus advance between $\sim$500–1500 m. Glaciers 05, 07, and 08 are all apparently still in an active phase – having entered this phase between 2010–2013, this makes their surge period $\sim$3–6 years so far. As well as having longer active phases, these are also the glaciers that are advancing at the slowest rates, although the sample size is too small to be able to assess a statistical or causal relationship between these two observations.

The third observation is that glaciers display remarkable similarities with regards to the timing of surge initiation, and largely enter their pre-surge advance phase between 2006–2008 – although glacier 08 begins slightly later, in $\sim$2010. The initiation of the subsequent rapid advance (active) phase differs by a few years – the earliest being glacier 02, which begins to rapidly advance in 2009 and begins to decelerate in 2011. This degree of coincidence between surge activity is remarkable, considering no glacier surges were observed in the study area between 1972–2016, and satellite imagery from 1972–1977 suggests that only two of the glaciers (01 and 03) were previously in phase.

5.3.2 Surge Velocities

Three glaciers were selected for detailed velocity profiling: glaciers 01, 03, and 06. Glaciers 03 and 06 were chosen due to their larger sizes increasing the likelihood of successful feature tracking across the glacier surface. Glacier 01, whilst not as large, was chosen as the bulk of the rapid terminus advance took place after the advent of Landsat 8 OLI availability (fig. 5.7). Detailed velocity change data is presented in the form of velocity profiles (figs. 5.9; 5.10; 5.12), where the profiles are sampled along manually derived glacier centrelines

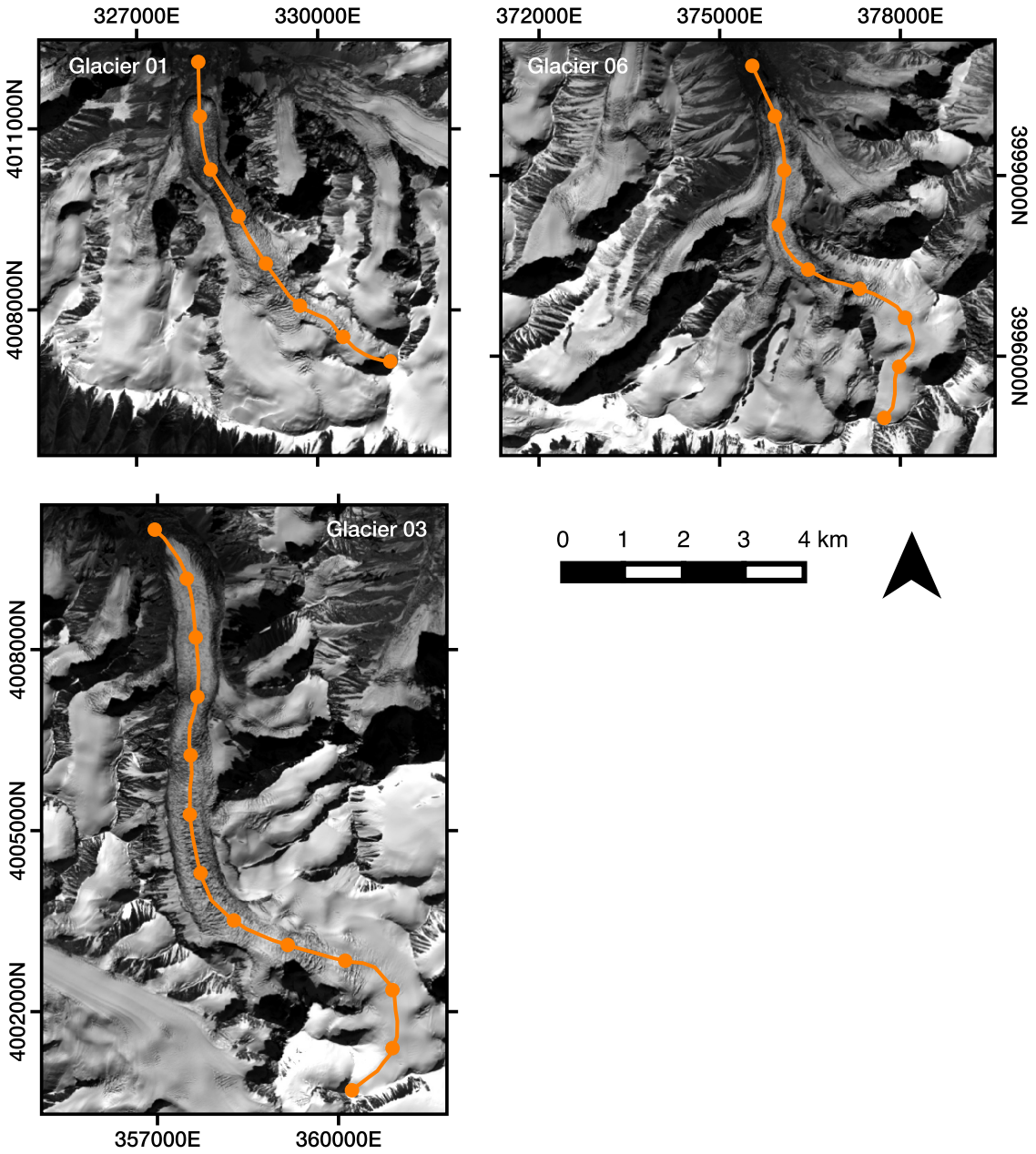

Fig. 5.8 Glacier centrelines used to extract velocity profiles for glaciers 01, 03, and 06, with markers every 1 km from the backwall. Background: Landsat 8 OLI image taken 2015-10-10.

presented in fig. 5.8. Elevation profiles, as sampled from the ASTER GDEM v.2.0, are also overlain for reference. In all cases, the upper 1–2 km of the glacier are not shown, as feature tracking tended to be particularly poor in this area (generally due to lack of crevassing). Velocity fields from the 2000–2002 quiescent phase can be compared with an alternative dataset for the 1999–2003 period, produced by Dehecq et al. (2015). Velocities from the two datasets are within error of each other and also display similar spatial distributions of slow and fast flow, suggesting that some confidence can be had in the results discussed here.

Glacier 01

From measurements taken during the quiescent phase (2000–2001), glacier 01 displayed slow velocities (<50 m a^{-1}) across the surface. By the time OLI imagery becomes available, glacier 01 has entered the active phase of the surge and is advancing rapidly ($\sim$500 m a^{-1} in 2013). This is broadly coincident with velocities displayed for this period, which exceed 500 m a^{-1} in the fastest region located 4–5 km from the headwall. This region is coincident with a rapid narrowing in the glacier, the steepest section of the elevation profile, and also the source of the surge bulge visible prior to the surge. The fastest velocities are displayed in summer 2014, in excess of 700 m a^{-1} for a limited number of measurements in the high-velocity zone. After this – and coincident with the start of a decelerating terminus advance rate (fig. 5.7) – velocities begin a slow but consistent reduction in velocity, decreasing to highs of only 300 m a^{-1} in winter 2015/2016 (although still not in line with 2000/2001 measurements). This deceleration is broadly linear: there is no apparent relationship between velocity and season visible in the data.

Glacier 03

In the quiescent phase, glacier 03 displayed similar velocities to glacier 01 (<50 m a^{-1}). Peak velocities, exceeding 1000 m a^{-1} in the high-velocity zone, are displayed immediately after measurements resume in 2013. Once again, this region coincides with a notable narrowing in the width of the glacier. The high velocity measurements are not continuous, but both

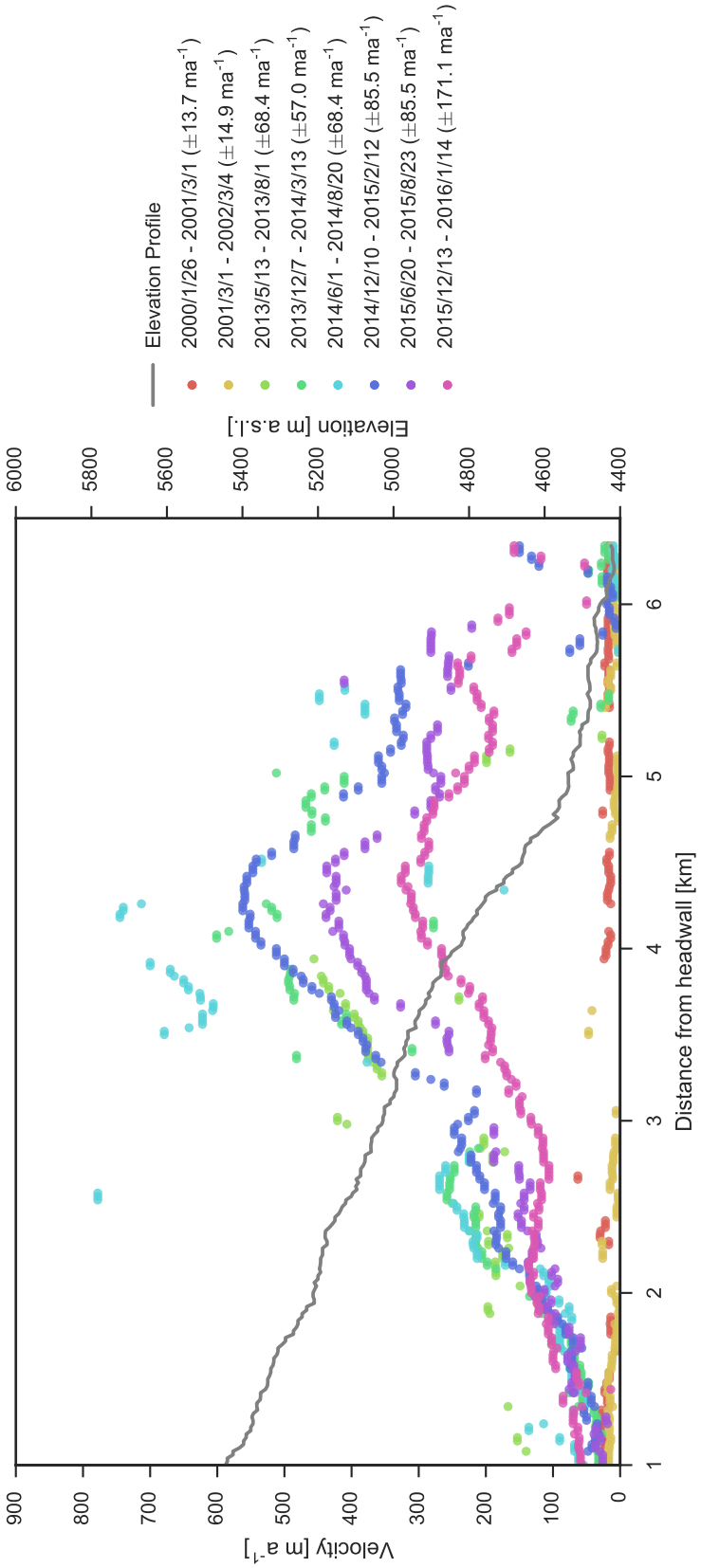

Fig. 5.9 Selected velocity profiles, and ASTER GDEM v.2.0 elevation profile, for glacier 01.

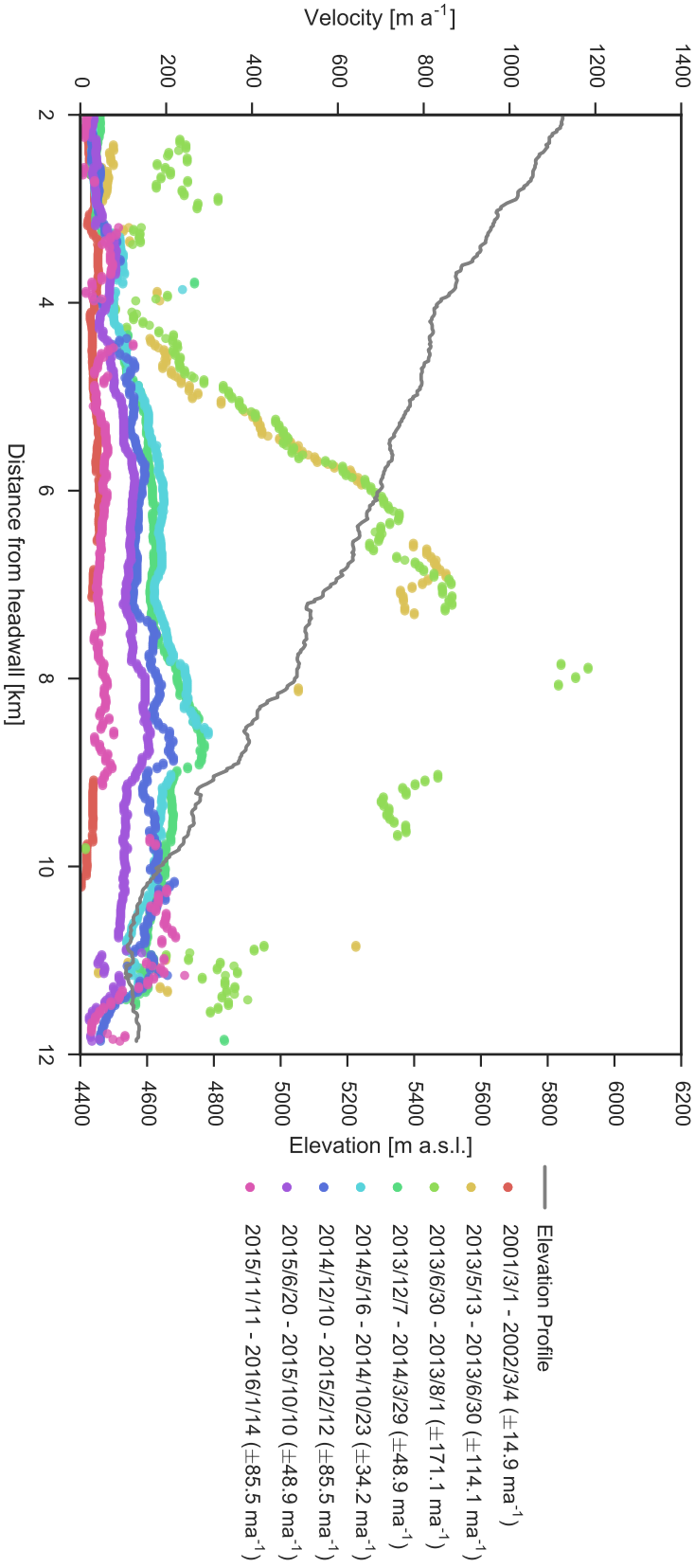

Fig. 5.10 Selected velocity profiles, and ASTER GDEM v.2.0 elevation profile, for glacier 03.

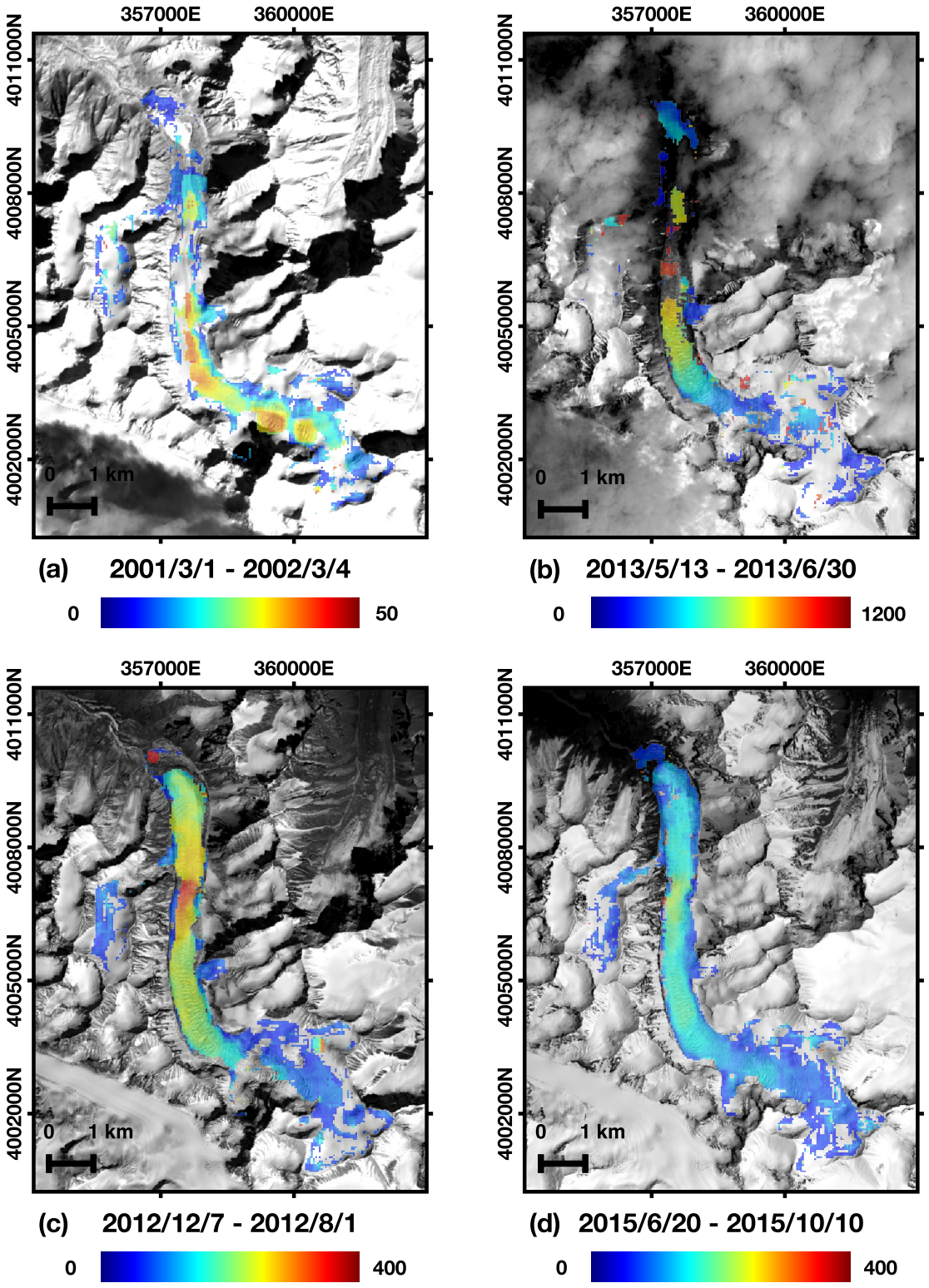

Fig. 5.11 Selected velocity fields for glacier 03, in m a^{-1}. Note the differing scales between subfigures.

of the measurements made in summer 2013 (May–June and June–August) overlap very well despite high uncertainties in excess of $\pm$100 m a^{-1} (due to low Δt between images), suggesting that these measurements are robust. However, unlike glacier 01, velocities do not display a gradual deceleration over the following years: instead, velocities decreased abruptly by winter 2013/2014 to highs of only 300 m a^{-1}. This termination is coincident with the beginning of the deceleration in terminus advance rate (fig. 5.7). After this, glacier velocities continued to decrease at a slower rate. Even after the rapid termination following summer 2013, the largest decreases in glacier velocity still apparently occur in transitions from summer to winter (i.e. summer 2014 to winter 2014/2015 and summer 2015 to winter 2015/2016). By winter 2015/2016, velocities have reached pre-surge levels.

Glacier 06

Once again, glacier 06 displays quiescent phase velocities of mostly <50 m a^{-1}, although some velocities as high as 70 m a^{-1} are apparent $\sim$4–4.5 km from the headwall. By 2013, the rapid advance phase of the glacier has terminated (fig. 5.7), and similarly the velocity dataset does not contain any profiles with velocities >300 m a^{-1}, as was clearly visible in the previous datasets. There are two high-velocity regions in the dataset, 4–4.5 km and 5.5–6 km from the headwall. The first is coincident with a notable steep region of the elevation profile, and the latter apparently coincident with a significant tributary joining from the west. As of winter 2015/2016, glacier velocities have not yet reached pre-surge levels: deceleration is seemingly occurring slowly. A feature not visible in previous datasets is a very clear difference between summer and winter velocity profiles. Only those in the summer show velocities in excess of 150 m a^{-1}, and winter profiles tend to display velocities 50–100 m a^{-1} lower in the high-velocity regions.

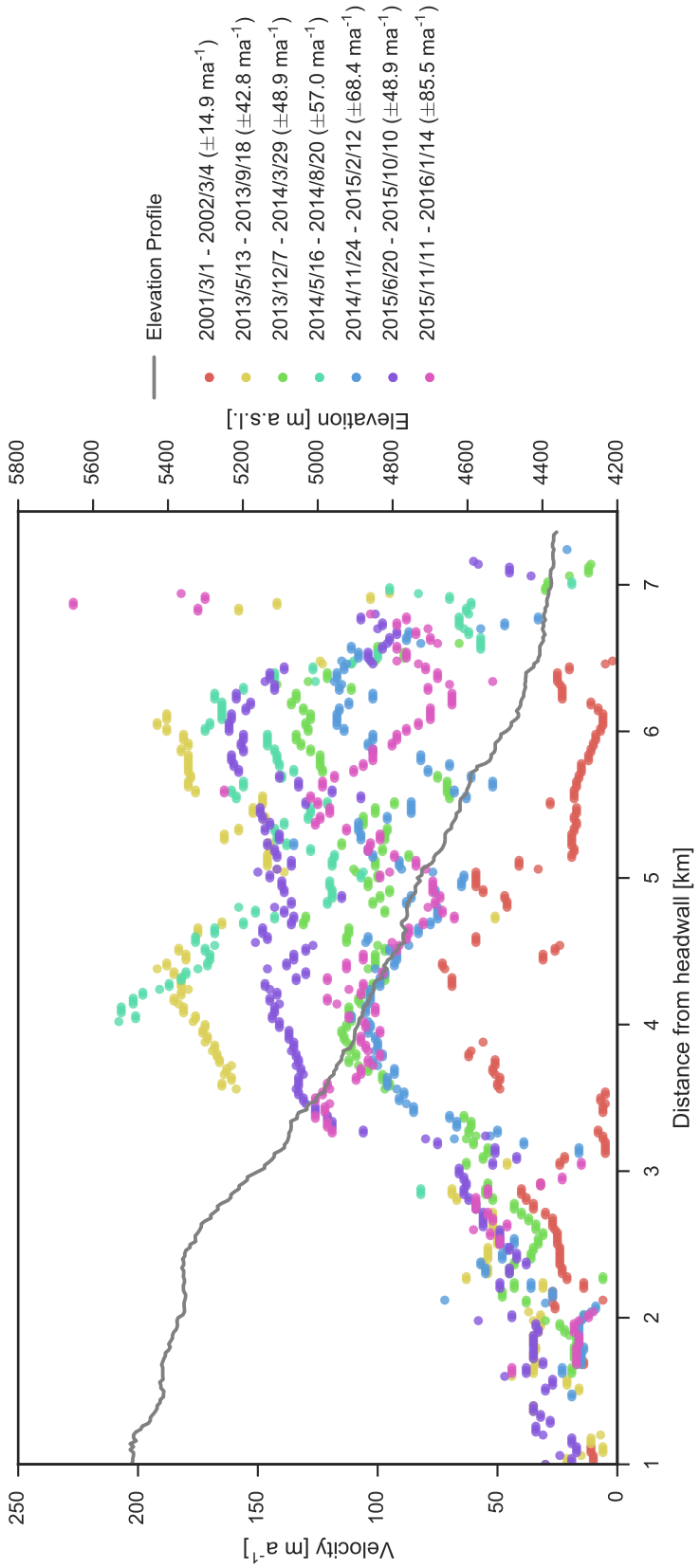

Fig. 5.12 Selected velocity profiles, and ASTER GDEM v.2.0 elevation profile, for glacier 06.

Chapter 6

Discussion

6.1 Glacier Surging in the West Kunlun Shan

A total of ten glaciers (11.3% of the total) exhibited clear active phases between 1972–2016. This agrees with the 12.6% reported for the Karakoram (Barrand and Murray, 2006). These surges occur even on smaller valley glaciers, which may be an order of magnitude smaller than the large glaciers of the Liushi region (Yasuda and Furuya, 2015). The presence of surging has implications for studies of glacier area (Shangguan et al., 2009) and elevation (Wu et al., 2014) changes in the Hotan River catchment. It implies that – as in regions to the west and east – reports of stability and even growth in glaciers may be biased by surging, even in sectors where glaciers are smaller than typical surge-type glaciers in the Karakoram and WKS.

It is possible that the total number of surges present in the study area is underestimated. First, limited geomorphic evidence for prior surges existed, leading to no type 2 and only one type 3 glacier being identified. This could be due to either sparse debris cover or lack of large tributary-trunk glacier systems (or both) to contribute to clear evidence such as looped moraines. As a result, it is difficult to ascertain evidence for surging glaciers where the active phase is not readily observed. Second, there are the six smaller glaciers that have been classified as ‘advancing’, which display ambiguous evidence: small rates of advance alongside surface crevassing across a partial section of the surface. It could be that a

proportion of these are true surges that should have been included in the analysis. However, in the interests of eliminating false positives from the analysis, a conservative assessment is justified.

6.2 Controls on Surging

6.2.1 Predicted Controls

The results of the statistical analysis show that in particular, larger glaciers are more likely to surge, with area, length, perimeter, and average width all displaying positive relationships with surge incidence. Other significant relationships exist between surge incidence and glacier slope, minimum elevation, elevation range, and complexity. Multivariate analysis was performed with the aim of excluding covariate predictors, and results identify two independent controlling variables: average glacier width (positive relationship) and minimum elevation (negative relationship).

The strong positive relationship between surging and a proxy for glacier size is broadly in line with global assessments (Sevestre and Benn, 2015) as well as studies from other regions (Clarke, 1991; Jiskoot et al., 1998). However, most studies conclude length is the dominant variable, whilst this study finds that length explains less of the total deviance than all other size-related variables, and instead finds average width to explain the most deviance from the null model. However, it should be noted that the average width variable is not a true measure but an estimate calculated from the area:length ratio. As the length variable only records the length of the main trunk, the average width is distorted by the presence of tributaries, which will increase the glacier area without increasing the measured length. As a result, average glacier width will be artificially inflated on complex glaciers, and will be highly covariate with area and length variables. Caution should be exerted before attempting to use this result to infer any direct causal relationships between average width and surge incidence. More research, with more sophisticated methods of calculating width, is necessary to explore this relationship.

The negative relationship with minimum glacier altitude is not commonly reported in the literature. Results of the univariate analysis show that significant relationships with elevation-related variables exist only for minimum elevation and elevation range (which is likely covariate with minimum elevation), and not for mean or maximum elevation. This suggests that the elevation control is not related to glaciers being at higher or lower altitudes as a whole. Instead, it specifically relates to glaciers extending into lower elevations – regardless of source altitude. This might suggest that the surge incidence is related specifically to action occurring in the ablation zone rather than the accumulation zone. Two possible causal links are suggested here: (i) an increased likelihood that glaciers will have warm beds at lower elevations; or (ii) an increased supply of surface meltwater to the base at lower elevations. However, this may also result from the covariation of glacier minimum elevation with some other variable, which is examined in section 6.2.3.

6.2.2 Comparison with Other Studies

Barrand and Murray (2006) performed logit analyses of surging glaciers for the Karakoram. In univariate analyses, they found glacier length, area, perimeter, average width, and debris cover to be significantly related to glacier surging (mean elevation and elevation range were not tested), from which the optimal predictor was glacier perimeter. Multivariate models did not significantly improve prediction. They interpreted this as glacier perimeter providing a significant proxy for avalanche activity, given the significance of avalanche and debris-fall material in Karakoram mass balances (Hewitt, 2007). Glacier perimeter does not exhibit similar dominance in this study (although it does form the second-most significant univariate variable). Furthermore, they found debris cover to be positively correlated with surging, whilst this study found no relationship, suggesting that surging here is relatively decoupled from debris cover (and thus avalanching) compared to the Karakoram. This conforms with the fact that the WKS is known to have relatively debris-free ice (Scherler et al., 2011b). However, Quincey et al. (2011) have identified surging on relatively clean-ice Karakoram glaciers, observing that these glaciers are sourced from, and terminate at, high elevations (>5000 m a.s.l.) in probable cold-ice regions. They suggest that these cold-ice glaciers could

be undergoing thermal changes at the base in response to climate change in the region. Surges in this study do not display the same restriction to the highest altitudes – possibly due to cold-based glaciers being able to exist at lower altitudes in the WKS. Despite this, the hypothesis could explain the relationship found here between surging and minimum elevation: lower elevations will be warmer, and thus could be influencing a shift in thermal regime at the base faster than other regions.

Barrand and Murray (2006) found a positive relationship with glacier complexity whilst this study found a negative relationship. Studies from other regions have also found complexity to be positively correlated with surge incidence (Clarke et al., 1986; Hamilton and Dowdeswell, 1996; Sevestre and Benn, 2015), making this result unusual. As with average area, the method used here applies a crude perimeter:length relationship to quantify glacier complexity, so results should be interpreted with caution. As with glacier minimum elevation, this could be a causal factor itself, or covary with some other unexamined factor.

Finally, Barrand and Murray (2006) found no relationship with mean glacier slope, whilst this study found a significant negative relationship. However, similar relationships have been identified since early work by Clarke et al. (1986) and Clarke (1991), who conclude that the relationship occurs due to the negative covariance between slope and the dominant variable, length. Coveriance is also likely to explain the relationship here, as slope was not found to be significant in the multivariate analysis.

6.2.3 Spatial Distribution

It is notable, given that the study area assesses two parallel ranges, that type 1 glaciers occur exclusively in the northernmost range (fig 5.1), suggesting that some controlling factor is significantly different between these two ranges. The short distances involved means any differences are unlikely to be climatic in origin. However, the northern and southern slopes of the WKS are known to display different topographies that can have effects on glacier hypsometry, with southern aspects displaying flatter, wider geometries and northern valleys displaying steep and high-relief geometries (Zhang et al., 1989). Indeed, a significant difference in minimum glacier elevations occurs between the two ranges: trunk glaciers in the

southern range commonly terminate at elevations >5000 m a.s.l., whilst in the northern range they are more likely to terminate between ∼4400–4600 m a.s.l.. Additionally, qualitatively examining glacier outlines reveals distinct differences in glacier morphology between the northern and southern ranges, with the southern range tending to consist of distinctive long, narrow tributaries that would result in a higher perimeter:area ratio (i.e. high complexity) for the non-surging population. Thus, the distribution bias to the northern range could be explained by differences in topographic controls (minimum glacier elevation and complexity) between the ranges.

However, an alternative explanation could be that an unexamined control displays distinct differences between the two ranges, and thus minimum glacier elevation and complexity merely covary with this third attribute. One candidate could be the geology of the ranges. The Karakax Fault Zone divides the two ranges (Lin et al., 2008; Styron et al., 2010). A geological analysis is beyond the scope of this study, but it is apparent that abrupt changes in geology can occur in the region (Yuan et al., 2002). Jiskoot et al. (1998) identified lithology as a significant factor explaining Svalbard surges, with surges most likely to overlie shale, mudstone and other sedimentary rocks, and least likely to overlie igneous rocks. Till deformation is thought to be an important surge process (Murray et al., 2000), hence any changes in the lithology or structure of basal till could influence surge behaviour and incidence. A lack of knowledge about basal conditions in the WKS limits the application of these findings to this study, but given the geological heterogeneity in the region, such characteristics could explain the differences between the ranges. A consideration of basal sediments is an ongoing research priority in the region, and should be further investigated with regards to surging in the future.

6.3 Surge Dynamics

6.3.1 Surge Cycle Descriptions

Historic imagery, length change and velocity data allow glacier dynamics to be quantified. Firstly, examination of early Landsat imagery shows evidence of previous maximum surge

extents for glacier 01 and 03 in the early 1970s. This suggests that periodicity for glacier surges is, at a minimum, $\sim$4 decades, but for some glaciers is likely much longer. The lower bound for this period is indicative of hydrological surging.

As velocity data are limited to the post-2013 period, information about the surge initiation is lacking. This makes exact surge period more difficult to ascertain. However, Mansell et al. (2012) present complete velocity and terminus advance data for surging tidewater glaciers in Svalbard, which show that periods of peak velocities coincide well with periods of rapid terminus advance, with acceleration occurring as the terminus begins to advance and peak speeds reached in the early-middle period of rapid advance. Assuming this is broadly applicable to the current study region (considering that tidewater glaciers will display unique ice-ocean interactions not present on land-terminating glaciers), the terminus advance data for this study would suggest that the active phase of surges began shortly after 2008, and lasted at least $\sim$2 years (glacier 03), exceeding $\sim$5 years for glaciers that have not yet terminated. This lower bound is indicative of hydrological surges, but the longer surges exceed reasonable hydrological surge periods.

Peak velocities, although only briefly observed in 2013 for the glaciers examined here, appear to be between 700–1200 m a^{-1} ($\sim$2–3 m d^{-1}) in the fast-flowing mid-sections. These findings agree with alternate studies: Yasuda and Furuya (2015) observe peak velocities of up to 500 m a^{-1} for the West Kunlun glacier in 2013–2014, although are slightly lower than those observed for larger Karakoram glaciers by Quincey et al. (2015), which can reach up to 2000 m a^{-1}. These figures are an order or magnitude lower than the velocities approached by Variegated Glacier (Kamb et al., 1985), and similar to those exhibited by Monacobreen and other Svalbard glaciers (Murray et al., 2003), indicative of a thermal surge.

Information on surge termination is more abundant. Two distinct forms of termination are identified in this study. The first is that of glacier 03, which peaks at 1200 m a^{-1} in May–June 2013 before rapidly decelerating between the June–August and December–March velocity fields. This rapid termination is reminiscent of hydrological surges. A viable mechanism would be the emergence of an efficient drainage system towards the end of the 2013 ablation season, which would evacuate water from the subglacial system and rapidly reduce P_w.

Between winter 2013/2014 and 2015/2016, glacier 03 continues to decrease slowly to pre-surge velocities, largely during the summer to winter periods, as more water is evacuated from the system during periods of efficient drainage. However, the termination of glacier 01 shows glacier velocities peaking at $\sim$700 m a^{-1} in summer 2014 and subsequently showing a steady, linear decline that has still not returned to pre-surge levels. This is more reminiscent of the termination of a thermal surge. Although the termination of glacier 06 was not observed (unless surge velocities were considerably lower for the glacier), indicators of subglacial hydrological activity are also evident. Peak glacier velocities for summers 2013, 2014, and 2015 range between 150–200 m a^{-1}, whereas winter velocities range between 100–130 m a^{-1}. Enhanced velocities in the summer are a clear indicator of greater subglacial P_w increasing basal sliding rates in the early-mid ablation season, before the development of an efficient drainage system (if indeed one develops). Hence, termination and post-termination behaviour in this study is indicative of both thermal and hydrological surging, and varies between glaciers.

Without pre-2013 velocity fields, evidence of surge propogation (e.g. Turrin et al., 2013) is limited. Only glacier 01 displayed any evidence of a clear surge front or bulge. Visual assessment of crevassing, particularly through the examination of animated imagery (appendix B), does not appear to suggest that crevasses propagate from any particular source on other glaciers. This propagation would probably be visible, especially in the case of thermal surging where the boundary would move downglacier over a period of years. Both behaviours (surge fronts and uniform acceleration) have been observed in the Karakoram (Quincey et al., 2015), but alternative explanations for surge fronts have been proposed. Quincey et al. (2015) identify that 'surge fronts' in the Karakoram may not represent a thermal or drainage boundary, but instead simply represent active ice overriding obstacles of stagnant ice and debris. As glacier 01 develops a surge bulge at a particularly narrow and steep section of the glacier, ahead of a region identified as rapidly decaying ice, it is interpreted here that a similar process is occurring, unrelated to traditional surge bulge mechanisms. Hence, although evidence is not conclusive, it is likely that glaciers display uniform acceleration across the glacier surface. This is similar to some of the Karakoram surges identified by

Quincey et al. (2015), who draw parallels with Monacobreen (Murray et al., 2003). In this case, a lack of surge front would be explained by the thermal front propagating faster that ice flow (Fowler et al., 2001). Alternatively, if the surge is hydrological, then a glacier-wide switch in drainage system could explain such rapid propagation (Björnsson, 1998).

6.3.2 Comparison with Adjacent Studies

In line with recent work in adjacent regions (Quincey et al., 2015; Yasuda and Furuya, 2015), surges display characteristics indicative of both thermal and hydrological mechanisms. Surge characteristics are in agreement with Karakoram studies: velocities conform to thermal surges; build-ups and terminations can be slow, lasting for months–years (glacier 01); and enhanced mid-late summer velocities are observed (glacier 06). Similarly, glacier 01 and 03 show that return periods can be as short as four decades, and surges last $\sim$2–5 years, both in line with hydrological surges. The extension of this behaviour beyond the Karakoram and into the WKS, even on considerably smaller glaciers, is strong evidence that unusual surge behaviour in the Karakoram is not necessarily anomalous. Instead, HMA glaciers probably display an internally consistent third mechanism, distinct from either traditional understandings of Alaskan- or Svalbard-type surges.

These observations cannot confirm the findings of Yasuda and Furuya (2013) that velocities are greater in the winter, which is distinctive evidence of hydrological surging. However, glacier 03 does display a clear rapid termination, from $\sim$1200 m a^{-1} to $\sim$300 m a^{-1} between summer 2013 and winter 2013/2014 (although subsequently it shows slower deceleration after this abrupt termination). This is evidence of an abrupt change from a distributed to efficient drainage system, and is a strong indicator that the surge has some hydrological component. At over 10 km^2, glacier 03 is the largest glacier examined in this study and hence likely the thickest, and most likely to exhibit temperate conditions at the base. Given that this occurs early in the observation period, one point of future study is to ascertain whether glacier 03, unlike glacier 06, displays greater winter velocities in the 2012/2013 period. If this is the case, it would be compelling evidence of surging more in line with hydrological mechanisms than thermal.

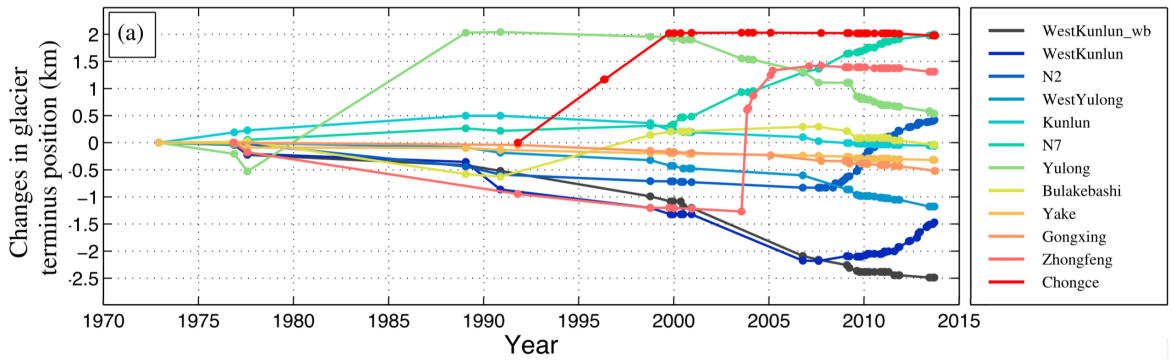

Fig. 6.1 Terminus advance rates of surge-type glaciers in the Liushi region from 1972–2014, reproduced from Yasuda and Furuya (2015). Note the temporal similarities between West Kunlun, N2, and the glaciers of this study (fig. 5.7)

6.4 Synchronicity of Surge Activity

6.4.1 Observations and Comments

Common descriptions of surging explicitly exclude the notion that surging can occur synchronously in adjacent glaciers (Cuffey and Paterson, 2010), or even adjacent tributaries (Hewitt, 2014). An unusual feature of this study is that glaciers 01–08 all began to enter the build-up phase between 2006–2008, despite no other surges occurring post-1990. In light of these results, it must also be noted that for the ambiguous 'advance' type glaciers, the transition to an advancing, crevassed state of uncertain surge status also occurs in the second half of the 2000s, coincident with the 'simultaneous' surges. Whilst this does not confirm that any of the smaller glaciers are indeed surge-type, it does suggest that there might be a common cause for both the surging and the more ambiguous advances. Additionally, Yasuda and Furuya (2015) observe two glacier surges in the Liushi Shan area beginning in 2008 and displaying similar advance rates and patterns – the West Kunlun Glacier and the unnamed glacier 'N2' (fig. 6.1, cf. fig. 5.7). The two glaciers are only $\sim$100 km southeast of the current study area, marking the closest observed surge-type glaciers to the current study area. The results described are an unusual finding given the common understanding that surges are internally regulated events, independent of external forcings such as climate (Benn and Evans, 2010; Hewitt, 2014; Murray et al., 2003; Sharp, 1988, and others).

One possibility is that the observed synchronicity is a coincidence, with independent surge cycles merely aligning. As a back-of-envelope calculation to assess this probability, simultaneous surge events were approached as a modification of the 'Birthday problem'. Instead of assessing the probability of a shared Birthday between N people in a set of 365 days, the probability of a shared surge event between N glaciers in a set of Y years (where Y is the length of surge cycle) was considered. Generous parameters were chosen. N was set to 17 (assuming that the ten surge type glaciers, one probable glacier, and six 'advance' glaciers are all viable). Although a minimum surge cycle period based on this study could be considered to be 40 years, surge initiation cannot be identified more accurately than a 2-year period, so Y was set to 20 (i.e. 40 / 2). A simple Monte Carlo simulation was performed to assess this problem using the parameters described, with glaciers given random surge initiation timings. Across 1 000 000 runs, the probability of two glaciers in the population sharing a surge event in the same two-year period was 0.72, but the probability of at least eight glaciers exhibiting simultaneous surges was $<2 \times 10^{-5}$. Hence, it is likely that the surges described in this study are not independent events.

Although a strict definition of surging is reliant only on internal dynamics, the interrelationship between external conditions and internal dynamics makes the distinction between internal surge and external speed-up difficult to apply in some cases (Benn and Evans, 2010). Indeed, at larger scales, surge activity is embedded in climatic controls on glacier behaviour (Sevestre and Benn, 2015). A limited number of prior examples of synchronous surge behaviour exist, which are examined here to assess the extent to which they can be applied to this study. Some, such as Kotlyakov et al. (2008) for the Pamir, suggest that glaciers in a connected drainage network may interact to initiate simultaneous surging – for instance, the advance of a tributary damming a trunk glacier and inducing a surge when released. However, this cannot apply to this study as the glaciers are discrete and located over a large range. Instead, two climatic explanations previously proposed in the literature are considered here: (i) long-term climate forcing, and (ii) short-term climate forcing.

6.4.2 Long-Term Climate Forcing

Long-term climate change has been proposed to result in switches to surge behaviour across a large area. Recent studies have identified an apparent increase in surge activity within the few decades in the Karakoram region (Copland et al., 2011; Hewitt, 2007, 2014). Hewitt (2007) identified 13 surges in the Karakoram Himalaya since 1985, more than any comparable period since the 1850s and at odds with known surge intervals. These observations have been approached with caution, as increased observational capability in the satellite era may explain some of the apparent increase. However, Copland et al. (2011) reviewed literature and satellite imagery from the 1960s onwards, highlighting that in the 14 years after 1990, double the number of surges were identified than in the 14 years prior to 1990 (26 and 13 surges, respectively), despite no significant difference in monitoring capability since the 1970s.

Studies highlight that this increase coincides with statistically significant increases in recorded winter and summer precipitation in the Karakoram region since 1961, as well as decreasing summer temperatures and temperature ranges (Archer and Fowler, 2004), both of which could favour positive mass balances (Copland et al., 2011; Hewitt, 2007) . In this sense, a transition to surge behaviour would be an inversion of the mechanism proposed by Dowdeswell et al. (1995) to explain reduced surge incidence in Svalbard. They noted a decrease from eighteen surging glaciers in mid-1930 to ten in 1970 and only five in 1990. They propose that negative glacier mass balances induced by warming (modelled to be up to 0.8 m a^{-1} $°C^{-1}$) have resulted in glaciers failing to accumulate necessary mass to initiate surge cycles, transitioning to a cold base and thus being incapable of rapid flow by basal sliding. Hence, it is possible that a transition to more positive mass balances – as is the case in regions of HMA – may force a regional-scale transition to surge activity. However, thickening and advance of non-surging glaciers occurs largely in the highest watersheds (Hewitt, 2005), and has only occurred since the 1990s (Bhambri et al., 2013). The sparse coverage of meteorological stations, largely located outside of the watersheds of surging

glaciers – and at far lower altitudes – make it difficult to extrapolate climatic observations to these highest altitudes.

An alternative mechanism, proposed by Hewitt (2007) and Quincey et al. (2011), suggests a climate-forced shift to surge-type conditions in the Karakoram could have been induced not by changing mass balances but by changing conditions at the base of glaciers, from predominantly cold to warm conditions. However, ice at depth largely reflects accumulation zone snow temperature, and thus changes in subglacial thermal regime by advection of accumulation zone ice alone would be slower than changes forced only since 1990 would allow. Hewitt (2005, 2007) thus proposed an alternative mechanism by which climate changes may induce a more rapid change in the basal conditions of glaciers in HMA. In steep, avalanche-fed glaciers and icefalls, the rate at which surface snow/ice reaches the bed is far more rapid, increasing response times from scales of centuries to years. As such, high-altitude thermal conditions may quickly affect the base of glaciers in HMA. If climate changes are indeed forcing a transition towards basal conditions conducive to surging, these processes could reduce the periods over which a transition to polythermal or temperate basal conditions occurs. Hewitt (2007) proposed this hypothesis to explain the remarkable coincidence of four surges in less than a decade in the tributaries of the Panmah Glacier, despite known surge intervals not supporting cycles being in phase. However, the effect of observed climate changes on glacier thermal regime is hard to predict, as large altitudinal range, avalanching, and latent heat transport via refreezing make conditions complex.

The above can be readily applied to this study. Surges apparently increase from two observed in the 1972–1990 period (with further evidence that glaciers 01 and 03 surged shortly prior to this), to eight surges in the 1990–2016 period. Whilst the smaller sample size gives less confidence in such a conclusion, there is definite evidence that an increase in surge activity occurred in the WKS. Additionally, a step-change to a warmer, wetter climate has been recorded since 1989 (see section 3.2.2). Seasonal temperature and precipitation data, as provided by the Chinese Meteorological Administration (`data.cma.cn`), are presented in figs. 6.2 and 6.3 for both Hotan and the mean of the nearest six meteorological stations (see appendix C for station IDs and locations). Notable step-changes in spring, summer, and

autumn temperatures can be observed in the 1990s – with the caveat that these are low-altitude meteorological stations and changes must be extrapolated to high-altitude glaciated catchments. Applying the same hypothesis as Hewitt (2007), it is possible to speculate that this warmer climate began a rapid shift in the thermal regime of glaciers starting in the 1990s, resulting in glaciers that were increasingly warm-bedded, and thus increasingly likely to surge, by the next decade. One point of evidence in favour of this is that the fastest regions of glaciers 01 and 03 were also the steepest regions (figs. 5.9, 5.10), and were already crevassed in the pre-surge period. This conforms to Hewitt's expectation that fast changes in thermal regimes could occur via crevassed sections and icefalls (Hewitt, 2007). It might be speculated that these sections experienced the most rapid, or most widespread, transition to a warmer base, explaining why they experience the most rapid surge velocities.

This hypothesis can explain why a high number of glaciers might have been 'primed' to surge by the mid-2000s. However, Hewitt (2007) only proposed this hypothesis to explain a clustering of surges within a period of ten years. An extra factor should also be considered to explain what might have triggered surging in the same two-year period.

6.4.3 Short-Term Climate Forcing

The relationship between surging and meltwater production means that on short timescales, exceptional climatic events may directly affect surge activity. This is most obvious for termination events: Eisen et al. (2005) identify that the 1995 termination of Variegated Glacier occurred after the two hottest days in the 78-year Yakutat record, with rapid meltwater production yielding an abrupt shift to an efficient subglacial drainage system. No analogous studies in HMA have, as yet, attributed surge activity to single climatic events. However, Quincey et al. (2009) identify particularly high velocities at Baltoro Glacier during summer 2005, with an apparent acceleration of $\sim$20–25% in some regions compared with earlier measurements. They attribute this to the severe winter snowfall of 2004, followed by a rapid melting of the deep winter snowpack introducing high volumes of meltwater to an inefficient subglacial system, thus enhancing P_w and glacier velocity. This indicates that meltwater can play an important role in determining periods of high glacier velocities in HMA.

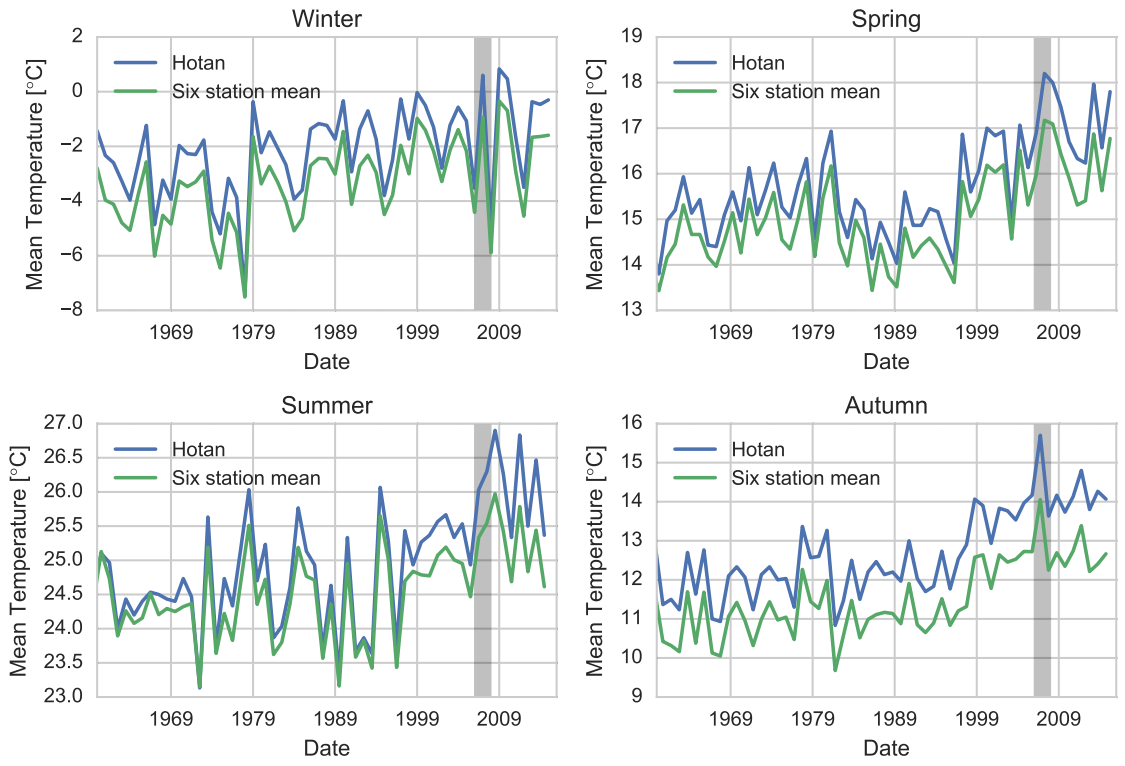

Fig. 6.2 Seasonal mean temperature data for southern Xinjiang, Q1 1960 – Q2 2015. 2006–2008 period of interest highlighted in grey.

Recent work by Dunse et al. (2015) has identified a potential relationship between extreme summer melt periods and thermal surge activity on Basin-3 outlet glacier of the Austfonna ice cap, Svalbard (fig. 6.4). They argue that strong summer surface melt can mobilise cold-based ice across multiple years (distinct from seasonal summer velocity increases), facilitating multi-annual accelerations due to fast basal motion. These hydro-thermodynamic processes work in the same way as a thermal surge described in section 2.1.1, inducing high basal P_w, fast velocities, and generating a positive feedback via frictional heating. This is distinct from a thermal surge, however: multi-annual accelerations were not uniform or gradual, and only when incorporating cryo-hydrological warming at the base due to surface meltwater penetration (e.g. latent heat release during meltwater refreezing, and direct heat transfer) can warming at the bed occur quickly enough to explain the observations. Hence, year-on-year increases in warm-bedded area, and thus P_w and velocity, are forced largely by consecutive high melt seasons. Dunse et al. (2015) again stress that surge activity,

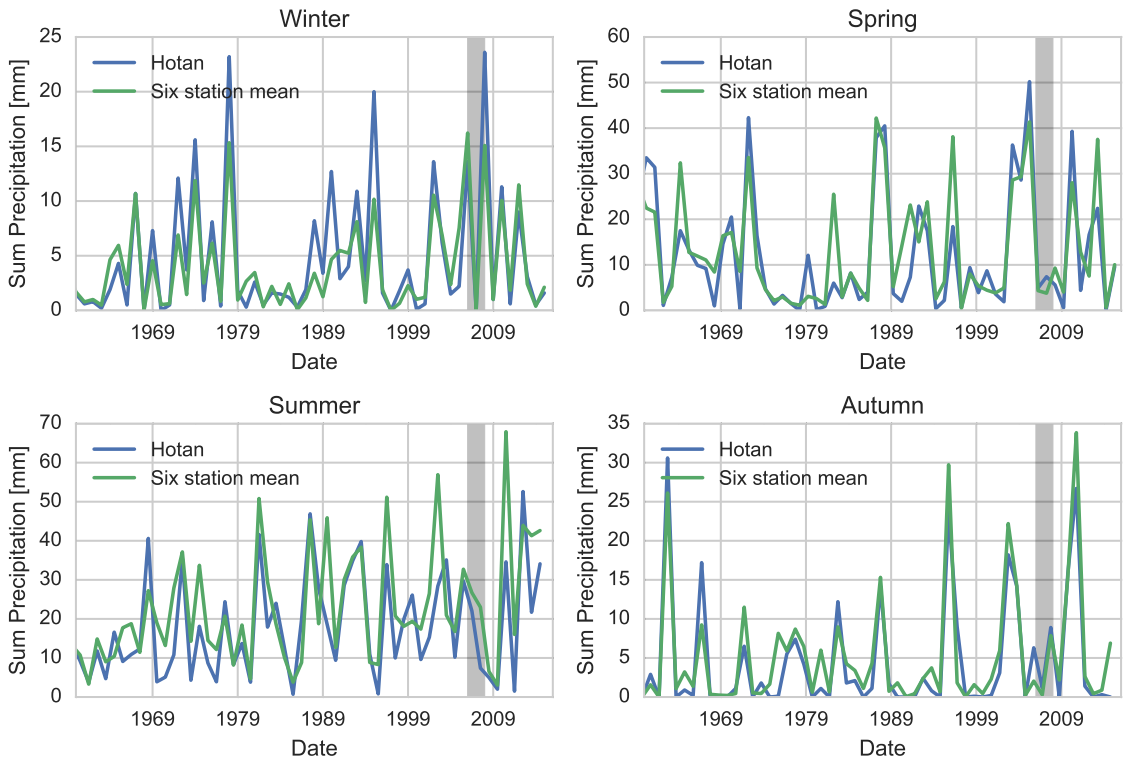

Fig. 6.3 Seasonal total precipitation data for southern Xinjiang, Q1 1960 – Q2 2015. 2006–2008 period of interest highlighted in grey.

as strictly defined, is an internally regulated process. External forcing by short-term melt conflicts with this view, but can only occur in systems already primed for surge activity, with hydro-thermodynamic contributions by surface meltwater merely mobilising the reservoir area.

The process as described by Dunse et al. (2015) can be readily applied to the glaciers in this study. First, the wider literature holds that cold and polythermal glaciers dominate the region, and it is apparent from flow velocities and the generally slow build-up and termination phases that a process akin to thermally forced surging dominates in the study area. Second, recent climatic warming would mean that a transition from cold to warm beds would likely already be occurring in the mid-2000s (analogous to phase 1 in fig. 6.4), meaning that thermal surges would be imminent for a number of glaciers. Third, the relatively rapid build-up, active, and termination phases – all far faster than traditional Svalbard thermal surges – could be explained by hydro-thermodynamic processes accelerating the expansion of

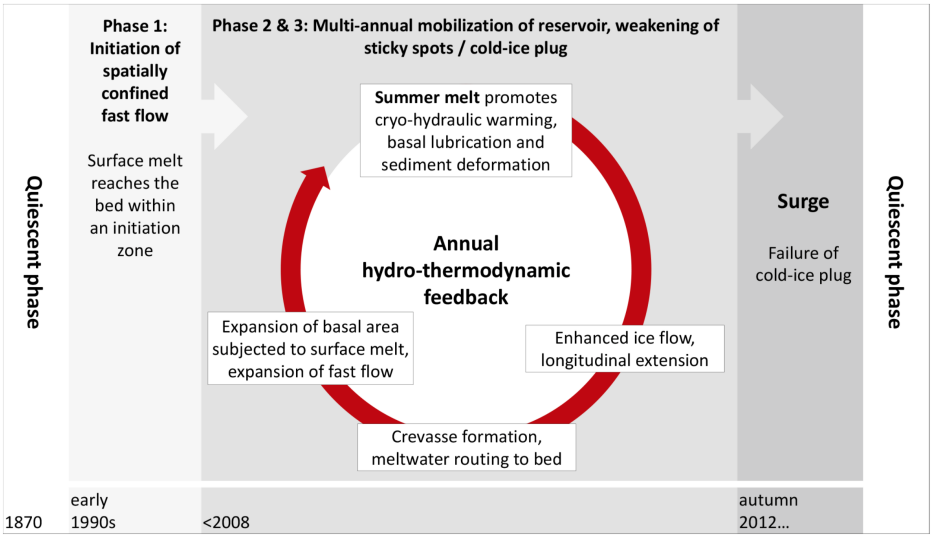

Fig. 6.4 Schematic illustration of hydro-thermodynamic summer melt feedback to induce surging in polythermal glaciers, reproduced from Dunse et al. (2015). Note that dates refer to the timings of the surge of Basin-3, Austfonna, not to those surges described in this study.

warm-based areas of the bed. This is supported by the observations from the Hotan weather station (fig. 6.2), where the periods autumn 2006, winter 2006/2007, spring 2007, and summer 2008 all display notably high – and in the case of the latter three, unprecedented – temperatures. It is speculated here that this period of high temperatures resulted in meltwater efficiently transmitting heat to the glacier beds – particularly at crevassed regions and icefalls as speculated by Hewitt (2007). This would coincide with phases 2 and 3 of fig. 6.4, before active phases initiate in the post-2008 period. This rapidly expanded the area of warm bed under the glaciers, especially considering they were already experiencing longer-term thermal regime change – and as such triggered the thermal surge in these glaciers. In subsequent seasons, further summer meltwater input into the basal system resulted in seasonal changes in velocity, especially as crevasses expanded across larger sections of the glacier surface, providing more efficient routes for meltwater to reach the subglacial system. In glacier 03, the largest glacier, the warm bed was able to develop to such an extent that an efficient subglacial system emerged, rapidly terminating the surge event.

6.5 Proposed Surge Mechanism

Given the theory and evidence examined in the above sections, a speculative series of events can be outlined that may have resulted in the surges of glaciers 01–08:

1. Prior to the late 20th century, glaciers in the study area existed in a largely cold or polythermal state. The low temperatures and precipitation prevalent in the region resulted in relatively low positive mass balances in reservoir zones, and thus quiescent phases were relatively long and surges were infrequent.

2. Recent anthropogenic climate change was expressed in southern Xinjiang province as a notable step-change to warmer and wetter climates, beginning in 1989.

3. The warmer climates began to force a transition to a warmer thermal regime in glaciers. This was accelerated by avalanching and regions of crevassing and icefalls (Hewitt, 2007), resulting in an efficient transfer of heat to the base of glaciers.

4. Warming at the base reduced the threshold glacier thickness at which glaciers underwent thermal surging. In some glaciers, it may have allowed thermal surging to occur for the first time. Regardless, by the mid-2000s a number of glaciers – possibly including the two glaciers in the Liushi region identified by Yasuda and Furuya (2015) – were approaching threshold profiles in their reservoir area: they were 'primed' to surge, as outlined by Hewitt (2007).

5. A particularly warm period between 2006–2008 considerably increased meltwater supply to the bed, mobilising the remaining cold-based ice and inducing thermal surges in those already close to the surge threshold, according to the hydro-thermodynamic mechanism of Dunse et al. (2015).

6. As described by Dunse et al. (2015), the influence of supraglacial meltwater rapidly accelerates the period over which thermal surges might otherwise occur. In glacier 03, temperatures may have been high enough for an efficient drainage system to occur, rapidly terminating surge velocities.

This hypothesis integrates a number of previous explanations from both HMA and wider surge literature. It links previously proposed changes in subglacial thermal regime of HMA glaciers (Hewitt, 2007; Quincey et al., 2011), to recent work by Dunse et al. (2015) that has proposed how supraglacial melt might be linked to rapid thermal surge initiations over shorter timescales (on the order of seasons). This potential forcing is supported by observations of unprecedented high temperatures at the nearest meteorological stations across the period that surges were initiating.

The hydro-thermodynamic surge mechanism could potentially explain a number of the unique HMA surge characteristics observed in this, and adjacent, studies. Increased surge velocities under this mechanism would still ultimately relate to mechanisms common in thermal surges, and hence explain why pre-surge accelerations can occur over periods of months–years, and why peak ice velocities align with previously observed thermal surges. However, the facilitating effect of surface meltwater would act to accelerate the thermal surge cycle, and hence explain why surge periods, and quiescent phases, are so much shorter than other thermal surges. Additionally, the influence of meltwater would explain the seasonal variations in velocity. It is not suggested here that this is necessarily a universal control across the HMA surge region: indeed, the synchronicity of glaciers observed here is likely a rare event, a product of the coincidence of both short-term temperature highs and longer-term thermal regime changes. However, this mechanism provides preliminary evidence of the interaction between high surface meltwater production and glacier surging in HMA, and provides motivation to further test this hypothesis across the wider region.

Chapter 7

Conclusion

7.1 Overview

The glaciers of northwest HMA represent the second global centre of surge activity (Sevestre and Benn, 2015) and also mark a region of anomalous glacier behaviour in the context of climate change. Despite this, studies of the area are scarce and understanding of glacial dynamics in the region is underdeveloped. This study set out to achieve three objectives relating to the glacier surging in a previously unexamined region of the WKS, relating to the (i) identification of surge glaciers, (ii) assessment of surge dynamics, and (iii) explanation of surge mechanisms, the results of which are summarised here.

Ten glaciers were observed to surge between 1972–2016 – 11.3% of the total. One further glacier displays possible evidence of surge activity, and six smaller glaciers show ambiguous evidence. This expands the record of surging glaciers in the WKS, which was previously limited to study of glaciers in the region surrounding Liushi Shan, showing that surging glaciers in the WKS can be smaller than previously identified. Statistical analysis showed that these glaciers were wider than non-surging glaciers, which is in line with previous findings, and terminated at lower altitudes, a new finding that here is linked to the increased likelihood of warm beds at lower altitudes. Distribution is biased to the northern range in the study area, which could be related to differing topographic controls to the north

and south of the range, but could also be linked to geological differences, a variable not examined here.

Glaciers in the WKS are reported as cold or polythermal in the literature, hence thermal surges might be expected to occur. Some observed surge dynamics align with this expectation, with relatively slow velocities as well as build-up and termination periods lasting months–years. However, Others are reminiscent of hydrological surges, including relatively short quiescent phases ($\sim$4 decades) and surge periods ($\sim$5 years). These factors have been previously identified in adjacent studies (Quincey et al., 2015; Yasuda and Furuya, 2015), suggesting that the unusual behaviours observed across various surge studies in HMA are indicative of a surge mechanism that is related to, but distinct from, traditional Svalbard-type thermal surging.

Finally, observations were made of eight glacier surges that are temporally coincident to an unusual degree, which conflicts with understandings of glacier surging as a behaviour forced entirely by internally regulated mechanisms. Although conclusions presented here are speculative, links were made to a hydro-thermodynamic mechanism recently proposed by Dunse et al. (2015) to explain surging of an outlet glacier of the Austfonna ice cap. This is supported by records of anomalously high temperatures during the surge initiation period, and can also be interpreted in the context of long-term climate changes in the region, recently linked to increased surge incidence in the Karakoram. Thus, this study proposes an alternative surge mechanism, distinct from previously proposed explanations (e.g. Yasuda and Furuya, 2015), that may be able to explain the unique and conflicting surge behaviours observed across HMA.

In conclusion, this study has expanded the record of surges in the WKS, and made an unusual discovery that further validates recent literature proposing a relationship between surging and climate. These findings are important both in terms of understanding more about regional glaciology and climate, but also towards better understanding surge behaviour as a whole.

7.2 Future Research

This study has provided a preliminary assessment of surging in a notably under-researched region. The findings provide a number of potential avenues for further research.

First, the marked difference in surge incidence between the northern and southern ranges of the study should be further investigated. This should be done in two stages. The first should consist of an expansion of the study area eastwards and westwards, as the small sizes and high density of glaciers in the area necessitated the study area being relatively small. This would determine whether the difference between the two ranges is true or an artefact of the small study size. Assuming that the difference are valid, a second investigation should examine geological differences between the two ranges, to determine whether it is possible that the nature and lithology of the subglacial environment impacted surge incidence in the area.

Second, velocity data covering the 2006–2013 period was severely limited in this study. The novel results motivate a more detailed assessment of velocities in these periods. A number of restricted-access satellites, both optical and radar, have been used to assess velocities in this region, including the AVNIR-2 and PALSAR sensors on the ALOS satellite, ASAR on ENVISAT, AMI on ERS-1 and 2, and the TerraSAR-X satellite (Quincey et al., 2009, 2015; Yasuda and Furuya, 2015). These data sources would allow for a detailed assessment of velocity changes to take place during the period otherwise limited by the SLC-off period for Landsat 7 ETM+ imagery. Additionally, surge initiations can can be compared to the hydro-thermodynamic initiation of Basin-3 of the Austfonna ice cap, which would predict velocity increases to occur in discrete steps over successive summers (Dunse et al., 2015). Comparisons would allow for the hydro-thermodynamic explanation proposed here to be further validated or refuted.

Finally, long-term meteorological data is limited in its application due to the marked difference in altitudes between meteorological stations and glaciated catchments. As the region is particularly arid, hydrological data, which exist for stations on the Karakash, Yurungkash, and Hotan rivers, acts as a useful proxy for glacier melt production (section

3.2.3). These data are difficult to access for researchers outside China, but papers where it is visually displayed (e.g. fig. 3, Xu et al., 2013) appear to show some anomaly in 2006 for the Hotan river station, which coincides with news reports of heavy flooding in the Hotan area (Xinjua News Agency, 2006). Access to these data at a monthly resolution could provide useful information about high-altitude meltwater production.

Incorporating a wider range of data from sources relating to geology, remote sensing, and hydrology would increase the confidence in the true nature and causes of the unusual behaviour observed here. Benn and Evans suggest that surging glaciers attract attention because 'like many instances of unusual or pathological behaviour, they offer a very instructive perspective on "normality"' (Benn and Evans, 2010, p.186–187). Indeed, being able to more effectively understand surge behaviour in the WKS would provide valuable clues as to the subglacial dynamics of glaciers in HMA, which is a notable source of data scarcity in an important and unusual region of the cryosphere.

References

Ageta, Y., Wenjing, Z., and Narawo, M. (1989). Mass balance studies on Chongce Ice Cap in the west Kunlun Mountains. *Bulletin of glacier research*, (7):37–43.

Archer, D. R. and Fowler, H. (2004). Spatial and temporal variations in precipitation in the Upper Indus Basin, global teleconnections and hydrological implications. *Hydrology and Earth System Sciences Discussions*, 8(1):47–61.

Atkinson, P., Jiskoot, H., Massari, R., and Murray, T. (1998). Generalized linear modelling in geomorphology. *Earth Surface Processes and Landforms*, 23(13):1185–1195.

Bajracharya, S. R. and Mool, P. (2010). Glaciers, glacial lakes and glacial lake outburst floods in the Mount Everest region, Nepal. *Annals of Glaciology*, 50(53):81–86.

Bao, W.-j., Liu, S.-y., Wei, J.-f., and Guo, W.-q. (2015). Glacier changes during the past 40 years in the West Kunlun Shan. *Journal of Mountain Science*, 12(2):344–357.

Barrand, N. E. and Murray, T. (2006). Multivariate controls on the incidence of glacier surging in the Karakoram Himalaya. *Arctic, Antarctic, and Alpine Research*, 38(4):489–498.

Bartholomew, I., Nienow, P., Mair, D., Hubbard, A., King, M. A., and Sole, A. (2010). Seasonal evolution of subglacial drainage and acceleration in a Greenland outlet glacier. *Nature Geoscience*, 3(6):408–411.

Benn, D. and Evans, D. (2010). *Glaciers and Glaciation.* Arnold, London, 2nd edition.

Benn, D. I., Bolch, T., Hands, K., Gulley, J., Luckman, A., Nicholson, L. I., Quincey, D., Thompson, S., Toumi, R., and Wiseman, S. (2012). Response of debris-covered glaciers in the Mount Everest region to recent warming, and implications for outburst flood hazards. *Earth-Science Reviews*, 114(1):156–174.

Benn, D. I. and Lehmkuhl, F. (2000). Mass balance and equilibrium-line altitudes of glaciers in high-mountain environments. *Quaternary International*, 65:15–29.

Bhambri, R., Bolch, T., Kawishwar, P., Dobhal, D. P., Srivastava, D., and Pratap, B. (2013). Heterogeneity in glacier response in the upper Shyok valley, northeast Karakoram. *The Cryosphere*, 7(5):1385–1398.

Björnsson, H. (1998). Hydrological characteristics of the drainage system beneath a surging glacier. *Nature*, 395(6704):771–774.

Björnsson, H., Pálsson, F., Sigurðsson, O., and Flowers, G. E. (2003). Surges of glaciers in Iceland. *Annals of Glaciology*, 36(1):82–90.

Bolch, T., Kulkarni, A., Kääb, A., Huggel, C., Paul, F., Cogley, J. G., Frey, H., Kargel, J. S., Fujita, K., Scheel, M., Bajracharya, S., and Stoffel, M. (2012). The State and Fate of Himalayan Glaciers. *Science*, 336(6079):310–314.

Borth, H., Tao, H., Fraedrich, K., Schneidereit, A., and Zhu, X. (2015). Hydrological extremes in the Aksu-Tarim River Basin: Mid-latitude dynamics. *Climate Dynamics*, pages 1–12.

Chen, Y., Takeuchi, K., Xu, C., Chen, Y., Xu, Z., et al. (2006). Regional climate change and its effects on river runoff in the Tarim Basin, China. *Hydrological Processes*, 20(10):2207–2216.

Clarke, G. K. (1991). Length, width and slope influences on glacier surging. *Journal of Glaciology*, 37(126):236–246.

Clarke, G. K., Schmok, J. P., Ommanney, C. S. L., and Collins, S. G. (1986). Characteristics of surge-type glaciers. *Journal of Geophysical Research: Solid Earth*, 91(B7):7165–7180.

Cogley, J. G. (2011). Present and future states of Himalaya and Karakoram glaciers. *Annals of Glaciology*, 52(59):69–73.

Cogley, J. G. (2016). Glacier shrinkage across High Mountain Asia. *Annals of Glaciology*.

Copland, L., Pope, S., Bishop, M. P., Shroder, J. F., Clendon, P., Bush, A., Kamp, U., Seong, Y. B., and Owen, L. A. (2009). Glacier velocities across the central Karakoram. *Annals of Glaciology*, 50(52):41–49.

Copland, L., Sharp, M. J., and Dowdeswell, J. A. (2003). The distribution and flow characteristics of surge-type glaciers in the Canadian High Arctic. *Annals of Glaciology*, 36(1):73–81.

Copland, L., Sylvestre, T., Bishop, M. P., Shroder, J. F., Seong, Y. B., Owen, L. A., Bush, A., and Kamp, U. (2011). Expanded and recently increased glacier surging in the Karakoram. *Arctic, Antarctic, and Alpine Research*, 43(4):503–516.

Cuffey, K. M. and Paterson, W. S. B. (2010). *The Physics of Glaciers*. Butterworth-Heinemann, Oxford, 4th edition.

Dehecq, A., Gourmelen, N., and Trouve, E. (2015). Deriving large-scale glacier velocities from a complete satellite archive: Application to the Pamir–Karakoram–Himalaya. *Remote Sensing of Environment*, 162:55–66.

Ding, Y., Liu, S., Li, J., and Shangguan, D. (2006). The retreat of glaciers in response to recent climate warming in western China. *Annals of Glaciology*, 43(1):97–105.

Dowdeswell, J., Hodgkins, R., Nuttall, A.-M., Hagen, J., and Hamilton, G. (1995). Mass balance change as a control on the frequency and occurrence of glacier surges in Svalbard, Norwegian High Arctic. *Geophysical Research Letters*, 22(21):2909–2912.

Dunse, T., Schellenberger, T., Hagen, J. O., Kääb, A., Schuler, T. V., and Reijmer, C. H. (2015). Glacier-surge mechanisms promoted by a hydro-thermodynamic feedback to summer melt. *The Cryosphere*, 9(1):197–215.

Eisen, O., Harrison, W. D., Raymond, C. F., Echelmeyer, K. A., Bender, G. A., and Gorda, J. L. (2005). Variegated Glacier, Alaska, USA: a century of surges. *Journal of Glaciology*, 51(174):399–406.

Fountain, A. G. and Walder, J. S. (1998). Water flow through temperate glaciers. *Reviews of Geophysics*, 36(3):299–328.

Fowler, A. (1987). A theory of glacier surges. *Journal of Geophysical Research: Solid Earth*, 92(B9):9111–9120.

Fowler, A., Murray, T., and Ng, F. (2001). Thermally controlled glacier surging. *Journal of Glaciology*, 47(159):527–538.

Gardelle, J., Berthier, E., and Arnaud, Y. (2012). Slight mass gain of Karakoram glaciers in the early twenty-first century. *Nature geoscience*, 5(5):322–325.

Gardner, A. S., Moholdt, G., Cogley, J. G., Wouters, B., Arendt, A. A., Wahr, J., Berthier, E., Hock, R., Pfeffer, W. T., Kaser, G., et al. (2013). A reconciled estimate of glacier contributions to sea level rise: 2003 to 2009. *Science*, 340(6134):852–857.

Gardner, J. S. and Hewitt, K. (1990). A surge of Bualtar Glacier, Karakoram Range, Pakistan: a possible landslide trigger. *Journal of Glaciology*, 36(123):159–162.

Grant, K. L., Stokes, C. R., and Evans, I. S. (2009). Identification and characteristics of surge-type glaciers on Novaya Zemlya, Russian Arctic. *Journal of Glaciology*, 55(194):960–972.

Guo, W., Liu, S., Wei, J., and Bao, W. (2013). The 2008/09 surge of central Yulinchuan glacier, northern Tibetan Plateau, as monitored by remote sensing. *Annals of Glaciology*, 54(63):299–310.

Hamilton, G. S. and Dowdeswell, J. A. (1996). Controls on glacier surging in Svalbard. *Journal of Glaciology*, 42(140):157–168.

Hewitt, K. (1969). Glacier surges in the Karakoram Himalaya (Central Asia). *Canadian Journal of Earth Sciences*, 6(4):1009–1018.

Hewitt, K. (1998). Glaciers receive a surge of attention in the Karakoram Himalaya. *Eos, Transactions American Geophysical Union*, 79(8):104–105.

Hewitt, K. (2005). The Karakoram Anomaly? Glacier Expansion and the 'Elevation Effect,' Karakoram Himalaya. *Mountain Research and Development*, 25(4):332–340.

Hewitt, K. (2007). Tributary glacier surges: an exceptional concentration at Panmah Glacier, Karakoram Himalaya. *Journal of Glaciology*, 53(181):181–188.

Hewitt, K. (2011). Glacier change, concentration, and elevation effects in the Karakoram Himalaya, Upper Indus Basin. *Mountain Research and Development*, 31(3):188–200.

Hewitt, K. (2014). *Glaciers of the Karakoram Himalaya: glacial environments, processes, hazards and resources*. Advances in Asian human-environmental research. Springer, Dordrecht.

Hewitt, K. and Liu, J. (2010). Ice-dammed lakes and outburst floods, Karakoram Himalaya: historical perspectives on emerging threats. *Physical Geography*, 31(6):528–551.

Huang, L., Wu, L., and Shen, B. (2009). Quantitative Estimation of Annual Runoff Variation from the Hotan River, China. *Journal of Sustainable Development*, 2(2):120.

Immerzeel, W., Kraaijenbrink, P., Shea, J., Shrestha, A., Pellicciotti, F., Bierkens, M., and De Jong, S. (2014). High-resolution monitoring of Himalayan glacier dynamics using unmanned aerial vehicles. *Remote Sensing of Environment*, 150:93–103.

Immerzeel, W. W., Van Beek, L. P., and Bierkens, M. F. (2010). Climate change will affect the Asian water towers. *Science*, 328(5984):1382–1385.

Jiskoot, H., Boyle, P., and Murray, T. (1998). The incidence of glacier surging in Svalbard: evidence from multivariate statistics. *Computers & Geosciences*, 24(4):387–399.

Jiskoot, H., Murray, T., and Boyle, P. (2000). Controls on the distribution of surge-type glaciers in Svalbard. *Journal of Glaciology*, 46(154):412–422.

Jiskoot, H., Murray, T., and Luckman, A. (2003). Surge potential and drainage-basin characteristics in East Greenland. *Annals of Glaciology*, 36(1):142–148.

Kamb, B. (1987). Glacier surge mechanism based on linked cavity configuration of the basal water conduit system. *Journal of Geophysical Research: Solid Earth*, 92(B9):9083–9100.

Kamb, B., Raymond, C. F., Harrison, W. D., Engelhardt, H., Echelmeyer, K. A., Humphrey, N., Brugman, M. M., and Pfeffer, T. (1985). Glacier Surge Mechanism: 1982-1983 Surge of Variegated Glacier, Alaska. *Science*, 227(4686):469–479.

Kapnick, S. B., Delworth, T. L., Ashfaq, M., Malyshev, S., and Milly, P. C. D. (2014). Snowfall less sensitive to warming in Karakoram than in Himalayas due to a unique seasonal cycle. *Nature Geoscience*, 7(11):834–840.

Ke, L., Ding, X., and Song, C. (2015). Heterogeneous changes of glaciers over the western Kunlun Mountains based on ICESat and Landsat-8 derived glacier inventory. *Remote Sensing of Environment*, 168:13–23.

Kotlyakov, V., Osipova, G., and Tsvetkov, D. (1997). Fluctuations of unstable mountain glaciers: scale and character. *Annals of Glaciology*, 24:338–343.

Kotlyakov, V., Osipova, G., and Tsvetkov, D. (2008). Monitoring surging glaciers of the Pamirs, central Asia, from space. *Annals of Glaciology*, 48(1):125–134.

Kääb, A., Berthier, E., Nuth, C., Gardelle, J., and Arnaud, Y. (2012). Contrasting patterns of early twenty-first-century glacier mass change in the Himalayas. *Nature*, 488(7412):495–498.

Kääb, A., Treichler, D., Nuth, C., and Berthier, E. (2015). Brief Communication: Contending estimates of 2003–2008 glacier mass balance over the Pamir–Karakoram–Himalaya. *The Cryosphere*, 9(2):557–564.

Lawson, W. (1996). Structural evolution of Variegated Glacier, Alaska, U.S.A., since 1948. *Journal of glaciology*, 42(141):261–270.

Lee, D. S., Storey, J. C., Choate, M. J., and Hayes, R. W. (2004). Four years of Landsat-7 on-orbit geometric calibration and performance. *Geoscience and Remote Sensing, IEEE Transactions on*, 42(12):2786–2795.

Lin, A., Kano, K.-i., Guo, J., and Maruyama, T. (2008). Late Quaternary activity and dextral strike-slip movement on the Karakax Fault Zone, northwest Tibet. *Tectonophysics*, 453(1):44–62.

Liu, S., Ding, Y., Shangguan, D., Zhang, Y., Li, J., Han, H., Wang, J., and Xie, C. (2006). Glacier retreat as a result of climate warming and increased precipitation in the Tarim river basin, northwest China. *Annals of Glaciology*, 43(1):91–96.

Liu, Y., Hou, S., Wang, Y., and Song, L. (2009). Distribution of borehole temperature at four high-altitude alpine glaciers in central Asia. *Journal of Mountain Science*, 6(3):221–227.

Mansell, D., Luckman, A., and Murray, T. (2012). Dynamics of tidewater surge-type glaciers in northwest Svalbard. *Journal of Glaciology*, 58(207):110–118.

Mayer, C., Fowler, A. C., Lambrecht, A., and Scharrer, K. (2011). A surge of North Gasherbrum Glacier, Karakoram, China. *Journal of Glaciology*, 57(205):904–916.

McNabb, R., Hock, R., O'Neel, S., Rasmussen, L., Ahn, Y., Braun, M., Conway, H., Herreid, S., Joughin, I., Pfeffer, W., et al. (2012). Using surface velocities to calculate ice thickness and bed topography: a case study at Columbia Glacier, Alaska, USA. *Journal of Glaciology*, 58(212):1151–1164.

Meier, M. F. and Post, A. (1969). What are glacier surges? *Canadian Journal of Earth Sciences*, 6(4):807–817.

Messerli, A. and Grinsted, A. (2015). Image georectification and feature tracking toolbox: ImGRAFT. *Geoscientific Instrumentation, Methods and Data Systems*, 4(1):23–34.

Messerli, A., Karlsson, N. B., and Grinsted, A. (2014). Brief Communication: 2014 velocity and flux for five major Greenland outlet glaciers using ImGRAFT and Landsat-8. *The Cryosphere Discussions*, 8(6):6235–6250.

Moon, T. and Joughin, I. (2008). Changes in ice front position on Greenland's outlet glaciers from 1992 to 2007. *Journal of Geophysical Research: Earth Surface*, 113(F2):F02022.

Murray, T., Dowdeswell, J. A., Drewry, D. J., and Frearson, I. (1998). Geometric evolution and ice dynamics during a surge of Bakaninbreen, Svalbard. *Journal of Glaciology*, 44(147):263–374.

Murray, T., Strozzi, T., Luckman, A., Jiskoot, H., and Christakos, P. (2003). Is there a single surge mechanism? Contrasts in dynamics between glacier surges in Svalbard and other regions. *Journal of Geophysical Research: Solid Earth*, 108(B5):2237.

Murray, T., Stuart, G. W., Miller, P. J., Woodward, J., Smith, A. M., Porter, P. R., and Jiskoot, H. (2000). Glacier surge propagation by thermal evolution at the bed. *Journal of Geophysical Research: Solid Earth*, 105(B6):13491–13507.

Narama, C., Kääb, A., Duishonakunov, M., and Abdrakhmatov, K. (2010). Spatial variability of recent glacier area changes in the Tien Shan Mountains, Central Asia, using Corona (~ 1970), Landsat (~ 2000), and ALOS (~ 2007) satellite data. *Global and Planetary Change*, 71(1–2):42–54.

Neckel, N., Kropáček, J., Bolch, T., and Hochschild, V. (2014). Glacier mass changes on the Tibetan Plateau 2003–2009 derived from ICESat laser altimetry measurements. *Environmental research letters*, 9(1):014009.

Nienow, P., Sharp, M., and Willis, I. (1998). Seasonal changes in the morphology of the subglacial drainage system, Haut Glacier d'Arolla, Switzerland. *Earth Surface Processes and Landforms*, 23(9):825–843.

NSIDC (2015). *Glacier Photograph Collection*. National Snow and Ice Data Center, Boulder, Colorado.

Nuimura, T., Sakai, A., Taniguchi, K., Nagai, H., Lamsal, D., Tsutaki, S., Kozawa, A., Hoshina, Y., Takenaka, S., Omiya, S., et al. (2015). The GAMDAM glacier inventory: a quality-controlled inventory of Asian glaciers. *The Cryosphere*, 9(3):849–864.

Owen, L. A. and Derbyshire, E. (1989). The Karakoram glacial depositional system. *Zeitschrift fiir Geomorphologie*, 76:33–73.

Paul, F. (2015). Revealing glacier flow and surge dynamics from animated satellite image sequences: examples from the Karakoram. *The Cryosphere*, 9(6):2201–2214.

Paul, F., Barry, R., Cogley, J., Frey, H., Haeberli, W., Ohmura, A., Ommanney, C., Raup, B., Rivera, A., and Zemp, M. (2010). Guidelines for the compilation of glacier inventory data from digital sources v1.0. *GlobGlacier*.

Peng, D., Wang, X., Zhao, C., Wu, X., Jiang, F., and Chen, P. (2014). Characterizing Air Temperature Changes in the Tarim Basin over 1960–2012. *PloS one*, 9(11):e112231.

Pfeffer, W. T., Arendt, A. A., Bliss, A., Bolch, T., Cogley, J. G., Gardner, A. S., Hagen, J.-O., Hock, R., Kaser, G., Kienholz, C., Miles, E. S., Moholdt, G., Mölg, N., Paul, F., Radić, V., Rastner, P., Raup, B. H., Rich, J., and Sharp, M. J. (2014). The Randolph Glacier Inventory: a globally complete inventory of glaciers. *Journal of Glaciology*, 60(221):537–552.

Pieczonka, T., Bolch, T., Junfeng, W., and Shiyin, L. (2013). Heterogeneous mass loss of glaciers in the Aksu-Tarim Catchment (Central Tien Shan) revealed by 1976 KH-9 Hexagon and 2009 SPOT-5 stereo imagery. *Remote Sensing of Environment*, 130:233–244.

Post, A. (1964). Variegated glacier. In *Glacier Photograph Collection*. National Snow and Ice Data Center, Boulder, Colerado, USA.

Post, A. (1965). Variegated glacier. In *Glacier Photograph Collection*. National Snow and Ice Data Center, Boulder, Colorado, USA.

Quincey, D., Copland, L., Mayer, C., Bishop, M., Luckman, A., and Belò, M. (2009). Ice velocity and climate variations for Baltoro Glacier, Pakistan. *Journal of Glaciology*, 55(194):1061–1071.

Quincey, D. J., Braun, M., Glasser, N. F., Bishop, M. P., Hewitt, K., and Luckman, A. (2011). Karakoram glacier surge dynamics. *Geophysical Research Letters*, 38(18):L18504.

Quincey, D. J., Glasser, N. F., Cook, S. J., and Luckman, A. (2015). Heterogeneity in Karakoram glacier surges. *Journal of Geophysical Research: Earth Surface*, 120(7):1288–1300.

Quincey, D. J. and Luckman, A. (2014). Brief Communication: On the magnitude and frequency of Khurdopin glacier surge events. *The Cryosphere*, 8(2):571–574.

Rankl, M., Kienholz, C., and Braun, M. (2014). Glacier changes in the Karakoram region mapped by multimission satellite imagery. *The Cryosphere*, 8(3):977–989.

Scambos, T. A., Dutkiewicz, M. J., Wilson, J. C., and Bindschadler, R. A. (1992). Application of image cross-correlation to the measurement of glacier velocity using satellite image data. *Remote Sensing of Environment*, 42(3):177–186.

Scherler, D., Bookhagen, B., and Strecker, M. R. (2011a). Hillslope-glacier coupling: The interplay of topography and glacial dynamics in High Asia. *Journal of Geophysical Research: Earth Surface*, 116(F2).

Scherler, D., Bookhagen, B., and Strecker, M. R. (2011b). Spatially variable response of Himalayan glaciers to climate change affected by debris cover. *Nature geoscience*, 4(3):156–159.

Sevestre, H. and Benn, D. I. (2015). Climatic and geometric controls on the global distribution of surge-type glaciers: implications for a unifying model of surging. *Journal of Glaciology*, 61(228):646–662.

Shangguan, D., Liu, S., Ding, Y., Ding, L., Xu, J., and Jing, L. (2009). Glacier changes during the last forty years in the Tarim Interior River basin, northwest China. *Progress in Natural Science*, 19(6):727–732.

Shangguan, D., Liu, S., Ding, Y., Li, J., Zhang, Y., Ding, L., Wang, X., Xie, C., and Li, G. (2007). Glacier changes in the west Kunlun Shan from 1970 to 2001 derived from Landsat TM/ETM+ and Chinese glacier inventory data. *Annals of Glaciology*, 46(1):204–208.

Sharp, M. (1988). Surging glaciers behaviour and mechanisms. *Progress in Physical Geography*, 12(3):349–370.

Shi, Y. and Liu, S. (2000). Estimation on the response of glaciers in China to the global warming in the 21st century. *Chinese Science Bulletin*, 45(7):668–672.

Shi, Y., Liu, S., Shangguan, D., Li, D., and Ye, B. (2006). Peculiar phenomena regarding climatic and glacial variations on the Tibetan Plateau. *Annals of Glaciology*, 43(1):106–110.

Shi, Y., Shen, Y., Kang, E., Li, D., Ding, Y., Zhang, G., and Hu, R. (2007). Recent and future climate change in northwest China. *Climatic change*, 80(3-4):379–393.

Stein, M. A. (1912). Ruins of Desert Cathay.

Styron, R., Taylor, M., and Okoronkwo, K. (2010). Database of active structures from the Indo-Asian collision. *Eos, Transactions American Geophysical Union*, 91(20):181–182.

Tang, X.-Y., Tang, X.-L., and Zhang, J.-M. (2014). Arid climate change features in xinjiang, china, during 1961-2011. *Journal of Applied Sciences*, 14(20):2570.

Tarr, R. S. (1907). Recent advance of glaciers in the Yakutat Bay region, Alaska. *Geological Society of America Bulletin*, 18(1):257–286.

Turrin, J., Forster, R. R., Larsen, C., and Sauber, J. (2013). The propagation of a surge front on Bering Glacier, Alaska, 2001–2011. *Annals of Glaciology*, 54(63):221–228.

Vaughan, D. G., Comiso, J. C., Allison, I., Carrasco, J., Kaser, G., Kwok, R., Mote, P., Murray, T., Paul, F., Ren, J., Rignot, E., Solomina, O., Steggen, K., and Zhang, T. (2013). Observations: Cryosphere. In Stocker, T. F., Qin, D., Plattner, G.-K., Tignor, M., Allen, S. K., Boschung, J., Nauels, A., Xia, Y., Bex, V., and Midgley, P. M., editors, *Climate Change 2013: The Physical Science Basis. Contribution of Working Group I to the Fifth Assessment Report of the Intergovernmental Panel on Climate Change*. Cambridge University Press, Cambridge, United Kingdom and New York, NY, USA. 317–382.

Wang, N., Yao, T., Pu, J., Zhang, Y., Sun, W., and Wang, Y. (2003). Variations in air temperature during the last 100 years revealed by δ18o in the Malan ice core from the Tibetan Plateau. *Chinese Science Bulletin*, 48(19):2134–2138.

Ward, M. (1989). The Kun Lun Shan: Desert Peaks of Central Asia. *The Alpine Journal*, 94:84–96.

Wiltshire, A. J. (2014). Climate change implications for the glaciers of the Hindu Kush, Karakoram and Himalayan region. *The Cryosphere*, 8(3):941–958.

Wu, H., Wang, N., Guo, Z., and Wu, Y. (2014). Regional glacier mass loss estimated by ICESat-GLAS data and SRTM digital elevation model in the West Kunlun Mountains, Tibetan Plateau, 2003–2009. *Journal of Applied Remote Sensing*, 8(1):083515–083515.

Xinjua News Agency (2006). Floods, Lightning Strikes Leave 25 dead in Xinjiang. *china.org.cn*. [online] Available at http://www.china.org.cn/english/China/178033.htm Accessed 2016-05-31.

Xu, C., Chen, Y., Chen, Y., Zhao, R., and Ding, H. (2013). Responses of surface runoff to climate change and human activities in the arid region of Central Asia: a case study in the Tarim River Basin, China. *Environmental management*, 51(4):926–938.

Yasuda, T. and Furuya, M. (2013). Short-term glacier velocity changes at West Kunlun Shan, Northwest Tibet, detected by Synthetic Aperture Radar data. *Remote Sensing of Environment*, 128:87–106.

Yasuda, T. and Furuya, M. (2015). Dynamics of surge-type glaciers in West Kunlun Shan, Northwestern Tibet. *Journal of Geophysical Research: Earth Surface*, 120(11):2015JF003511.

Yi, S. and Sun, W. (2014). Evaluation of glacier changes in high-mountain Asia based on 10 year GRACE RL05 models. *Journal of Geophysical Research: Solid Earth*, 119(3):2504–2517.

Yuan, C., Sun, M., Zhou, M.-f., Zhou, H., Xiao, W.-j., and Li, J.-l. (2002). Tectonic evolution of the West Kunlun: geochronologic and geochemical constraints from Kudi Granitoids. *International Geology Review*, 44(7):653–669.

Zhang, Q., Xu, C.-Y., Tao, H., Jiang, T., and Chen, Y. D. (2009). Climate changes and their impacts on water resources in the arid regions: a case study of the Tarim River basin, China. *Stochastic Environmental Research and Risk Assessment*, 24(3):349–358.

Zhang, W., An, R., Yang, H., and Jiao, K. (1989). Conditions of glacier development and some glacial features in the West Kunlin Mountains. *Bulletin of glacier research*, (7):49–58.

Zhang, Z. and Jiao, K. (1987). Modern glaciers on the south slope of West Kunlun Mountains (in Aksayqin Lake and Guozha Co Lake drainage areas). *Bulletin of glacier research*, (5):85–91.

Zhao, L., Ping, C.-L., Yang, D., Cheng, G., Ding, Y., and Liu, S. (2004). Changes of climate and seasonally frozen ground over the past 30 years in Qinghai–Xizang (Tibetan) Plateau, China. *Global and Planetary Change*, 43(1):19–31.

Appendix A

Table of Satellite Data

Table A.1 Dates, sensors, and long-form IDs for Landsat imagery used in this study.

Year	Day of Year	Sensor	ID
1972	301	LS1 MSS	LM11570351972301AAA04
1973	043	LS1 MSS	LM11570351973043AAA05
1976	289	LS2 MSS	LM21570351976289XXX01
1976	307	LS2 MSS	LM21570351976307XXX01
1976	325	LS2 MSS	LM21570351976325AAA07
1976	343	LS2 MSS	LM21570351976343AAA02
1976	361	LS2 MSS	LM21570351976361AAA03
1977	013	LS2 MSS	LM21570351977013XXX03
1977	031	LS2 MSS	LM21570351977031XXX03
1977	049	LS2 MSS	LM21570351977049XXX03
1977	067	LS2 MSS	LM21570351977067AAA03
1977	085	LS2 MSS	LM21570351977085AAA03
1977	103	LS2 MSS	LM21570351977103AAA03
1977	121	LS2 MSS	LM21570351977121AAA02
1977	175	LS2 MSS	LM21570351977175XXX03

Continued on next page

Table A.1 – *Continued from previous page*

Year	Day of Year	Sensor	ID
1977	193	LS2 MSS	LM21570351977193XXX03
1977	210	LS2 MSS	LM21570351977210AAA01
1977	211	LS2 MSS	LM21570351977211AAA03
1977	229	LS2 MSS	LM21570351977229AAA03
1977	246	LS2 MSS	LM21570351977246TGS02
1977	247	LS2 MSS	LM21570351977247AAA03
1977	265	LS2 MSS	LM21570351977265AAA03
1989	051	LS5 MSS	LM51460351989051ISP00
1989	339	LS5 TM	LT51460351989339ISP00
1989	355	LS5 TM	LT51460351989355ISP00
1990	038	LS5 TM	LT51460351990038ISP00
1990	054	LS5 TM	LT51460351990054ISP00
1990	214	LS5 TM	LT51460351990214ISP00
1991	009	LS5 TM	LT51460351991009ISP00
1991	025	LS5 TM	LT51460351991025ISP00
1991	057	LS5 TM	LT51460351991057ISP00
1991	073	LS5 TM	LT51460351991073ISP00
1991	089	LS5 TM	LT51460351991089ISP00
1991	105	LS5 TM	LT51460351991105SGI00
1991	137	LS5 TM	LT51460351991137ISP00
1991	313	LS5 TM	LT51460351991313ISP00
1991	345	LS5 TM	LT51460351991345ISP00
1992	012	LS5 TM	LT51460351992012ISP00
1992	028	LS5 TM	LT51460351992028ISP00
1992	044	LS5 TM	LT51460351992044ISP00

Continued on next page

Table A.1 – *Continued from previous page*

Year	Day of Year	Sensor	ID
1992	060	LS5 TM	LT51460351992060ISP00
1992	076	LS5 TM	LT51460351992076ISP00
1992	092	LS5 TM	LT51460351992092ISP00
1992	124	LS5 TM	LT51460351992124ISP00
1992	156	LS5 TM	LT51460351992156ISP00
1992	316	LS5 TM	LT51460351992316ISP00
1992	364	LS5 TM	LT51460351992364ISP00
1993	030	LS5 TM	LT51460351993030ISP00
1993	046	LS5 TM	LT51460351993046ISP00
1993	062	LS5 TM	LT51460351993062ISP00
1993	078	LS5 TM	LT51460351993078ISP00
1993	094	LS5 TM	LT51460351993094ISP00
1993	126	LS5 TM	LT51460351993126ISP01
1993	142	LS5 TM	LT51460351993142ISP00
1993	158	LS5 TM	LT51460351993158ISP00
1993	174	LS5 TM	LT51460351993174ISP00
1993	206	LS5 TM	LT51460351993206ISP00
1993	222	LS5 TM	LT51460351993222ISP00
1993	238	LS5 TM	LT51460351993238ISP00
1993	270	LS5 TM	LT51460351993270ISP00
1993	302	LS5 TM	LT51460351993302ISP00
1993	318	LS5 TM	LT51460351993318ISP00
1993	334	LS5 TM	LT51460351993334ISP00
1994	001	LS5 TM	LT51460351994001ISP00
1994	017	LS5 TM	LT51460351994017ISP00

Continued on next page

Table A.1 – *Continued from previous page*

Year	Day of Year	Sensor	ID
1994	033	LS5 TM	LT51460351994033ISP00
1994	049	LS5 TM	LT51460351994049ISP00
1994	065	LS5 TM	LT51460351994065ISP00
1994	097	LS5 TM	LT51460351994097ISP01
1994	129	LS5 TM	LT51460351994129ISP40
1994	161	LS5 TM	LT51460351994161ISP00
1994	193	LS5 TM	LT51460351994193ISP40
1994	209	LS5 TM	LT51460351994209ISP00
1994	225	LS5 TM	LT51460351994225ISP00
1994	241	LS5 TM	LT51460351994241ISP00
1994	257	LS5 TM	LT51460351994257ISP00
1994	273	LS5 TM	LT51460351994273ISP00
1994	289	LS5 TM	LT51460351994289ISP01
1994	305	LS5 TM	LT51460351994305ISP00
1994	337	LS5 TM	LT51460351994337ISP00
1995	004	LS5 TM	LT51460351995004ISP00
1995	020	LS5 TM	LT51460351995020ISP00
1995	068	LS5 TM	LT51460351995068ISP00
1995	084	LS5 TM	LT51460351995084ISP00
1995	308	LS5 TM	LT51460351995308ISP01
1995	340	LS5 TM	LT51460351995340ISP00
1996	023	LS5 TM	LT51460351996023ISP00
1996	039	LS5 TM	LT51460351996039ISP00
1996	055	LS5 TM	LT51460351996055ISP00
1996	071	LS5 TM	LT51460351996071ISP00

Continued on next page

Table A.1 – *Continued from previous page*

Year	Day of Year	Sensor	ID
1996	087	LS5 TM	LT51460351996087ISP00
1996	103	LS5 TM	LT51460351996103ISP00
1996	135	LS5 TM	LT51460351996135ISP00
1996	151	LS5 TM	LT51460351996151ISP00
1996	167	LS5 TM	LT51460351996167ISP00
1996	199	LS5 TM	LT51460351996199ISP00
1996	215	LS5 TM	LT51460351996215ISP00
1996	231	LS5 TM	LT51460351996231ISP00
1996	247	LS5 TM	LT51460351996247ISP00
1996	263	LS5 TM	LT51460351996263ISP00
1996	295	LS5 TM	LT51460351996295ISP00
1996	311	LS5 TM	LT51460351996311ISP00
1997	009	LS5 TM	LT51460351997009ISP00
1997	025	LS5 TM	LT51460351997025ISP00
1997	057	LS5 TM	LT51460351997057SGI00
1997	121	LS5 TM	LT51460351997121SGI00
1997	137	LS5 TM	LT51460351997137SGI00
1997	201	LS5 TM	LT51460351997201SGI00
1997	217	LS5 TM	LT51460351997217ISP00
1997	233	LS5 TM	LT51460351997233ISP00
1997	265	LS5 TM	LT51460351997265ISP00
1997	281	LS5 TM	LT51460351997281ISP00
1998	108	LS5 TM	LT51460351998108XXX01
1998	140	LS5 TM	LT51460351998140ULM03
1998	236	LS5 TM	LT51460351998236BIK04

Continued on next page

Table A.1 – *Continued from previous page*

Year	Day of Year	Sensor	ID
1998	252	LS5 TM	LT51460351998252BIK01
1998	268	LS5 TM	LT51460351998268BIK02
1999	047	LS5 TM	LT51460351999047AAA02
1999	063	LS5 TM	LT51460351999063XXX01
1999	079	LS5 TM	LT51460351999079XXX02
1999	111	LS5 TM	LT51460351999111XXX02
2000	130	LS5 TM	LT51460352000130XXX01
2001	100	LS5 TM	LT51460352001100SGI00
2001	164	LS5 TM	LT51460352001164SGI00
2001	212	LS5 TM	LT51460352001212SGI00
2008	120	LS5 TM	LT51460352008120BJC01
2008	152	LS5 TM	LT51460352008152KHC01
2008	168	LS5 TM	LT51460352008168KHC01
2008	184	LS5 TM	LT51460352008184KHC01
2008	200	LS5 TM	LT51460352008200KHC01
2008	216	LS5 TM	LT51460352008216KHC01
2008	264	LS5 TM	LT51460352008264KHC01
2008	280	LS5 TM	LT51460352008280KHC01
2008	296	LS5 TM	LT51460352008296KHC01
2008	328	LS5 TM	LT51460352008328KHC01
2009	010	LS5 TM	LT51460352009010KHC02
2009	074	LS5 TM	LT51460352009074KHC00
2009	090	LS5 TM	LT51460352009090KHC00
2009	106	LS5 TM	LT51460352009106KHC00
2009	122	LS5 TM	LT51460352009122KHC00

Continued on next page

Table A.1 – *Continued from previous page*

Year	Day of Year	Sensor	ID
2009	138	LS5 TM	LT51460352009138KHC00
2009	154	LS5 TM	LT51460352009154KHC00
2009	170	LS5 TM	LT51460352009170KHC00
2009	186	LS5 TM	LT51460352009186KHC00
2009	202	LS5 TM	LT51460352009202KHC00
2009	218	LS5 TM	LT51460352009218KHC00
2009	234	LS5 TM	LT51460352009234KHC00
2009	250	LS5 TM	LT51460352009250KHC00
2009	266	LS5 TM	LT51460352009266KHC00
2009	282	LS5 TM	LT51460352009282KHC00
2009	298	LS5 TM	LT51460352009298KHC00
2009	330	LS5 TM	LT51460352009330KHC00
2009	346	LS5 TM	LT51460352009346KHC00
2010	013	LS5 TM	LT51460352010013KHC00
2010	029	LS5 TM	LT51460352010029KHC00
2010	093	LS5 TM	LT51460352010093KHC00
2010	141	LS5 TM	LT51460352010141KHC00
2010	157	LS5 TM	LT51460352010157KHC00
2010	173	LS5 TM	LT51460352010173KHC00
2010	189	LS5 TM	LT51460352010189KHC00
2010	205	LS5 TM	LT51460352010205KHC00
2010	237	LS5 TM	LT51460352010237KHC00
2010	269	LS5 TM	LT51460352010269KHC00
2010	285	LS5 TM	LT51460352010285KHC01
2010	301	LS5 TM	LT51460352010301KHC00

Continued on next page

Table A.1 – *Continued from previous page*

Year	Day of Year	Sensor	ID
2010	317	LS5 TM	LT51460352010317KHC00
2010	333	LS5 TM	LT51460352010333KHC00
2010	349	LS5 TM	LT51460352010349KHC00
2011	032	LS5 TM	LT51460352011032KHC00
2011	048	LS5 TM	LT51460352011048KHC00
2011	064	LS5 TM	LT51460352011064KHC00
2011	096	LS5 TM	LT51460352011096KHC00
2011	112	LS5 TM	LT51460352011112KHC00
2011	128	LS5 TM	LT51460352011128KHC00
2011	160	LS5 TM	LT51460352011160KHC04
2011	192	LS5 TM	LT51460352011192KHC00
2011	256	LS5 TM	LT51460352011256KHC00
2011	272	LS5 TM	LT51460352011272KHC01
1999	199	LS7 ETM+ SLC-on	LE71460351999199EDC01
1999	215	LS7 ETM+ SLC-on	LE71460351999215SGS01
1999	231	LS7 ETM+ SLC-on	LE71460351999231SGS00
1999	295	LS7 ETM+ SLC-on	LE71460351999295SGS00
2000	026	LS7 ETM+ SLC-on	LE71460352000026EDC00
2000	074	LS7 ETM+ SLC-on	LE71460352000074SGS00
2000	122	LS7 ETM+ SLC-on	LE71460352000122SGS00
2000	154	LS7 ETM+ SLC-on	LE71460352000154SGS00
2000	218	LS7 ETM+ SLC-on	LE71460352000218SGS00
2000	282	LS7 ETM+ SLC-on	LE71460352000282SGS00
2001	012	LS7 ETM+ SLC-on	LE71460352001012SGS01
2001	060	LS7 ETM+ SLC-on	LE71460352001060SGS00

Continued on next page

Table A.1 – *Continued from previous page*

Year	Day of Year	Sensor	ID
2001	092	LS7 ETM+ SLC-on	LE71460352001092SGS00
2001	124	LS7 ETM+ SLC-on	LE71460352001124SGS00
2001	252	LS7 ETM+ SLC-on	LE71460352001252SGS00
2001	268	LS7 ETM+ SLC-on	LE71460352001268EDC00
2002	031	LS7 ETM+ SLC-on	LE71460352002031SGS00
2002	063	LS7 ETM+ SLC-on	LE71460352002063SGS00
2002	111	LS7 ETM+ SLC-on	LE71460352002111SGS00
2002	191	LS7 ETM+ SLC-on	LE71460352002191SGS00
2002	223	LS7 ETM+ SLC-on	LE71460352002223SGS00
2002	239	LS7 ETM+ SLC-on	LE71460352002239SGS00
2002	255	LS7 ETM+ SLC-on	LE71460352002255SGS00
2002	271	LS7 ETM+ SLC-on	LE71460352002271SGS00
2002	287	LS7 ETM+ SLC-on	LE71460352002287SGS00
2002	335	LS7 ETM+ SLC-on	LE71460352002335SGS00
2003	034	LS7 ETM+ SLC-on	LE71460352003034SGS00
2003	066	LS7 ETM+ SLC-on	LE71460352003066SGS00
2003	082	LS7 ETM+ SLC-on	LE71460352003082ASN00
2003	130	LS7 ETM+ SLC-on	LE71460352003130ASN00
2009	208	LS7 ETM+ SLC-off	LE70112092009208EDC00
2011	182	LS7 ETM+ SLC-off	LE70112092011182EDC00
2003	274	LS7 ETM+ SLC-off	LE71460352003274ASN01
2003	290	LS7 ETM+ SLC-off	LE71460352003290ASN01
2004	037	LS7 ETM+ SLC-off	LE71460352004037ASN01
2004	069	LS7 ETM+ SLC-off	LE71460352004069ASN01
2004	117	LS7 ETM+ SLC-off	LE71460352004117ASN02

Continued on next page

Table A.1 – *Continued from previous page*

Year	Day of Year	Sensor	ID
2004	165	LS7 ETM+ SLC-off	LE71460352004165ASN01
2004	229	LS7 ETM+ SLC-off	LE71460352004229ASN01
2004	261	LS7 ETM+ SLC-off	LE71460352004261ASN01
2004	309	LS7 ETM+ SLC-off	LE71460352004309PFS00
2004	341	LS7 ETM+ SLC-off	LE71460352004341PFS00
2005	007	LS7 ETM+ SLC-off	LE71460352005007ASN00
2005	071	LS7 ETM+ SLC-off	LE71460352005071ASN01
2005	087	LS7 ETM+ SLC-off	LE71460352005087PFS00
2005	103	LS7 ETM+ SLC-off	LE71460352005103ASN00
2005	247	LS7 ETM+ SLC-off	LE71460352005247ASN00
2005	263	LS7 ETM+ SLC-off	LE71460352005263PFS00
2006	026	LS7 ETM+ SLC-off	LE71460352006026PFS00
2006	170	LS7 ETM+ SLC-off	LE71460352006170PFS00
2006	186	LS7 ETM+ SLC-off	LE71460352006186ASN00
2006	202	LS7 ETM+ SLC-off	LE71460352006202ASN00
2006	250	LS7 ETM+ SLC-off	LE71460352006250PFS01
2006	282	LS7 ETM+ SLC-off	LE71460352006282PFS00
2006	314	LS7 ETM+ SLC-off	LE71460352006314PFS00
2006	346	LS7 ETM+ SLC-off	LE71460352006346SGS00
2007	029	LS7 ETM+ SLC-off	LE71460352007029SGS00
2007	061	LS7 ETM+ SLC-off	LE71460352007061SGS00
2007	077	LS7 ETM+ SLC-off	LE71460352007077SGS00
2007	093	LS7 ETM+ SLC-off	LE71460352007093SGS00
2007	109	LS7 ETM+ SLC-off	LE71460352007109SGS00
2007	173	LS7 ETM+ SLC-off	LE71460352007173PFS00

Continued on next page

Table A.1 – *Continued from previous page*

Year	Day of Year	Sensor	ID
2007	269	LS7 ETM+ SLC-off	LE71460352007269PFS00
2007	285	LS7 ETM+ SLC-off	LE71460352007285PFS00
2007	301	LS7 ETM+ SLC-off	LE71460352007301PFS00
2007	317	LS7 ETM+ SLC-off	LE71460352007317PFS00
2008	032	LS7 ETM+ SLC-off	LE71460352008032SGS00
2008	112	LS7 ETM+ SLC-off	LE71460352008112SGS00
2008	128	LS7 ETM+ SLC-off	LE71460352008128ASN00
2008	160	LS7 ETM+ SLC-off	LE71460352008160PFS00
2008	192	LS7 ETM+ SLC-off	LE71460352008192PFS00
2008	256	LS7 ETM+ SLC-off	LE71460352008256ASN00
2008	272	LS7 ETM+ SLC-off	LE71460352008272ASN00
2009	082	LS7 ETM+ SLC-off	LE71460352009082SGS00
2009	226	LS7 ETM+ SLC-off	LE71460352009226ASN00
2009	242	LS7 ETM+ SLC-off	LE71460352009242ASN00
2009	258	LS7 ETM+ SLC-off	LE71460352009258SGS00
2009	274	LS7 ETM+ SLC-off	LE71460352009274ASN00
2009	306	LS7 ETM+ SLC-off	LE71460352009306SGS00
2010	085	LS7 ETM+ SLC-off	LE71460352010085ASN00
2010	101	LS7 ETM+ SLC-off	LE71460352010101SGS00
2010	245	LS7 ETM+ SLC-off	LE71460352010245ASN00
2010	277	LS7 ETM+ SLC-off	LE71460352010277ASN00
2010	293	LS7 ETM+ SLC-off	LE71460352010293SGS00
2010	309	LS7 ETM+ SLC-off	LE71460352010309ASN00
2011	104	LS7 ETM+ SLC-off	LE71460352011104PFS00
2011	136	LS7 ETM+ SLC-off	LE71460352011136PFS00

Continued on next page

Table A.1 – *Continued from previous page*

Year	Day of Year	Sensor	ID
2011	216	LS7 ETM+ SLC-off	LE71460352011216PFS00
2011	264	LS7 ETM+ SLC-off	LE71460352011264PFS00
2011	280	LS7 ETM+ SLC-off	LE71460352011280PFS00
2011	296	LS7 ETM+ SLC-off	LE71460352011296PFS00
2011	312	LS7 ETM+ SLC-off	LE71460352011312PFS00
2011	344	LS7 ETM+ SLC-off	LE71460352011344PFS00
2012	011	LS7 ETM+ SLC-off	LE71460352012011PFS00
2012	027	LS7 ETM+ SLC-off	LE71460352012027PFS00
2012	075	LS7 ETM+ SLC-off	LE71460352012075PFS00
2012	139	LS7 ETM+ SLC-off	LE71460352012139PFS02
2012	299	LS7 ETM+ SLC-off	LE71460352012299PFS02
2012	315	LS7 ETM+ SLC-off	LE71460352012315PFS00
2013	045	LS7 ETM+ SLC-off	LE71460352013045PFS00
2013	061	LS7 ETM+ SLC-off	LE71460352013061PFS00
2013	077	LS7 ETM+ SLC-off	LE71460352013077PFS00
2013	093	LS7 ETM+ SLC-off	LE71460352013093PFS00
2013	133	LS8 OLI	LC81460352013133LGN01
2013	181	LS8 OLI	LC81460352013181LGN00
2013	197	LS8 OLI	LC81460352013197LGN00
2013	213	LS8 OLI	LC81460352013213LGN00
2013	261	LS8 OLI	LC81460352013261LGN00
2013	325	LS8 OLI	LC81460352013325LGN00
2013	341	LS8 OLI	LC81460352013341LGN00
2014	056	LS8 OLI	LC81460352014056LGN00
2014	072	LS8 OLI	LC81460352014072LGN00

Continued on next page

Table A.1 – *Continued from previous page*

Year	Day of Year	Sensor	ID
2015	011	LS8 OLI	LC81460352015011LGN00
2014	088	LS8 OLI	LC81460352014088LGN00
2014	136	LS8 OLI	LC81460352014136LGN00
2014	152	LS8 OLI	LC81460352014152LGN00
2014	168	LS8 OLI	LC81460352014168LGN00
2014	232	LS8 OLI	LC81460352014232LGN00
2014	280	LS8 OLI	LC81460352014280LGN00
2014	296	LS8 OLI	LC81460352014296LGN00
2014	328	LS8 OLI	LC81460352014328LGN00
2014	344	LS8 OLI	LC81460352014344LGN00
2015	043	LS8 OLI	LC81460352015043LGN00
2015	139	LS8 OLI	LC81460352015139LGN00
2015	171	LS8 OLI	LC81460352015171LGN00
2015	203	LS8 OLI	LC81460352015203LGN00
2015	219	LS8 OLI	LC81460352015219LGN00
2015	235	LS8 OLI	LC81460352015235LGN00
2015	283	LS8 OLI	LC81460352015283LGN00
2015	315	LS8 OLI	LC81460352015315LGN00
2015	331	LS8 OLI	LC81460352015331LGN01
2015	347	LS8 OLI	LC81460352015347LGN00
2015	363	LS8 OLI	LC81460352015363LGN00
2016	014	LS8 OLI	LC81460352016014LGN00

Appendix B

Supplementary Material

Supplementary material is made available in the form of gifs, available at `https://www.repository.cam.ac.uk/handle/1810/256047`. These gifs display stacked Landsat 2 MSS (band 4, 60 m resolution), Landsat 5 TM (band 1, 30 m resolution), Landsat 7 ETM+ (band 8, 15 m resolution), and Landsat 8 OLI (band 8, 15 m resolution) imagery from 1972–2016, visualising the surges of 8 glaciers in the West Kunlun Shan, Xinjiang, China. Frames are annotated in the form YYYY_DDD, where YYYY is the year and DDD is the DoY. Landsat data is provided by the USGS at `earthexplorer.usgs.gov`.

Scale bars and coordinates either on or beside the gif imagery was deemed inappropriate due to (i) rapidly changing contrast between summer/winter imagery and (ii) a desire to keep files of a reasonable size. Instead, relevant scale bars and coordinates are presented in figure B.1.

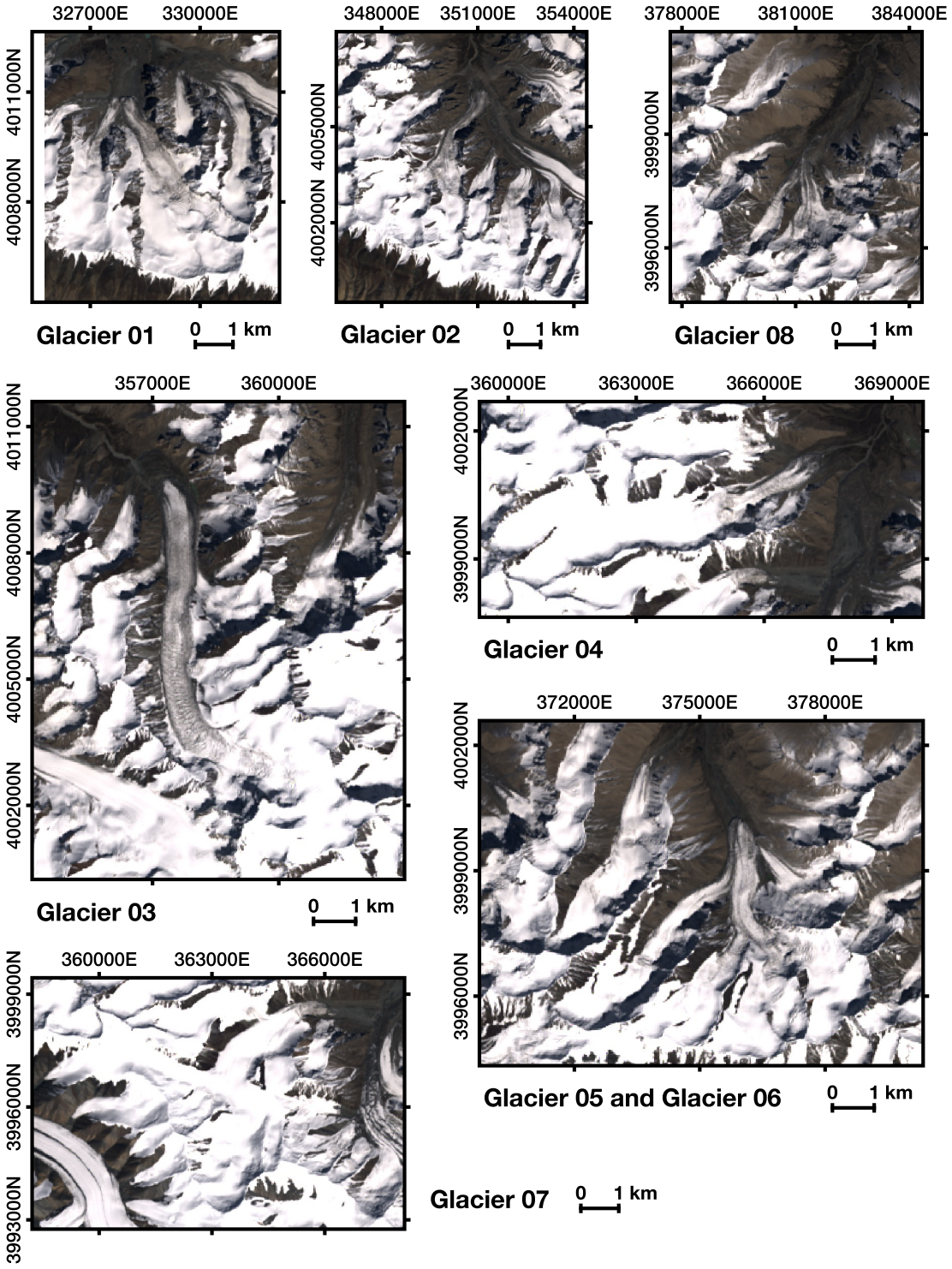

Fig. B.1 Location and scale data for supplementary animations. Background image is Landsat 7 ETM+ imagery, 2000 DoY 282. Coordinate data given in UTM 44N.

Appendix C

Meteorological Stations

Table C.1 Information on meteorological stations, including Name and ID provided by the Chinese Meteorological Administration, location, and temporal coverage.

Name	ID	Lat.	Long.	Elevation	Temperature	Precipitation
Shache	51811	38.43	77.27	1231.2	1953-7 – 2015-6	1951-7 – 2015-6
Pishan	51818	37.62	78.28	1375.4	1959-1 – 2015-6	1959-1 – 2015-6
Hotan	51828	37.13	79.93	1375	1953-2 – 2015-6	1953-2 – 2015-6
Yutian	51931	36.85	81.65	1422	1955-11 – 2015-6	1955-11 – 2015-6
Minfeng	51839	37.07	82.72	1409.5	1956-12 – 2015-6	1956-12 – 2015-6
Andehe	51848	37.93	83.65	1262.8	1960-1 – 1998-12	1960-1 – 1998-12

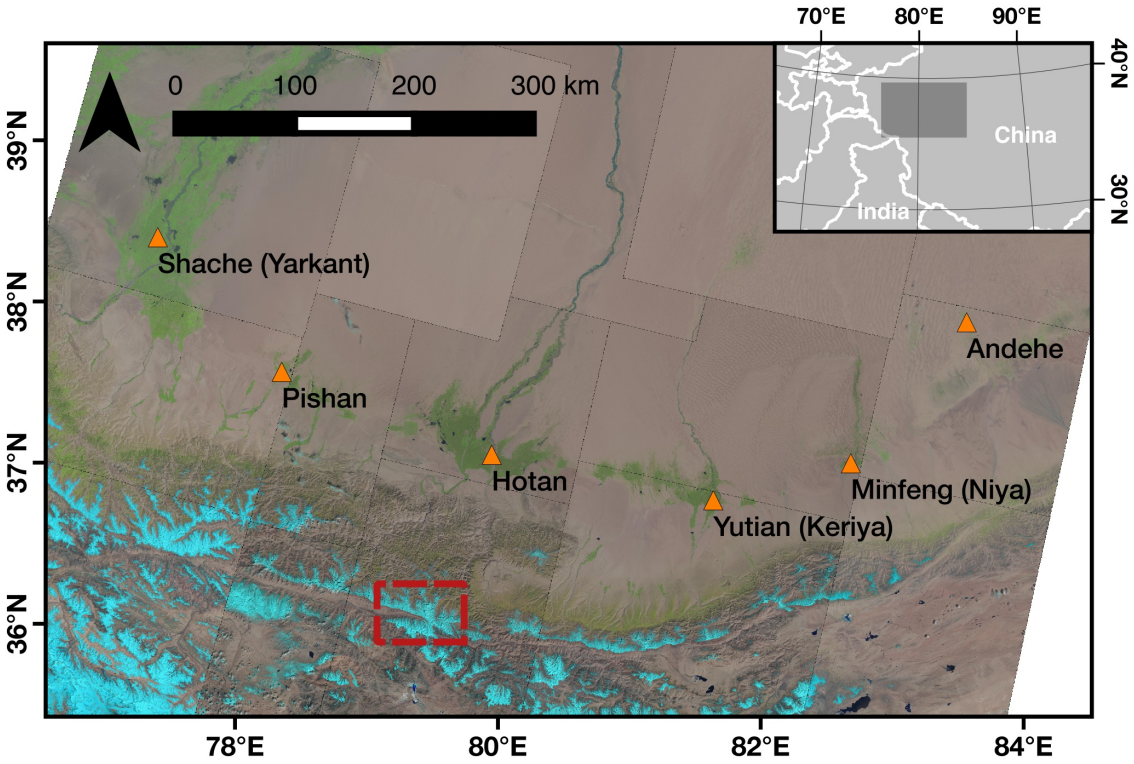

Fig. C.1 Location of meteorological stations relative to the study area (red box). Alternative names are given in brackets.